PhD Thesis

Control Design for Space Applications

Hassrizal Bin Hassan Basri

Supervisors:
Dr. Anthony Rossiter

June 2021

Abstract

Spacecraft operation requires a crucial and robust control scheme to accomplish their missions. Hence, sliding mode control (SMC) is one of the robust control approaches capable of fulfilling the spacecraft control operation requirements. Classical SMC, however, produces chattering in the control inputs, which can cause wear and tear in the moving mechanical parts, for instance, actuator. Thus, many researchers introduced modifications in the SMC to attenuate the chattering drawbacks. SMC control development can be divided into two groups; low-order sliding mode control (LOSMC) and high-order sliding mode control (HOSMC). In details, HOSMC requires a sophisticated control algorithm compared to the LOSMC but with a more significant dynamics response. Thus, a new LOSMC is required, producing similar results as HOSMC but less complexity in the control algorithm. Several selected SMC approaches are evaluated on the spacecraft's attitude and orbit control subsystem (ACS) applications; spacecraft attitude and orientation model (SAOM) and spacecraft rendezvous and docking manoeuvres (SRDM). This analysis is a vital medium for evaluating the existing SMC techniques, strengths, and weaknesses for a new LOSMC control development. First, the proposed LOSMC is analysed on the SAOM and SRDM, where the outcomes are compared to the HOSMC. Then, an optimisation technique (particle swarm optimisation (PSO)) is implemented on the new LOSMC and HOSMC. The PSO helps the SAOM and SRDM improving the transient trajectory. The new LOSMC is designed and can perform as the HOSMC with a low complexity algorithm. Finally, this will provide helpful SMC information of the SMC control strategies with their performances on the SAOM and SRDM.

Contents

Abbreviations

ACS Attitude and Orbit Control Subsystem

AFSMC Adaptive Fuzzy Sliding Mode Control

ANSTSMC Adaptive Non-Singular Terminal Sliding Mode Control

CME Coronal Mass Ejection

CBL Constant Boundary Layer

DBL Decaying Boundary Layer

DBLEF Decaying Boundary Layer Thorough Error Feedback

DBLSF Decaying Boundary Layer and Sewitching Function Method Thorough Error Feedback

DSMC Dynamic Sliding Mode Control

EKF Extended Kalman Filtering

EORM Equations of Rotational Motion

FFPT Failure for a Period of Time

FSMC Fuzzy Sliding Mode Control

GPS Global Positioning Satellite

HEO High Earth Orbit

HOSMC Higher Order Sliding Mode Control

ISMC Integral Sliding Mode Control

ISS International Space Station

KF Kalman Filtering

LEO Low Earth Orbit

LFSG Linear Feedback with State Dependent Gains

LIUT Lock-in Unknown Time

LOE Loss of Effectiveness

LOSMC Low Order Sliding Mode Control

LTI Linear Time Invariant

MEO Medium Earth Orbit

MIMO Multi-Input Multi-Output

MSMEFC Minimum Sliding Mode Error Feedback Control

MT Magnetic Torquers

PSO Particle Swarm Optimisation

RCG Relay with Constant Gains

ROOM Reduction of Error Method

RSG Relay with State Dependent Gains

RW Reaction Wheels

SAOM Spacecraft Attitude and Orientation model

SCS Supplemental Communications System

SDBL State-Dependent Boundary Layer

SFD Switching Function Designs

SMC Sliding Mode Control

SRDM Spacecraft Rendezvous and Docking model

STSMC Super-Twisting Sliding Mode Control

UKF Unscented Kalman Filtering

UV Ultraviolet

Nomenclature

A Inertial-fixed or Fixed-frame Origin

α Angular Acceleration of Moving-frame

B Moving-frame Origin / Center of Mass

$d(t)$ Disturbances and Uncertainties

J Inertia Matrix in the Body-Fixed Frame

$u_{eq}(t)$ Equivalent Control Input

$u_{smc}(t)$ Control Input Law

$u_n(t)$ Switching Function Control Input

$u(t)$ Scalar Inputs

λ Gain for States Error of Switching Surface Design

$V(x, \dot{x})$ Lyapunov Function

P A Point on Moving-frame

θ Rotation along Y axis (Pitch)

r_{BA} Vector distance at B from A

ψ Rotation along X axis (Roll)

r_{PA} Vector distance at P from A

r_{PB} Vector distance at P from B

s Sliding Surface Coefficients for States of Switching Surface Design

$e(t)$ Deviation between the Reference Inputs and Measured Outputs

S A Set of Switching Function Coefficients

$\sigma(t)$ Sliding Surface

$sgn(.)$ Signum Function

$x_d(t)$ Desired States Output

v_{PA} Vector Velocity between P and A

M_P Moment about P

$x(t)$ System State-Variables

τ Torque Input

a_{BA} Vector Acceleration between B and A

a_{PA} Vector Acceleration between P and A

v_{BA} Vector Velocity between B and A

Ω Angular Velocity of Moving-frame

ω Angular Velocity

xyz Moving-frame Axis

XYZ Inertial-frame or Fixed-frame Axis

ϕ Rotation along Z axis (Yaw)

List of Figures

List of Tables

Chapter 1

Introduction

A spacecraft is a vehicle travels in outer space to accomplish a variety of missions and purposes such as communications [8], Earth observation [9], meteorology [8], navigation [10], planetary colonisation [11], and transportation of humans and cargo [12]. The development of human crewed or auto manoeuvring spacecraft has and continues to have a significant impact on human civilisation [13]. Generally, a spacecraft made of six subsystems which attitude and orbit control subsystem (ACS) is among them [14]. The ACS provides, for instance, payload and antennas achieved stability and coarse pointing accuracy in the spacecraft missions [15]. Furthermore, the ACS is also stabilising and de-tumbling the spacecraft angular velocity while gathering the orbit and attitude information [16]. Therefore, a spacecraft needs a crucial control scheme to complete the missions with existing challenges in space such as solar storm and sun and moon gravitational force [17]. Thus, many researchers have proposed various control algorithms to achieve the precision and optimisation of the ACS.

A few typical specifications for assessing these strategies, especially for small spacecraft operation, have been robustness, energy efficiency, minimum maintenance, and weight reduction [18]. Among the possible robust control schemes, sliding mode control (SMC) attributes such as low complexity, computer-implementable, less weight, and low-cost control make this is the suitable approach to be implemented as the ACS controller [19–21]. Hence, it is essential to understand the range of limitations of these SMC approaches before further improvements can be made. Therefore, this research will explore various SMC control algorithms on ACS applications.

SMC is a particular type of variable structure control systems (VSCS)

family were characterised by a suite of feedback control laws (switching surface) and decision rule (switching function). The advantages of the VSCS are insensitive towards the disturbances and uncertainties, and the dynamics behaviour potentially follow the switching surface particular design [22]. There are two stages in designing the SMC; the switching surface design (continuous) and the control law (discontinuous) [23]. The continuous part drives the state trajectories of the controlled system to the designed transient performance requirements, while the discontinuous feature will help maintain the state on robust condition. Unfortunately, using just the basic concept of SMC, chattering is the main drawback produced by the high-frequency switching due to the un-modelled dynamics in the switching function that can cause wear and tear, for instance, to the actuator. Thus, many researchers proposed SMC algorithms to suppress the chattering phenomena in the classical SMC while maintaining the robustness and control outputs accuracy, where can be categorised as low-order sliding mode control (LOSMC), [24] and high-order sliding mode control (HOSMC) [25].

The HOSMC requires a complex control algorithm compared to the LOSMC (for double integrators case) but attributes to evaluable at the finite-time convergence which guarantees of the all-dimension chain of integrators [26]. Besides that, HOSMC offers better control output accuracy. Thus, the primary focus of this research study is to develop a new LOSMC technique comparable to HOSMC performances.

1.1 Thesis Outline

The thesis structures outlined as below:

- **Chapter 1** introduces the research topic and purposes of this thesis. Next, the thesis outline and key contributions are explained for each chapter. Furthermore, the relevance of the author's publications is listed at the end of this chapter.

- **Chapter 2** reviews the ACS structures and applications. Following, the general spacecraft challenges in space are presented. Some of the published papers focus on the SMC algorithms on the ideal spacecraft scenarios are reviewed, including the strengths and weakness.

- **Chapter 3** elaborates on the SMC fundamental design concepts, developments and general control techniques. Existing LOSMC and HOSMC characteristics are presented.

- **Chapter 4** reproduces some of the technical paper results using HOSMC approaches for simulation technique skills validation.

- **Chapter 5** analyses the existing SMC on the SAOM for LOSMC and HOSMC technique. The controller parameters are manually adjusted to tailor SMC for a spacecraft instead of 'theory' development.

- **Chapter 6** introduced a new LOSMC to the SAOM where the controller behaviour are carefully evaluated through simulations. Finally, PSO tunes the new LOSMC and a HOSMC; then, the performances are contrasted.

- **Chapter 7** evaluates the SRDM using existing LOSMC and HOSMC. First, the SRDM is well-derived from the fundamental structure. Then, the developed LOSMC is implemented on the SRDM, where the characteristics are compared to the HOSMC. Finally, PSO is injected into the new LOSMC and the existing HOSMC for optimisation comparison.

- **Chapter 8** gives a summary of the thesis and discusses future works.

1.2   Key Contributions

Key contributions of this thesis are highlighted below:

1. A survey of SMC techniques is undertaken, including an evaluation of strengths and weaknesses. A particular novelty of this thesis is that the presentation focuses on the potential applications to spacecraft.

2. Following a careful evaluation of the performance of conventional SMC techniques on some ideal spacecraft scenarios, modifications to the boundary layer technique in SMC and implementation of an optimisation method are proposed to improve behaviour for spacecraft. The efficacy of the proposed algorithms is demonstrated with simulations.

3. A vital information about the common existing SMC characteristics on spacecraft classical scenarios throughout simulations are carefully validated and presented. A potency LOSMC algorithm is developed over the findings.

4. A new LOSMC is proposed, including the analysis of the controller characteristics. The designed controller behaviour on the possible spacecraft scenarios is presented and contrasted to a HOSMC method. The efficiency of the developed method is validated with simulations.

1.3 List of Publications

The author's publications with relevance to this thesis are listed below:

- ***P1:*** **Hassrizal H. B.** and J. A. Rossiter (2016), "A Survey of control strategis for spacecarft attitude and orientation," 11th International Conference on Control (UKACC), IEEE, Belfast, 2016.

- ***P2:*** **Hassrizal H. B.** and J. A. Rossiter (2017). "Application of decaying boundary layer and switching function method thorough error feedback for sliding mode control on spacecraft's attitude," 25th Mediterranean Conference on Control and Automation (MED), IEEE, 2017.

- ***P3:*** **Hassrizal H. B.**, J. A. Rossiter, and A. R. Firdaus (2018). "Feasibility study of switching function approaches in sliding mode control for a spacecraft's attitude control system," 5th International Conference on Control, Decision and Information Technologies (CoDIT), IEEE, 2018.

- ***P4:*** **Hassrizal H. B.**, J. A. Rossiter, M. N. Nasir, and S. M. Othman (2019). "Particle swarm algorithm sliding mode control on spacecraft's attitude with switching function method thorough error feedback," 2019 International Conference on Man Machine Systems (ICoMMS 2019), IOP, 2019.

Chapter 2

Literature Review

2.1 Introduction

Spacecraft applications need robust and energy efficiency control methods to produce a-high-accuracy outputs for the system. Furthermore, the system needs an optimisation technique to maximise the performances in term of state trajectories and power consumption. Thus, this chapter reviews, elaborate, and concludes the definition of spacecraft with its structures, spacecraft's applications, and existing optimisation control algorithms for the applications. Finally, the possible optimisation control methods on SAOM is proposed for further investigation and analysis.

2.2 Earth's Orbits and Challenges

In space, the scientist categorise three orbits relative to the Earth; low Earth orbit (LEO), medium Earth orbit (MEO) and high Earth orbit (HEO). The definition of these orbit is shown in Table 2.1 [27].

Table 2.1: Orbits Distance From Earth.

Orbit	Distance from the Earth's surface
Low Earth Orbit (LEO)	2000 km
Medium Earth Orbit (MEO)	2000 km to 20350 km
High Earth Orbit (HEO)	over 20350 km

Kepler's laws widely used to explain the planetary or object motion in these orbits. In total, there are three Kepler's laws explain about the planetary motion [3].

1. The first law said that the planets follow elliptical paths around the sun. The interaction between these two-body orbits mostly referred to as Keplerian orbits.

2. The second law stated that equal areas are swept out in similar times.

3. The third law said that the period of a planet is proportional to three-halves power of its semi-major axis.

2.2.1 Earth's Orbits

Each orbit attributes to specific spacecraft operations. The most common and vital spacecraft applications, for instance, weather forecast, communication, broadcasting, surveillance of a pre-selected region, military purposes, global positioning satellite (GPS), gather and distribute information daily for human uses. Hence, the correct spacecraft location in orbit, attitude and orientation are the keys to the success of a task.

Firstly, in LEO, the travel speed of the object orbiting the Earth must be greater than 8 kms^{-1} to avoid the object enter the Earth atmosphere because of gravity. Because of the high speed, the object can orbit the Earth as much as 50 times a day. The well-known International Space Station (ISS) and Hubble space telescope are located in this orbit. The speed of these objects can be reduced by the atmospheric drag, a type of uncertainties, in this region, although the amount is minimal. Thus, a robust attitude and orientation controller is required to fix this error. Furthermore, the nominated controller also helps the spacecraft to maintain its position long enough in any pre-specified region while orbiting at high speed around the Earth.

Next, in MEO, the objects travel twice a day around the Earth. MEO operation, such as GPS navigation, provides and coordinates the human location on the Earth surface. Four GPS navigation satellites are needed to produce an accurate position on Earth.

Finally, HEO, also known as the High Altitude Geostationary region, is suitable, such as weather forecast, communication, and broadcasting satellite operations. In this orbit, objects maintain their position relative to a point on the Earth at all time. Thus, for instance, a television antenna can always point in the same direction since the satellite location does not change relative to the television antenna.

In conclusion, the position of a satellite or a spacecraft (both of them named as spacecraft) is essential to make sure the missions are successful, although there exist uncertainties and disturbances produce by either internal of the spacecraft or space phenomena. Hence, a robust attitude and orientation control must complete the spacecraft missions and bring benefits to human needs.

2.2.2   Spacecraft Challenge in Space

Multiple factors contribute to spacecraft performance degradation across time. One of the reasons is the external disturbances and uncertainties impacting the spacecraft when orbiting the Earth. For example, ISS requires re-boosting several times each year. In addition, the ISS attitude is decreasing about a kilometre every 12 days because of the atmospheric drag in LEO. This phenomenon occurs because the upper atmosphere heated by the solar storms that are increasing the ISS drag and accelerates the orbit decay [28]. Thus, spacecraft experience low aerodynamic torque indeed.

A most potent solar storm happens when particles that are thrown out send coronal mass ejection (CME) and consider the most violent and energetic that can disturb the interplanetary magnetic field and planetary magnetospheres [29]. Previously, the significant gravitational impact on spacecraft only considers on Earth gravitational (see section 2.2 for details [30]). However, if the position is not appropriately chosen, the sun and the moon gravity can influence the spacecraft performance [17]. Therefore, insensitive control strategies need to encounter these problems to ensure the spacecraft position, attitude, and orientation are guaranteed. Table 2.3 summarised the typical type of disturbances and uncertainties and the effect towards spacecraft in space [17].

Table 2.2: Gravitational Acceleration due to the Earth and the Sun.

Location	Earth	Sun
Earth's Surface	$9.81 \ ms^{-2}$	$6 \times 10^{-6} \ ms^{-2}$
LEO	$9 \ ms^{-2}$	$6 \times 10^{-6} \ ms^{-2}$
200000 km from the Earth	$10 \times 10^{-6} \ ms^{-2}$	$6 \times 10^{-6} \ ms^{-2}$
6 million km from the Earth	$10 \times 10^{-6} \ ms^{-2}$	$6 \times 10^{-6} \ ms^{-2}$

Table 2.3: Typical Disturbances and Uncertainties in Space.

Disturbance/Uncertainties	Affect to the spacecraft
Solar radiation	Ultraviolet (UV) light from the sun will darken the solar panel and ultimately reduce the efficiency and thus power output produced by the solar panel. Hence, the spacecraft must be energy efficient to counter this degradation.
Solar storm	The solar wind consists of energetic particles, protons and electrons. The particles put pressure on spacecraft (this phenomena also creates aurora). The most powerful solar storm is sending CME that has a significant impact on the earth magnetic field. The CME's speed can varies between less than $100kms^{-1}$ to greater than $1200kms^{-1}$ [31]. This phenomenon causes the spacecraft to lose its attitude control [32].
Atmosphere drag in LEO	The spacecraft attitude will change due to the atmospheric drag slowing the speed. Thus in LEO, the spacecraft consumes high power to counter the gravitational Earth field to maintain altitude and speed by using their thrusters.
Sun and moon gravitational force	The gravitational forces of the sun and the moon cause periodic variations in all of the orbital elements, but only the right ascension of the ascending node, argument of perigee and mean anomaly experience secular variations.

In real case scenarios, the value of these disturbances and uncertainties can be seen as in Table 2.4 [4] where shows the comparison between two different satellite sizes. FireSat II can be categorized as a very small satellite

and orbiting the earth. On the other hands, Supplemental Communications System (SCS) is a small Earth-pointing spacecraft.

Table 2.4: Disturbances and Uncertainties Value of FireSat II and SCS [4].

Disturbance/Uncertainties	FireSat II	SCS
Solar radiation	$9.6 \mathrm{x} 10^{-7} Nm$	$6.6 x 10^{-6} Nm$
Solar storm	$2.1 \mathrm{x} 10^{-5} Nm$	$4.6 \mathrm{x} 10^{-7} Nm$
Atmosphere drag in LEO	$3.7 \mathrm{x} 10^{-7} Nm$	$8.7 \mathrm{x} 10^{-12} Nm$
Sun and moon gravitational force	$1.5 \mathrm{x} 10^{-6} Nm$	$3.0 \mathrm{x} 10^{-7} Nm$

2.3 Spacecraft's Subsystem

The internal spacecraft system generates the next element that contributes to the spacecraft out-performance. Generally, the spacecraft is built by six subsystems as follow [33–35]:

1. A structural subsystem.

2. A telemetry subsystem.

3. A power subsystem.

4. A thermal control subsystem.

5. A communication payload subsystem.

6. An attitude and orbit control subsystem.

Thus, this thesis focus on the sixth subsystem, which is the attitude and orbit control subsystem (ACS). In ACS, there are two control parameters involved: the attitude and orbit of the other satellite subsystems and the payload. Attitude control consists two main aspects [36]:

1. Firstly, the orientation of a spacecraft referred to reference objects, for instance, earth, sun, moon and stars.

2. Finally, the dynamic of a spacecraft is required since they must change the orientation time-to-time according to the needs. This task can be done by controlling the rotation and rotation rate in ACS.

Then, ACS functions about maintaining or obtaining the spacecraft at a target orbit. Besides that, ACS also used to avoid collisions with other objects. The connection between these parameters can be represented in Figure 2.1.

The actuator receives the control commands from the onboard control unit. The control command decisions are based on the nominal values and deviations from the sensors. The sensors inputs are the angles, spin rates, or position measurements which translate in data form. The actuator will apply the necessary torques or forces to re-orient the spacecraft to the desired attitude according to the deviation between desired orientation and current position, as detected by sensors until the variation is equal to zero [37]. This

13
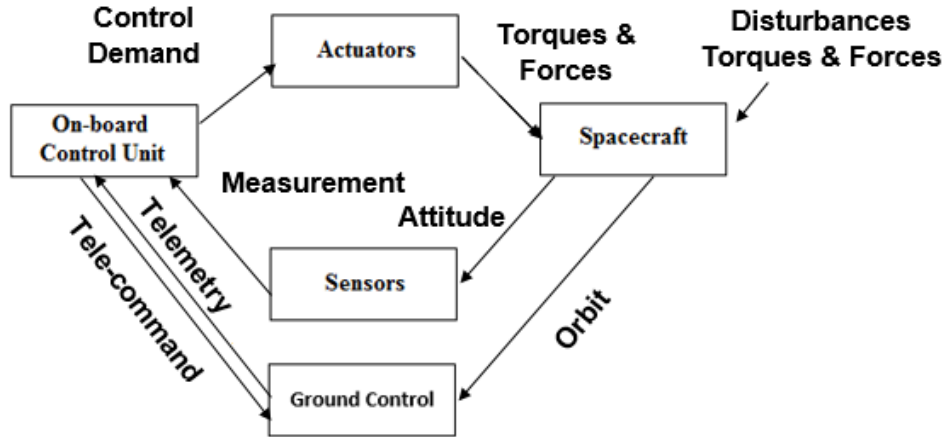
Figure 2.1: ACS Components and Control Cycles [1].

process is simplified in Figure 2.2. The standard type of actuators used in ACS is reaction wheels and magnetic torquers. The spacecraft models derived in linear and non-linear systems where the controller's design based on these actuators. A common challenge for researchers is the practical consideration and rejection of the disturbances and uncertainties which exist in space and on the spacecraft and how as shown in Table 2.3 and 2.5. On the other hands, the orbit control performs the orbit correction manoeuvres task.
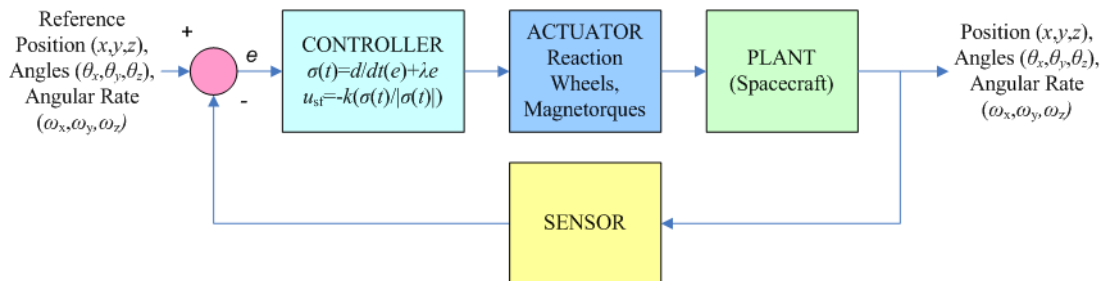
Figure 2.2: Attitude Control Block Diagram Process.

2.3.1 Reaction Wheels

Reaction wheels (RW), also known and operated as a momentum wheel, consist of a rotating mass attached to an electric motor; devices on a spacecraft are aligned on X (roll), Y (pitch) and Z (yaw) axis (Figure 2.3). Sometimes, the RW has the fourth device which is used for redundancy purpose. The pointing accuracy of RW can achieve up to 0.001^0 precision [38]. Unfortunately, RW suffers from degradation, for example, loss of effectiveness (LOE), stuck fault (lock-in unknown time (LIUT) and failure for a period of time (FFPT) [39]. One of the malfunctions to an RW happened to the Mars Odyssey spacecraft in 2012. The Mars Odyssey detected one of its three RW, which are used to control orbiter orientation in space produces unusual readings. Then, the spacecraft has to enter the safe mode before the recovery actions are taken. The orbiter carries a spare RW on-board, in case one of the three in use fails. Besides that, RW is heavy and thus require substantial space inside the spacecraft. Moreover, they have low power efficiency, require high energy to operate and also are unsuitable for small satellites. Furthermore, flywheels or batteries are required to supply the power to RW during an eclipse. Nevertheless, researchers have developed spacecraft using RW as the main actuator in MEO and HEO since, in these orbits, the interaction between a spacecraft and the Earth magnetic field is low.
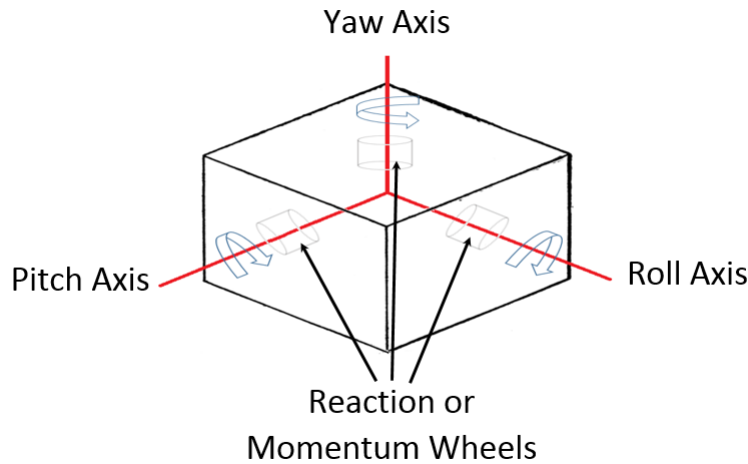
Figure 2.3: Reaction Wheels Direction.

2.3.2 Magnetic Torquer

Magnetic torquers (MT), also known as magnetorquers, utilise an electrical current run around a piece of metal (torque rods with an iron core or air coils [40]), that creates an electromagnet. Within space in LEO, this electromagnet will be subject to a force causing it to align itself along the Earth's magnetic field and thus generate a torque on the spacecraft. These magnetic controls are relatively light but low accuracy (1^0) [41]. They can also can be used to compensate for the natural magnetic effects of satellite components [38]. A MT is available as long as sufficient electric power is available. With the advantages of smaller size, less weight and energy, and negligible degradation due to no moving parts, MT are widely used for small satellites in LEO. Nevertheless, MT requires more complex control design since various uncertainties exist such as non-clean magnetic fields inside the spacecraft that interfere with the magnetic interaction between the spacecraft and the Earth [42]. The use of MT also introduces challenges, for example the system is only controllable in two axes at any time. The axes being perpendicular to the local geomagnetic field vector [43].

2.3.3 Summary of between Reaction Wheels and Magnetic Torquer Actuator

Based on the description of both actuators, it can be said these actuators have advantages and disadvantages. The selection of actuator type when designing the spacecraft is dependent on their missions, for example considering the reliability, accuracy and location in space. A summary of spacecraft actuator characteristics is shown in Table 2.5.

Furthermore, the typical performance range of these attitude actuators can be summarised in Table 2.6 [4].

2.3.4 Actuators Challenges in Space

There are several issues which from challenges for an attitude controller. Some actuators made from mechanical moving parts and one primary component is motor. A motor will degrade in time thus affecting spacecraft attitude performance. Fault-tolerant strategies to cope with scenarios such as LOE, LIUT and FFPT may come at the price of a significant disruption to a spacecraft's performance [44]. Besides that, internal noise from sources

Table 2.5: Characteristics Summary of Reaction Wheels and Magnetic Torquer Actuators.

Actuator	Reaction Wheels (RW)	Magnetics Torquers (MT)
Characteristics	RW has a high pointing accuracy of 0.001^0. The RW, however requires high energy consumption, large size and needs a separate power source (flywheel or battery) during an eclipse event.	The MT is small, low weight and consumes low power but low accuracy (1^0). It also free of degradation due to having no moving parts. The control design for MT, however is complex.
Orbit	The RW have been implemented on spacecraft in LEO, MEO and HEO but is unsuitable for small spacecraft due to the size requirement.	The MT is only suitable for spacecraft in LEO since near to the Earth, there is a large enough magnetic field compared to MEO and HEO to determine the spacecraft orientation and position.
Challenges	The RW degrades over time (LOE, LIUT, FFPT) since it uses moving parts.	The MT produces non-clean magnetic fields generated by current flowing inside the actuator that can cause interference.

within a satellite will have an impact similar to a disturbance torque form. For magnetic actuators, the magnetic fields generated by the coil will be affected by the material within the MT since non-clean magnetics exists where the currents are flowing, for instance in the harness, solar panels, permanent magnets and solenoid valves can lead to unwanted disturbances to the spacecraft's attitude [3]. This problem will be a massive challenge for spacecraft to maintain their attitude and orientation.

Table 2.6: Typical Performance of RW and MT.

Actuator	Performance	Mass (kg)	Power (W)
RW	Maximum torques: $0.01Nm$ to $1Nm$ Practical momentum storage capacity: $0.4Nms$ to $3000Nms$	2 to 20	10 to 100
MT	$1Am^2$ to $4000Am^2$	0.4 to 50	0.6 to 16

2.4 Sliding Mode Control

VSCS earliest work was introduced by Emel'yanov and Barbashin from Soviet Union in the late 1950s [45–48]. However, Itkis and Utkin introduced VSCS to the world by publishing a book [46] and a paper [47] in the mid-1970s. VSCS contains a set of continuous subsystems with suitable switching function where the 'control law' of the subsystem is intentionally changed by some external factors with rules applied [47, 49]. VSCS is designed to make sure the states drive and lie around a switching surface by utilizing a high-speed switching control law, wherein this region; a controlled system is robust-guaranteed [22, 49]. VSCS holds two main advantages. Firstly, the switching function selection determines the dynamic of the compensated system. Then, the closed-loop controlled system becomes insensitive or robust towards to disturbances and uncertainties [22]. Nowadays, VSCS with sliding mode, known as sliding mode control (SMC), widely introduced into many critical application models, for instance, faults tolerant control on piloted simulator evaluation [50], a nonlinear longitudinal model of Boeing 747-100/200 [51], and damaged aircraft [52].

SMC is well-known as one of the robust controllers; capable of handling high-order nonlinear dynamic systems with high complexity. Some of the SMC's major contribution features are low sensitivity towards plant parameter variations and disturbances, low cost, low computational burden, processors with energy efficiency and low complexity [53–55]. SMC design consists of two crucial components; switching function design and control law design. The switching function is designed based on the output requirements while the control law selection will make the switching function converge to the

plant state [22, 49].

In SMC, however, the major challenge is the chattering effect produces by high-switching frequency which were negelected in system outputs [56–58]. The chattering can cause, for example, law control accuracy, wear and tear to the mechanical parts, which contributes to the hardware's maintenance or replacement, and high heat losses in power circuits [19, 58]. Thus, many researchers introduced modification approaches in SMC to improve the classical SMC deficiency such as boundary layer technique [19, 59–61], SMC hybrid with other control methods [62–65], and higher-order sliding mode control [5, 66, 67].

The proposed approaches can eliminate the chattering while maintaining the accuracy of the outputs, but they also have pros and cons to the compensated systems. Then, some SMC essential criteria are set to make sure the SMC algorithms are suitable to be implemented on small spacecraft applications. The SMC characteristics on the chosen small spacecraft operations must be simple mathematical operators, required low computational load, robust, high outputs accuracy, energy efficiency and low cost.

2.4.1   A Review of Sliding Mode Control Approaches

Many criteria must be taken into account when designing an attitude control system: computational time, control power consumption, the robustness of the intended control towards internal and external disturbances and uncertainties, accuracy of the output, improvements from previously compensated attitude control system and capability of the spacecraft to process the designed controller. By considering all these criteria, it is possible to ensure the spacecraft can accomplish its mission for long periods and also to ensure the appropriateness of the designed attitude control systems for specific spacecraft characteristics.

Sliding mode control (SMC), Fuzzy SMC, Unscented Kalman Filter (UKF) (an improvement of Kalman Filter and Extended Kalman Filter (EKF)) and adaptive control are examples of spacecraft attitude controllers. The performances and capability of these controllers are reviewed here to compare and contrast their efficiency. These controllers tested with linear and non-linear spacecraft models with various types of disturbances and uncertainties.

2.4.1.1 Modification in Sliding Mode Control

Sliding mode control (SMC) is well-known as one of the robust control strategy which is relatively insensitive towards disturbances and uncertainties. SMC officially introduced in a survey paper year 1977 [47]. Since then, SMC triggers the researcher interest to apply the control algorithm in both fundamentals and system applications. Interestingly, SMC is easy to implement and has low computational costs. Due to these advantages, SMC is convenient for small spacecraft in LEO, but it suffers from a chattering phenomenon which is a drawback. The chattering causes wear and tear on the actuator in spacecraft application. In response, researchers proposed Fuzzy SMC (FSMC), Minimum Sliding Mode Error Feedback (MSMEFC), Adaptive Non-Singular Terminal SMC (ANSTSMC), Adaptive Fuzzy SMC (AFSMC) and Integral SMC (ISMC) as alternatives to suppress this problem and improved overall performance, including transient response, effectiveness and accuracy. The modified approaches have been implemented on RW [39, 44, 65] and MT [55]. Modified SMC has been shown to give good precision, effectiveness and convergence to the required position infinite time, in the presence of various disturbances and uncertainties.

AFSMC [65] and ANSTSMC [39] can produce robust and high-efficiency attitude and orientation spacecraft output. Both methods, however, need high computational burden to eliminate the chattering in SMC. Thus, AFSMC and ANTSMC are unsuitable for implementing on small spacecraft. Originally, AFSMC was introduced because of fixed fuzzy rules contribute to a non-robust system. The AFSMC is divided into two components where equivalent control terms are used to deal with the uncertainties while hitting control is used to achieve the attitude precision. The equivalent control term is the approximation of the control law to produce zero steady-state value. Moreover, hitting control functions act as the chattering remover. Due to the high computational load, AFSMC limits the on-line spacecraft application. Finally, based on the result [65], the AFSMC is able produced precise attitude control subject to fewer disturbances and uncertainties. The AFSMC needs some modifications to tackle the spacecraft system with an enormous challenge. Hence, MSMEFC [44] is one of the solutions for ANSTSMC in term of computational load. In MSMEFC, the uncertain disturbances are offset by an equivalent control error to improve the control performance. A cost function contains all the information of sliding mode error, and the equivalent control error is derived to estimate the optimal equivalent control

error where this estimation will feedback to the conventional SMC to produce the MSMEFC result. As a result, the MSMEFC not only computes in energy efficiency but also robust towards faults inside the actuator (LOE, LIUT and FFPT) and perturbations. The MSMEFC have not considered the orbital manoeuvres inside the analysis because sometimes orbital manoeuvres required due to the severe perturbations such as debris avoidance [68]. The AFSMC, MSMEFC and ANSTSMC analysed on RW actuator base model.

On the other hands, most researchers considered MT as the spacecraft's actuator to produce small spacecraft size, weight and less energy consumption. An ISMC [55] used purely magnetic attitude control with realistic non-linear parameters. The control torque vector at the output of the controller acts on the spacecraft after successive manipulations. As the result, the disturbances, however can't be fully eliminated because of the difference between the control torque vector generated by the controller and the applied control torque vector (control torque error).

2.4.1.2 Unscented Kalman Filter

Some researchers introduced an UKF controller [62] as an improvement on a Kalman Filter (KF) and EKF [63] for spacecraft attitude state and parameter estimation. The development has been made since KF is used to estimating a linear system while EKF limited estimating up to first-order terms for non-linear systems by neglecting higher-order terms. Ignoring the higher-order terms can lead to instability. Based on the result, UKF was able to converge, despite poor initial estimates of the parameters, through numeric simulation; using simulated noisy measurements bring better convergence characteristics and greater accuracy than the EKF [62]. Furthermore, UKF is also easier to implement because this control method is derivative-free [69]. EKF computes the output by using a Jacobian; the Jacobian leads to more complexity and computational demand. Compared to UKF, this method approximates the state/measurement estimate and the associated uncertainty by a statistical linear regression through a well-chosen set of a set of samples determined from the apriori mean and covariance of the state known as "sigma points" and thus is less complex [70].

This thesis, however, focused on several SMC algorithms implement on a few spacecraft applications. Hence, the maintenance and replacement are unsuitable and challenging to apply for these and also for general applications. Then, in this chapter, the solutions for the problem with advantages and dis-

advantages are discussed where the objectives are to relate SMC approaches with spacecraft applications.

Next, among the essential rules in SMC such as system's stability, robustness conditions, optimal parameters selection and reachability conditions in SMC will be investigated and elaborated in this chapter. The main objective of this review to explore, select and enhance the suitable SMC control algorithms with core requirements being low cost, robustness, precision, high efficiency and low computational load on several spacecraft operations. However, in this review, the SMC control approaches are specific on general small-spacecraft-task-models where operate in low Earth orbit (LEO). Some of the must-do-missions are spacecraft attitude and orientation (SAOM), and spacecraft rendezvous, and docking manoeuvres (SRDM).

2.4.1.3   Comparison Between Spacecraft Attitude Controllers

Table 2.7 elaborated the comparison between spacecraft attitude controllers based on existing strategies. The comparison are based on the advantages and the disadvantages with the room of improvements to utilise the optimum spacecraft attitude and orientation outputs.

Table 2.7: Comparisons between existing Spacecraft Attitude Control Strategies.

Controller	Advantages	Disadvantages	Improvements
SMC	The SMC is a low complexity, low computational burden, less weight and low cost control method. The SMC also a robust control strategy where the output can converge in finite time with sufficient precision. Hence, the SMC is suitable for various type of the attitude and orientation spacecraft control.	The SMC produces a chattering effect to the system. It caused wear and tear to the actuator.	A modification in SMC switching function is required to suppress the chattering drawback.

Table 2.7 – *Continued from previous page*

Controller	Advantages	Disadvantages	Improvements
AFSMC	Fixed fuzzy rules lead to limited robustness which makes the system become unstable. However, it solved the chattering phenomena caused by the switching function in SMC. Then, adaptive fuzzy rules are introduced not only to counter instability but also produced the precise attitude of the spacecraft.	The AFSMC is a complex fuzzy parameter which leads to a high computational load. As such, the AFSMC is unsuitable to use in small spacecraft. Besides that, it only robust towards to minimum disturbances and uncertainties in space and the spacecraft.	To use in small spacecraft, a modification inside switching function of SMC is proposed instead of combine the SMC with the other controller methods, such as Fuzzy. The modification can minimise the computational burden of the spacecraft.
MSMEFC	The MSMEFC is an enery efficiency and robust control method suitable for realistic disturbances and uncertainties generated by the spacecraft and in space. The MSMEFC contains a cost function which is used to offset the disturbances and uncertainties to improve control performance. Hence, the MSMEFC is suitable for small spacecraft.	The MSMEFC considered fault actuator as uncertainties but sometimes there are serious perturbations happens in space.	One of the ways to reject the serious perturbations effect is intoducing orbital manoeuvres with minimum energy consumption to the spacecraft.

Table 2.7 – *Continued from previous page*

Controller	Advantages	Disadvantages	Improvements
ISMC	The ISMC is implemented on a magnetic actuator. This controller has small size, weight and low energy consumption, thus is suitable for small spacecraft.	The ISMC is influenced by the disturbances and uncertainties because the variance of the control torque and the applied control torque vector which resulting impreciseness output.	More research on fundamental problem specific to the purely magnetic attitude control problem is required to overcome the disadvantages.
UKF	The UKF is able to converge and estimate higher-order non-linear parameter which bring better converge characteristics and greater accuracy than the EKF although with poor initial estimates. Furthermore, the UKF is easy to implement since it uses no derivatives This control method has low computational requirements and low complexity.	The UKF has not been tested with real case perturbations in space and the spacecraft.	The UKF can be tested with the real case of disturbances and uncertainties such as fault-tolerant in actuator.

2.4.2 Conclusion

Table 2.7 summarises the strengthens and weaknesses of common approaches to spacecraft attitude control and hence gives insight to where improvements would be beneficial. SMC is robust but it has chattering as the drawback. One proposed alternative of Adaptive Fuzzy requires an additional cost function inside the SMC thus increasing complexity and computational load more than is allowable. Integral SMC cannot adequately eliminate disturbances and uncertainties which bring to the impreciseness output of the spacecraft attitude. According to the MSMEFC advantages, this method is suitable to be implemented for both small and huge spacecraft due to the energy efficiency and high robustness. This can be achieved because the MSMEFC do modification inside the SMC algorithm by adding cost function without compound with another type of controllers. As such, in order to minimise the size, low the complexity and optimize the small spacecraft performance with greater accuracy, modification in SMC algorithm is one of the ways to achieve the objectives while implement on magnetics actuator.

Overall, some of the control strategies discussed in this chapter manage to control the linear and non-linear attitude and orientation of spacecraft systems. The controllers must be robust against the disturbances and uncertainties which exist in space and the spacecraft. Besides that, the spacecraft attitude and orientation outputs must be precise, effective and can converge to the desired position infinite time while being efficient with the spacecraft's power consumption. A low computational process load, small size, and ease of implementation must also be considered when designing a controller, especially for the small spacecraft. Based on Table 2.7, the MSMEFC and UKF demonstrate these criteria better than the alternative controllers. Nevertheless, although the results shown by both methods give precise attitude output, these methods also can consider serious perturbations and how to maintain the desired attitude and orientation in space. Hence, one of the possible methods to resist serious perturbations by using orbital manoeuvre. The orbital manoeuvre required a control method to achieve a precise new desired attitude using minimum energy consumption. One of the solutions is using the state-dependent boundary layer method of SMC.
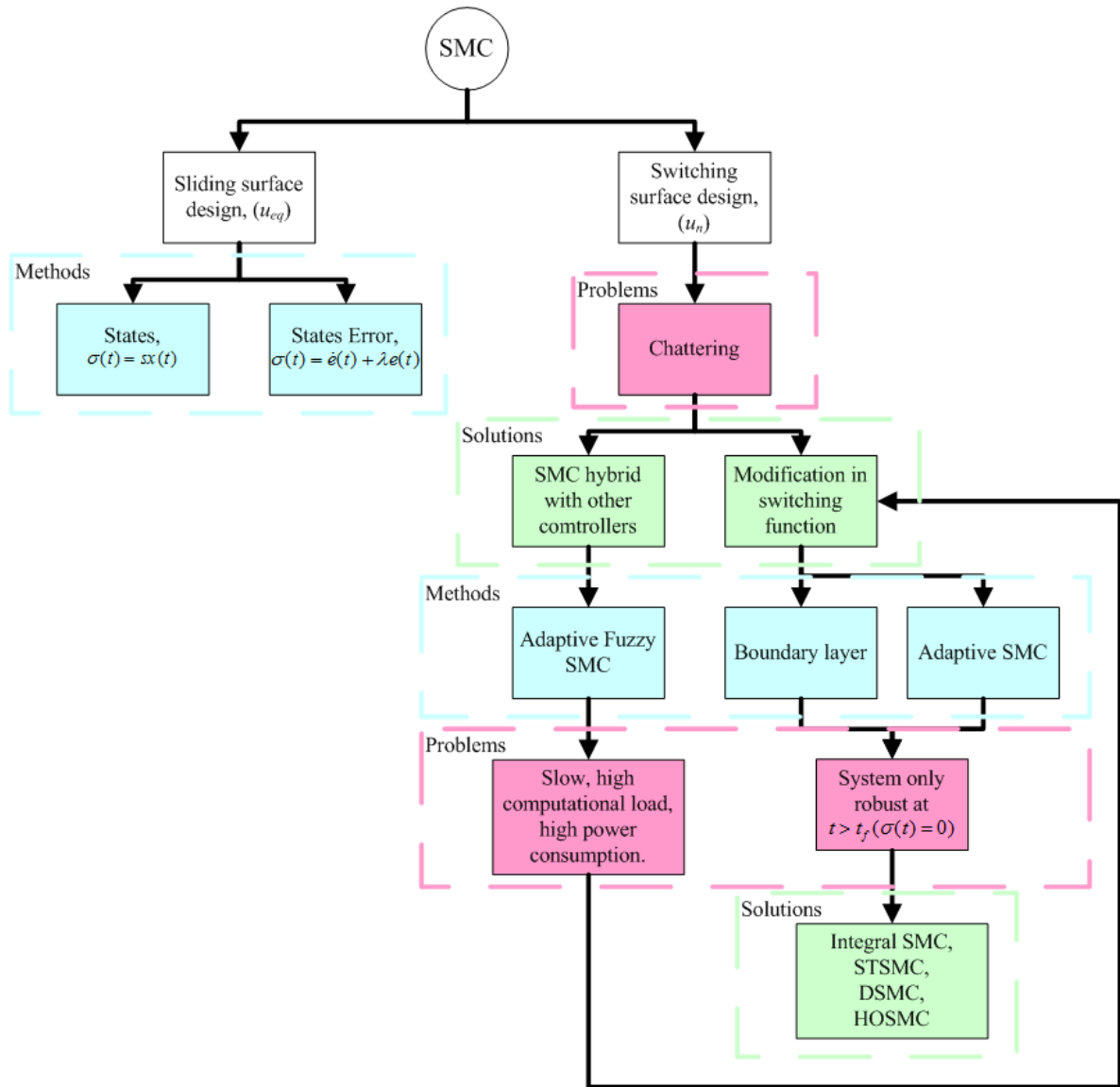
Figure 2.4: Flow Chart of the SMC Characteristics and Solutions.

The SMC control methodology summary is shown in Figure 2.4, where the controller development can be divided into two parts: sliding surface design and switching surface design. The designer can develop the sliding surface $\sigma(t)$ in SMC either using states $(\sigma(t) = sx(t))$ or state errors

$(\sigma(t) = \dot{e}(t) + \lambda e(t))$ where $\sigma(t)$ is sliding surface, s and λ are refer to sliding surface coefficients, $x(t)$ denotes to state variables (for example, roll, pitch and yaw orientation) and $e(t)$ attributes to state variables error value. The sliding surface is the characteristic equation to determine the controlled system transient performance, depending to s and λ values.

On the other hand, the switching surface design used to force the system's state variables, containing along the sliding surface with existing bounded disturbances until the system achieve the equilibrium condition. The drawbacks of this advantage are chattering phenomena in controller input. Hence, some of the existing algorithms attenuate this problem by modifying the switching surface or hybridising the SMC with other controllers. From the literature, examples of modification in SMC by introducing boundary layer technique and an adaptive SMC. Furthermore, for the hybrid SMC method, the researcher introduced the AFSMC method. However, the hybrid SMC method requires high computational load, high power consumption and slow computational output, which is unsuitable for small spacecraft operations. Thus, modification in the switching function is proposed in this research.

Modification in SMC also have drawbacks where the system only robust when the state variables start hitting the sliding surface. The literature suggests using ISMC, dynamic sliding mode contrl (DSMC), and HOSMC to avoid this condition for improvement. Thus, in this research, the SMC controller development focus is implementing modification in switching surface design where the sliding surface structure is developed using states and states error.

Chapter 3

Existing Sliding Mode Control Formulation

3.1 Introduction

SMC is one of the VSCS approaches. VSCS is a viable high-speed switching feedback control [22, 49]. This control law provides a practical and robust means of controlling non-linear systems. Hence, this chapter elaborated the classical SMC formulation design, which is in the low order form. SMC, however, range to higher-order methodologies such as super-twisting sliding mode control (STSMC) and DSMC. Later, the formulation of higher-order SMC concepts are reviewed with STSMC and DSMC methods considered in the spacecraft's control design including the classical SMC approaches. Beforehand, the outputs of these algorithms are reproduced to make sure the simulation techniques are validate justify where STSMC referred to the paper [2] while DSMC attributed to the paper [5].

3.1.1 Sliding Mode Control

The main purpose of the SMC algorithm is to compute the double integrator of the state variables or errors is equal to the inputs [22]. However, in this section, state variables $(\ddot{x}(t))$ as in Eq. 3.1 is used to define the SMC control input development. In the end, the relationship between state variables $(x(t))$ and its dynamic $(\dot{x}(t))$ is obtained to show that the controlled system able to achieve equilibrium condition where in this research, the state vari-

ables represent by spacecraft orientation parameters (roll, pitch and yaw) in angular form and spacecraft relative positions (x, y and z axis).

$$\ddot{x}(t) = u(t). \tag{3.1}$$

Consider the uses of feedback control law applied on the scalar inputs ($u(t)$) in Eq. 3.2.

$$u(t) = -kx(t), \tag{3.2}$$

where k is a control input feedback gain that can influences the system's characteristic and strictly positive scalar to ensure stability. Then, substituted Eq. 3.1 into Eq. 3.2 and becomes

$$\ddot{x}(t) = -kx(t), \tag{3.3}$$

Next, multiplying Eq. 3.3 with $\dot{x}$ and produces Eq. 3.4. The integration of Eq. 3.4 as in Eq. 3.5.

$$\dot{x}\ddot{x} = -kx\dot{x}, \tag{3.4}$$

$$\begin{aligned} \int \dot{x}\ddot{x} &= -\int kx\dot{x}. \\ \dot{x}^2 + kx^2 &= r, \end{aligned} \tag{3.5}$$

Eq. 3.5 generates a circle graph with $\sqrt{r}$ as radius with origin as the center when $k = 1$. In other words, r is a constant value, generates from the integration, also known as initial conditions and strictly positive to produce a circular direction around the equilibrium point for state variables trajectory direction. However, from Eq. 3.5, with the different k values selection, the state variables trajectories around the equilibrium points can be ellipse direction and illustrated in Figure 3.1 where $0 < k_1 < 1$ and $1 < k_2$. The range of k_1 and k_2 values determine the controlled system transient performance. Hence, to optimum the system trajectories, consider a control law below which is combination of k_1 and k_2 condition in Figure 3.1.

$$u(t) = \begin{cases} -k_1 x(t), & \text{if } x\dot{x} < 0. \\ -k_2 x(t), & \text{otherwise.} \end{cases} \tag{3.6}$$
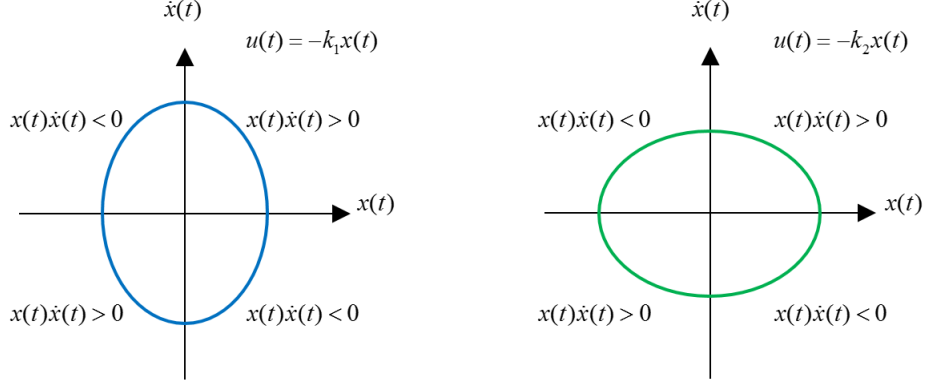
Figure 3.1: The ellipse graph of $\dot{x}(t)$ against $x(t)$ based on Eq. 3.5 with $0 < k_1 < 1$ and $1 < k_2$.

Based on the control law, the phase portrait between $\dot{x}(t)$ against $x(t)$ is illustrated in Figure 3.2, produces a spiral converging to the origin and an asymptotically stable motion results. On the other hands, it also can mathematically be proven by considering the Lyapunov function $(V(x, \dot{x}))$ in Eq. 3.7 and its dynamic in Eq. 3.8.

$$V(x, \dot{x}) = \dot{x}^2 + x^2, \tag{3.7}$$

$$
\begin{aligned}
\dot{V}(x, \dot{x}) &= 2\dot{x}x + 2\ddot{x}\dot{x}, \\
&= 2\dot{x}(x + u) = \begin{cases} 2x\dot{x}(1 - k_1), & \text{if } x\dot{x} < 0, \\ 2x\dot{x}(1 - k_2), & \text{if } x\dot{x} > 0. \end{cases}
\end{aligned}
\tag{3.8}
$$

The energy is always negative towards time refer to how the gains are constructed. The distance of the states trajectory is always decreasing from the origin which is similar as illustrated in Figure 3.2. However, the system using control law in Eq. 3.6 (state planes of linear structures control law [71]) needs more time to achieve equilibrium points. Then, a more significant variable structure law is introduced in Eq. 3.9 [22, 49] to improve the system's performance which is comparable to a sign function as in Eq. 3.10. Eq. 3.9 used to robustly control the perturbed higher order systems [72].
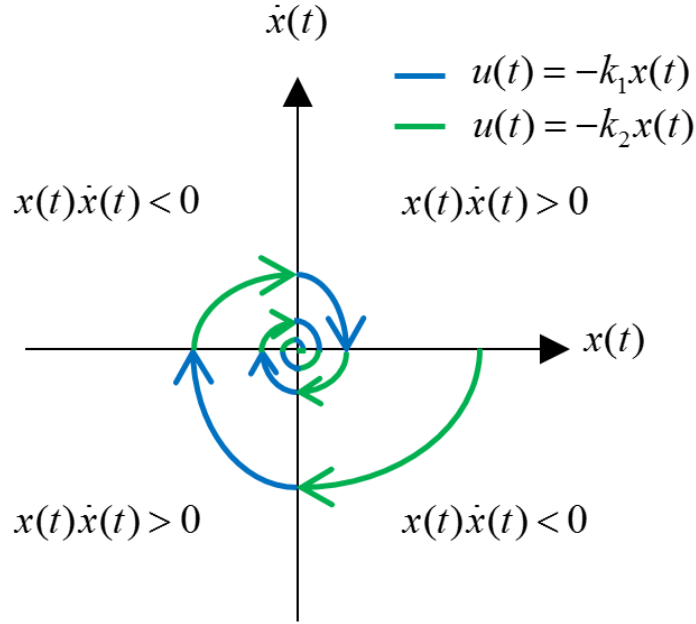
Figure 3.2: Phase portrait of the system in VSCS.

$$
u(t) =
\begin{cases}
-1, & \text{if } s(x, \dot{x}) > 0. \\
1, & \text{if } s(x, \dot{x}) < 0.
\end{cases}
\tag{3.9}
$$

$$
u(t) = -sgn(\sigma(x, \dot{x})) = -\frac{|\sigma(x, \dot{x})|}{\sigma(x, \dot{x})}.
\tag{3.10}
$$

where the $\sigma(x, \dot{x})$ is the switching surface as in Eq. 3.11 and $sgn(.)$ is the sign function.

$$
\sigma(x, \dot{x}) = mx + \dot{x}.
\tag{3.11}
$$

where m is a positive gain used to determine the control structure is in use at any point in the phase plane.

To guarantee the trajectory of the states for a system converges to the origin, obtains the dynamics of the Eq. 3.11 and becomes

$$\begin{aligned}
\sigma\dot{\sigma} &= \sigma(m\dot{x} + \ddot{x}) &&< 0, \\
&= \sigma(m\dot{x} - sgn(\sigma)) &&< 0, &&(3.12) \\
&= |\sigma|(m|\dot{x}| - 1) &&< 0.
\end{aligned}$$

or similarly can be written as

$$\lim_{\sigma \to 0^+} \dot{\sigma} < 0 \quad \text{and} \quad \lim_{\sigma \to 0^-} \dot{\sigma} > 0. \tag{3.13}$$

As the result of $m|\dot{x}| < 1$ property, the system trajectories on either side of the sliding surface line point towards the sliding surface line [22]. Figure 3.3 illustrates the effect of this property and also the effect when $\sigma(x, \dot{x}) = 0$. Eq. 3.12 also used to determine the reachability condition.
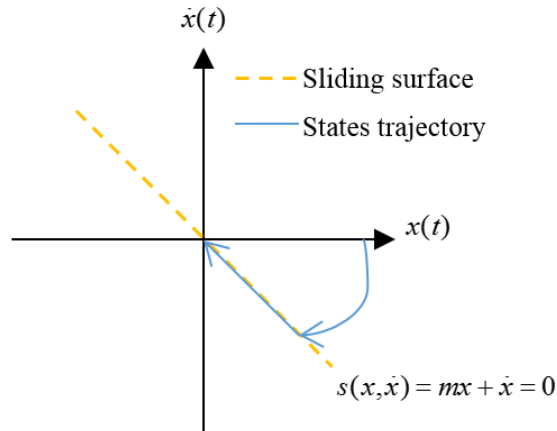
Figure 3.3: Phase portrait when $m|\dot{x}| < 1$ and $\sigma(x, \dot{x}) = 0$.

3.1.2 Sliding Control Laws

In this section, the basis development of the conventional SMC control input law is elaborated and discussed. Beforehand, consider a linear time invariant (LTI) system below.

$$\dot{x}(t) = Ax(t) + Bu(t) + f(t, x, u). \tag{3.14}$$

where $A \in \Re^{nxn}$ represents the system matrix, $B \in \Re^{nxm}$ with $1 \leq m < n$ refers to the input matrix. Matrix B can be assumed has full rank. $x(t)$ is state variables, $u(t) \in \Re^{mxm}$ is input of the system and $f(t, x, u)$ is unknown parameter uncertainty or non-linearities in the system but bounded by some known functions of the state.

A control law used to force the states return to the origin from any initial conditions although there are uncertainties acted on the system [22]. Thus, in SMC, the sliding control laws expression is presented in Eq. 3.15 where in the end, Eq. 3.1 is obtained. The control input laws $(u_{smc}(t))$ consist of two main parts; equivalent control $(u_{eq}(t))$ and switching function $(u_n(t))$. $u_{eq}(t)$ is a linear static output feedback component while $u_n(t)$ is the non-linear and discontinuous about the sliding surface [73].

$$u_{smc}(t) = u_{eq}(t) + u_n(t). \tag{3.15}$$

The equivalent control was proposed by Utkin [47] where used to maintain an ideal sliding motion on switching surface [22]. The switching surface can be designed using two approaches:

1. State-variables Switching Surface (SVSS)

2. State-errors Switching Surface (SESS)

3.1.2.1 The $u_{eq}(t)$ Design using State-variables Switching Surface

The SVSS as in Eq. 3.16, then, the dynamics as in Eq. 3.17.

$$\sigma(t) = Sx(t), \tag{3.16}$$

where $S \in \Re^{mxn}$ is a set of the switching surface coefficients.

$$\frac{d}{dt}(\sigma(t)) = S\frac{d}{dt}x(t), \qquad (3.17)$$
$$\dot{\sigma}(t) = S\dot{x}(t),$$

Replaced Eq. 3.14 to Eq. 3.17 produces Eq. 3.18.

$$S\dot{x}(t) = S(Ax(t) + Bu(t) + f(t, x, u)) = 0. \qquad (3.18)$$

The equivalent control is derived by considering the system states hitting the sliding surface (Eq. 3.19) with its dynamic in Eq. 3.20 and ideal sliding motion takes place [74].

$$\sigma = Sx(t) = 0, \qquad (3.19)$$

$$\dot{\sigma} = S\dot{x}(t) = 0, \qquad (3.20)$$

Replaced Eq. 3.14 with $f(t, x, u) = BD\zeta(t, x)$ that is assumed to satisfying the matching condition into Eq. 3.19 and produces Eq. 3.21.

$$S\dot{x} = SAx(t) + SBu(t) + SBD\zeta(t, x) = 0, \quad \text{for all} \quad t \geq t_{ss}. \qquad (3.21)$$

where t_{ss} is the system states starting time hitting the sliding surface. Thus, the u_{eq} of the sliding control laws as in Eq. 3.22.

$$u_{eq}(t) = -(SB)^{-1}(SAx(t) + SBD\zeta(t, x)). \qquad (3.22)$$

Then, substituting Eq. 3.22 into Eq. 3.14 gives Eq. 3.23.

$$
\begin{aligned}
\dot{x}(t) &= Ax(t) + B(-(SB)^{-1}(SAx(t) + SBD\zeta(t, x)))) + f(t, x, u), \\
&= Ax(t) - B(SB)^{-1}SAx(t) - B(SB)^{-1}SBD\zeta(t, x)) + BD\zeta(t, x), \\
&= (I - B(SB)^{-1}S)Ax(t) + (I - B(SB)^{-1}S)BD\zeta(t, x),
\end{aligned}
$$
$$(3.23)$$

34

with $I \in \Re^{nxn}$ is an identity matric. However, the property of $(I-B(SB)^{-1}S)B = 0$. Hence, Eq. 3.23 becomes

$$\dot{x} = (I - B(SB)^{-1}S)Ax(t). \tag{3.24}$$

Based on Eq. 3.24, the uncertainties contribute by $BD\zeta(t,x)$ are rejected by the equivalent control. Thus, the sliding mode control clearly insensitive or robust to the matched uncertainties [75].

Finally, substitute Eq. 3.22 and 3.10 in Eq. 3.15. Thus, the control laws in SMC as in Eq. 3.25.

$$u_{smc}(t) = -(SB)^{-1}SAx(t) - \rho(t,x)\frac{|\sigma|}{\sigma}. \tag{3.25}$$

where $\rho(t,x)$ is a positive gain that determines the signum function's amplitude where is greater than the size of the bounded uncertainties value in the system to eliminate the perturbations.

3.1.2.2 The $u_{eq}(t)$ Design States-error Switching Surface

Using SESS (Eq. 3.26) to design the $u_{eq}(t)$, hence the error and error dynamics are presented in Eq. 3.27.

$$\begin{aligned} \sigma(t) &= \frac{d}{dt}(e(t)) + \lambda e(t), \\ &= \dot{e}(t) + \lambda e(t), \end{aligned} \tag{3.26}$$

$$\begin{aligned} e(t) &= x(t) - x_d(t), \\ \frac{d}{dt}(e(t)) &= \dot{x}(t). \end{aligned} \tag{3.27}$$

where $x_d(t)$ is desired states and consider $x_d(t)$ is constant and λ contributes to switching surface gradient that influenced the state trajectories performance. Thus, $\dot{x}_d(t) = 0$. Next, replaced Eq. 3.27 into Eq. 3.26 and produces Eq. 3.28 (sliding surface and sliding surface dynamics).

$$
\begin{aligned}
\sigma(t) &= \dot{x}(t) + \lambda x(t) - x_d(t), \\
\frac{d}{dt}(\sigma(t)) &= \ddot{x}(t) + \lambda \dot{x}(t).
\end{aligned}
\tag{3.28}
$$

Sliding surface dynamics is set to zero ($\sigma(t) = 0$) to ensure the robustness can be achieved and with states identity (Eq. 3.29), then Eq. 3.28 becomes Eq. 3.30.

$$
\begin{aligned}
x(t) &= x_n(t), \quad \text{with} \quad n = 1, 2, 3 \\
\dot{x}(t) &= x_{n+1}, \\
\ddot{x}(t) &= \dot{x}_{n+1},
\end{aligned}
\tag{3.29}
$$

$$
\dot{\sigma}(t) = \dot{x}_{n+1} + \lambda x_{n+1} = 0.
\tag{3.30}
$$

where n denotes the system's order. Replaced Eq. 3.14 into Eq. 3.30 and get Eq. 3.31.

$$
Ax(t) + Bu_{eq}(t) + f(t, x, u) + \lambda x_{n+1} = 0,
\tag{3.31}
$$

Hence, the sliding surface ($u_{eq}(t)$) using states error as in Eq. 3.32.

$$
u_{eq}(t) = -(B)^{-1}Ax(t) - (B)^{-1}\lambda x_{n+1}(t) - B^{-1}f(t, x, u).
\tag{3.32}
$$

3.1.3 Reachability Condition in Sliding Mode Control

In SMC, the control input design can be analysed at two phases (Figure 3.4):

1. States trajectory at finite-time reaching phase ($\sigma(x, \dot{x}) \neq 0$ where $0 < t < t_{ss}$).

2. States trajectory around the sliding surface ($\sigma(x, \dot{x}) = 0$ where $t \geq t_{ss}$).

where t_{ss} is the states trajectory finite-time hitting the sliding surface.

The control input, $u_{smc}(t)$ is designed to make sure that the so-called reachability condition is satisfy [22, 47, 75]. The reachability condition is a
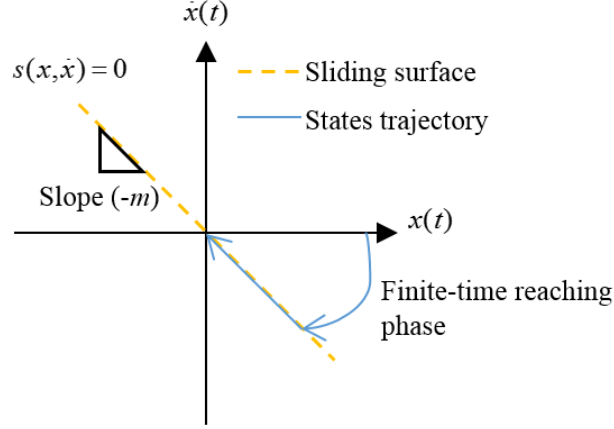
Figure 3.4: The finite-time reaching phase in SMC is the system states trajectory between the initial condition and sliding surface.

sufficient condition to ensure that at each time instant, the system state trajectories will move towards the sliding surface (referred as finite-time reaching phase in Figure 3.4 [76]). This criteria can be achieved if a controlled system satisfy Eq. 3.12 conditions. However, with the appearance of external disturbances and uncertainties, Eq. 3.12 can be represented into Eq. 3.33 and Eq. 3.34 (for multi-input systems).

$$\sigma\dot{\sigma} \leq -\eta|\sigma|, \tag{3.33}$$

$$\sigma^T\dot{\sigma} \leq -\eta\|\sigma\|. \tag{3.34}$$

where η is a positive design scalar ensuring the sliding mode achieved in finite time.

Eq. 3.34 can be demonstrated by substituting Eq. 3.25 into Eq. 3.14. Then replaced the expression into Eq. 3.19 and get Eq. 3.35.

$$
\begin{aligned}
\dot{\sigma} &= S(Ax(t) + B(-(SB)^{-1}SAx(t) - \rho(t,x) + f(t,x,u))), \\
&= SAx(t) - SB(SB)^{-1}SAx(t) - SB\rho(t,x)(SB)^{-1}\frac{\|\sigma\|}{\sigma}.
\end{aligned}
\tag{3.35}
$$

Chapter 4

Higher-order SMC: Simulation Skills Validation

4.1 Introduction

HOSMC is introduced to produce a smooth control that capable maintaining the originality of the SMC, such as, chattering attenuation, insensitive to the disturbances and uncertainties, and fast dynamic response [2,77,78]. HOSMC was introduced in 1996 [79], and since then, the methodology is expended by the researchers. However, the HOSMC requires a complicated algorithm compared to the LOSMC [78], where the LOSMC approaches is discussed in Chapter 4. Thus, in this chapter, there are two types of HOSMC are presented per below:

1. Super-twisting sliding mode control (STSMC).

2. Dynamic sliding mode control (DSMC).

The purpose of this Chapter is to reproduce the existing HOSMC methods to validate the author simulation skills. This is an essential step before further simulation and analysis are made across the study. HOSMC is selected due to the complexity algorithm, hence, suitable to confirm the simulation techniques.

4.2 Dynamic Sliding Mode Control Design

DSMC is one of the HOSMC family. In this section, the DSMC is implemented on a system in Eq. 4.1.

$$\dot{x} = A(x,t) + B(x,t)u. \tag{4.1}$$

where $x \in \Re^n$ denotes the state-variables, $u \in \Re$ refers to the scalar input, $A(x,t)$ and $B(x,t)$ are vector fields represent the system's dynamic and input. The switching function is defined in Eq. 4.2.

$$\sigma = \sigma(x,t), \tag{4.2}$$

Then, consider a sliding dynamics of a system in (4.3) [5]:

$$\ddot{\sigma} = f(t,\sigma) + u. \tag{4.3}$$

with $f(t,\sigma) = 2\sigma^2 - \sigma - 2sin(2t - 0.5)$ and $u = -K_{kd}sgn(J_{kd})$. The term of $-2sin(2t - 0.5)$ is generated by a tracking signal.

For DSMC, there are two non-linear sliding surfaces (χ_{kd} and J_{kd}) are constructed [80] below.

$$\chi_{kd} = a_{kd}|\sigma|^{0.5}sgn(\sigma) - b_{kd}|\chi_{kd} + \sigma|^{0.5}sgn(\chi_{kd} + \sigma),$$
$$J_{kd} = \chi_{kd} + \sigma. \tag{4.4}$$

where $a_{kd} > 0, b_{kd} > 0$ and $a_{kd} \neq b_{kd}$. The J_{kd} and σ are the sliding dynamics implemented on the system (Eq. 4.3). a_{kd} and b_{kd} value are determined using theorem below.

$$|J_{kd}(0)| \leq \left(\frac{b_{kd}}{a_{kd}}\right)^2 |\sigma(0)|. \tag{4.5}$$

In [5], the parameters in Eqs. 4.3, 4.4, and 4.5 are set in Table 4.1. The simulation used to investigate the DSMC performance on a system with a tracking signal.

Table 4.1: Parameter setup in [5].

Parameter	Value
$J_{kd}(0)$	0.1
$\sigma(0)$	1
$\dot{\sigma}(0)$	0.5
a_{kd}	1
b_{kd}	2

4.2.1 Results

Figure 4.1a shows the literature results [5] while Figure 4.1b illustrates the author's simulation results with $a_{kd} \neq b_{kd}$. On the other hand, the comparisan between literature (Figure 4.2a) and author's simulation (Figure 4.2b) is presented in Figure 4.2 with $a_{kd} = b_{kd}$ condition.

There is slightly different for the $a_{kd} \neq b_{kd}$ result. This happens due to the initial condition of the paper [5] is different to the simulation setup as suggested in Table 4.1. The literature [5] set the $\sigma(0) = 1$, but the Figure 4.1a(a) shows the sliding function ($\sigma(0)$) start at 2. Similarly to the $\dot{\sigma}(0)$, the literature is set to 0.5 while the Figure 4.1a(c) illustrates almost 0.

On the other hand, in Figure 4.2, for $a_{kd} = b_{kd}$ condition, the literature and current results produced similar graph pattern for all parameters. In conclusion, the simulation technique for the DSMC is validated. However, for $a_{kd} \neq b_{kd}$, the variant happens due to the intial condition setup.
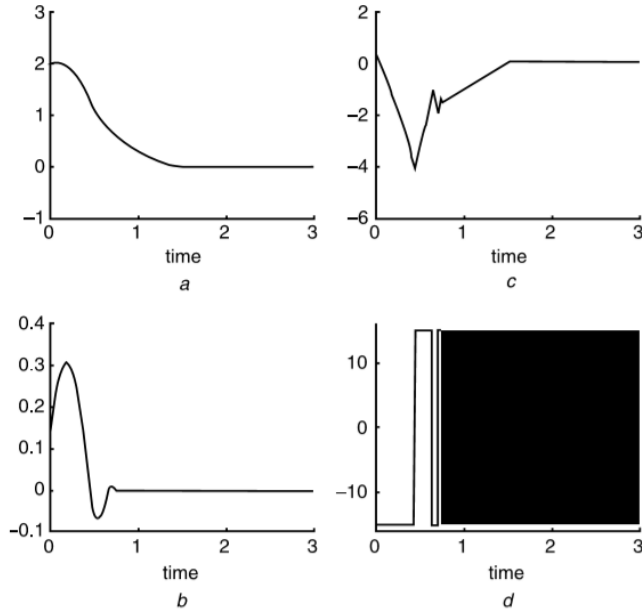
(a) Literature: Sliding dynamics response with discontinuous control with $a_{kd} \neq b_{kd}$ [5]. (a) Sliding function, σ (b) Sliding function, J (c) Sliding dynamic, $\dot{\sigma}$ (d) Discontinuous control, u.
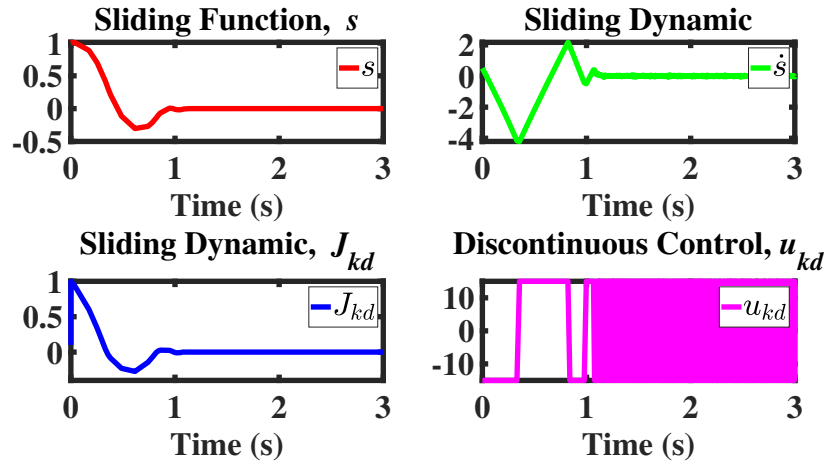
(b) Current: Sliding dynamics response with discontinuous control with $a_{kd} \neq b_{kd}$.

Figure 4.1: Literature and current results using DSMC with $a_{kd} \neq b_{kd}$.
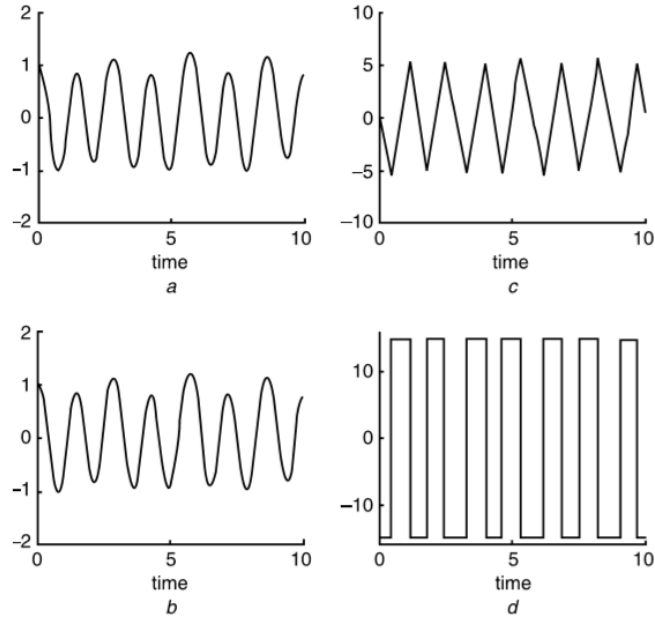
(a) Literature result: Sliding dynamics response with discontinuous control with $a_{kd} = b_{kd}$ [5].
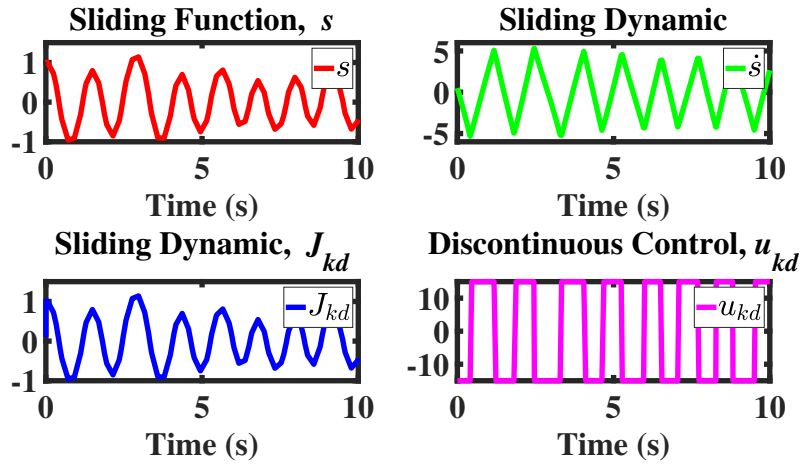
(b) Present result: Sliding dynamics response with discontinuous control with $a_{kd} = b_{kd}$.

Figure 4.2: Literature and current results using DSMC with $a_{kd} = b_{kd}$.

4.3 Sliding Mode Control: A Tutorial

This paper consider a simple second-order scaled pendulum (4.6) implemented on a super-twisting controller.

$$\ddot{y} = -a_{1ss}sin(y) + u_{ss}, \tag{4.6}$$

where y denotes the angular position and $\ddot{y}$ refers to angular acceleration of a scaled pendulum. The $a_{1ss} > 0$ is a scalar while the $a_1 sin(y)$ is a bounded uncertainty. The control or torque applied to the suspension point represents by u_{ss}. For compensated system, however, u_{ss} is represented by (4.7).

$$u_{ss} = u_{eqss} + u_{st}. \tag{4.7}$$

with u_{eqss} is the equivalent control while u_{st} is the discontinuous control part.

On the other hand, consider a sliding variable dynamics (4.8).

$$\dot{\sigma} = \phi(\sigma, t) + \gamma(\sigma, t)u_{st}, \tag{4.8}$$

where the cumulative disturbance term is assumed bounded, $|\phi(\sigma, t)| \leq \Phi$, and the positive constant of an unknown smooth function, $0 \leq \Gamma_m \leq \gamma(\sigma, t) \leq \Gamma_M$ [81]. Thus, the super-twisting controller algorithm design is elaborated in Eq. 4.9 until Eq. 4.11.

$$u_{st} = \dot{u_{1ss}} + u_{2ss}, \tag{4.9}$$

with

$$\dot{u_{1ss}} = \begin{cases} -u_{st}, & \text{if } |u_{st}| > U_{ss}. \\ -W_{ss}sgn(\sigma), & \text{if } |u_{st}| \leq U_{ss}. \end{cases} \tag{4.10}$$

and

$$u_{2ss} = \begin{cases} -\lambda_{u2ss}|s_0|^{0.5}sgn(\sigma), & \text{if } |s| > s_0. \\ -\lambda_{u2ss}|s|^{0.5}sgn(\sigma), & \text{if } |s| \leq s_0. \end{cases} \tag{4.11}$$

with s_0 is boundary layer width around the sliding surface and U_{ss} is the maximum control input. In (4.10) and (4.11), the W_{ss} and λ_{u2ss} are constant and can be computed based on Eq. 4.12.

$$
\begin{aligned}
W_{ss} &= \frac{\Phi}{\Gamma_m}, \\
\lambda_{u2ss} &= \frac{4\Phi\,\Gamma_M(W_{ss} + \Phi)}{\Gamma_m^2\,\Gamma_m(W_{ss} - \Phi)}.
\end{aligned}
\tag{4.12}
$$

Finally, the constructed super-twisting algorithm is implemented on a simple scaled pendulum system to validate the controller performance. The system's output expected to be chattering free sustaining the advantages of the classical SMC [82].

4.3.1 Controller design on a simple scaled pendulum

The sliding surface using states-error for the system (Eq. 4.6) as in Eq. 4.13:

$$
\sigma = \dot{e} + \lambda_{ss}e,
\tag{4.13}
$$

with error of the scaled pendulum, $e = y - y_d$. y_d denotes the desired angular pendulum output. Thus, the sliding dynamics of Eq. 4.13 as in Eq. 4.14 until Eq. 4.16:

$$
\dot{\sigma} = \ddot{e} + \lambda_{ss}\dot{e},
\tag{4.14}
$$

but

$$
\begin{aligned}
\dot{e} &= \dot{y}. \\
\ddot{e} &= \ddot{y}.
\end{aligned}
\tag{4.15}
$$

Replaced Eq. 4.15 and Eq. 4.6 into Eq. 4.14, thus produced Eq. 4.16:

$$
\dot{\sigma} = -a_{1ss}sin(y) + \lambda_{ss}\dot{y} + u,
\tag{4.16}
$$

Then, the equivalent control of Eq. 4.16, when the states hitting the sliding surface ($\dot{\sigma} = \sigma = 0$) as in Eq. 4.17:

$$u_{eqss} = a_{1ss}sin(y) - \lambda_{ss}\dot{y}, \tag{4.17}$$

Substituted Eq. 4.8 into Eq. 4.16 produces Eq. 4.18:

$$u_{eqss} = a_{1ss}sin(y) - \lambda_{ss}\dot{y}, \tag{4.18}$$

Then, replaced Eq. 4.18 and Eq. 4.7 into Eq. 4.16 and becomes

$$\dot{\sigma} = -a_{1ss}sin(y) + u_{st}. \tag{4.19}$$

In [2], the paramater are set as in Table 4.2.

Table 4.2: Paramater in [2].

Paramater	Value
λ_{ss}	1
a_{1ss}	1
U_{ss}	10
s_0	0.01
$[y(0), \dot{y}(0)]$	$[1, 0.1]$

Thus, Eq. 4.19 becomes

$$\dot{\sigma} = -sin(y) + u_{st}. \tag{4.20}$$

Compare Eq. 4.20 with Eq. 4.8 to compute the Φ, Γ_m and Γ_M value as in Table 4.3. Finally, the sliding dynamic parameters for the simulation skills validation represents in Table 4.3.

Table 4.3: The sliding dynamic parameters in [2].

Paramater	Value
$\gamma(\sigma,t)$	1
$\phi(\sigma,t)$	1
Γ_m	0.9
Γ_M	1.1
$\Phi(\sigma,t)$	1.1
W_{ss}	1.3
λ_{u2}	8.92

4.3.2   Results

This section compared the result in [2] with current results. Figure 4.3 (current result) and Figure 4.4 (literature result) show that both results are identitical. Therefore, this can be concluded that the simulation technique is verified.
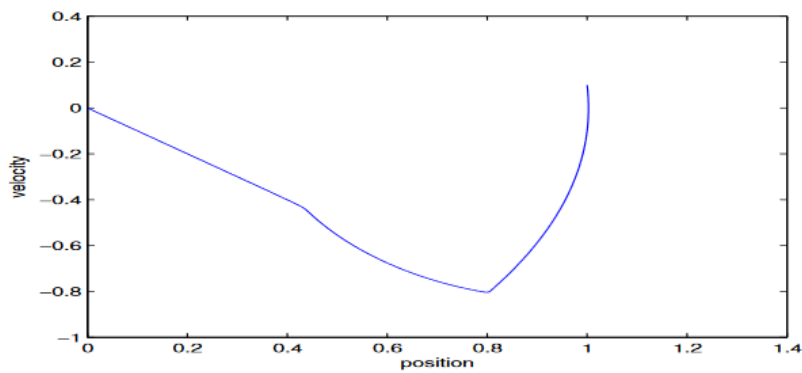
Figure 4.3: Literature result: Phase plane potrait of a simple scaled pendulum using STSMC [2].
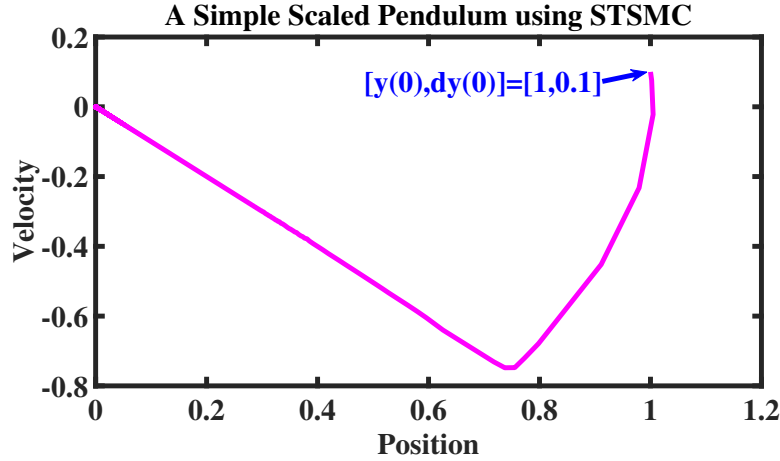
Figure 4.4: Present result: Phase plane potrait of a simple scaled pendulum using STSMC.

4.4 Conclusion

Two existing HOSMC controllers (DSMC and STSMC) have been simulated to validate the simulation skills before further evaluation and analysis were made using SMC on space applications. The DSMC is implemented on a system with a tracking signal, while the STSMC is simulated on a simple scaled pendulum system. The simulation outcomes are compared to the results in [5] for DSMC and [2] for STMC.

In [5], there are two conditions for the results: $a_{kd} = b_{kd}$ and $a_{kd} \neq b_{kd}$. The $a_{kd} = b_{kd}$ shows that the literature and simulation results are comparable for the sliding function (s), sliding dynamic $(\dot{(s)}$ and $J_{kd})$ and discontinuous control (u_{kd}) parameters. However, the comparison shows that there is a slightly variant for $a_{kd} \neq b_{kd}$ condition. Initially, Table 4.1 shows the intial setup ontained from [5]. For instance, s initial value is 1 but from the result (Figure 4.1a) illustrates that the $\sigma(0) = 2$. Hence, this is the main reasons for the difference.

For STSMC, the phase plane portrait result in [2] (Figure 4.3) is mostly comparable to the simulation (Figure 4.4). There is a slight difference for the minimum peak were less than $-0.8\ rads^{-1}$ for the simulation but oppositely for [2]. In this case, further investigation on the difference can not be made because of insufficient information in [2]. Nevertheless, this comparison is

acceptable.

Therefore, this can be concluded that the simulation technique is verified. Hence, the development of the SMC approaches on space applications can proceed.

Chapter 5

Spacecraft's Attitude and Orientation with Sliding Mode Control Techniques Formulation, Results and Analysis

5.1 Introduction

ACS is essential for a spacecraft operation. ACS supply information, such as, coarse pointing accuracy and also payload and antenna stability for a spacecraft mission. Thus, this chapter elaborates the fundamental and a basic application in the ACS which is SAOM. Thus, the chapter is divided into several portions:

1. Formulation of spacecraft's attitude and orientation which involved the spacecraft's position, velocity and acceleration between moving-frame (spacecraft) and fixed-frame (ECI). The formulation includes the development of rotational motion for a body in space using Euler's equation and equations of rotation motion. In the end, the model presented in a state-space model.

2. Feasibility study of SMC's switching function approaches (SFD) for a SAOM with state-variables and state-errors switching surface. The

SFD is chosen among the most common in SMC which used to attenuate chattering in the conventional SMC. This topic covered the switching surface formulations, SFD designs and results.

3. Introducing a new decaying boundary layer and switching function method thorough error feedback (DBLSF) for SMC which categorised as LOSMC. The DBLSF implemented on the developed SAOM model to eliminate the chattering drawbacks in SMC. This method is designed using state-errors switching surface, and then, controlled outputs are compared to the existing SFD approaches. Then, a PSO is introduced to the SAOM to enhance its performance.

4. A HOSMC (STSMC) introduced to the SAOM. The results of this technique are compared to the DBLSF (LOSMC). Then, PSO is enforced to the STSMC. At the end, the comparison on both methodolgies (DBLSF and STSMC) are evaluate of strengths and weaknesses.

The performance of LOSMC (SFD approaches and DBLSF) and HOSMC (STSMC) are presented, designed and analysed on the SAOM model. Then, PSO is implemented on DBLSF and STSMC where the attractive point of this chapter is to evaluate and compare the performance between DBLSF (developed method) and STSMC with and without PSO.

5.2 The Formulation of Position, Velocity and Acceleration between Moving-frame and Fixed-frame

In this section, the formulation of position, velocity and acceleration between moving-frame (ECI) and fixed-frame (spacecraft) is constructed. Figure 5.1 shows the relationship vector between P (a point on the spacecraft) and A for SAOM formulation. The symbols for the modelling as in Table 5.1.
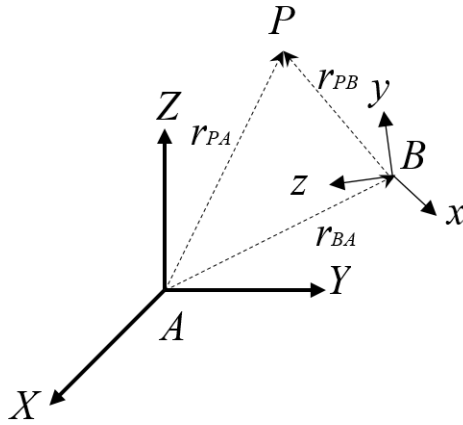
Figure 5.1: Inertial and Moving Axis Reference.

Later, any vectors that relate w.r.t. fixed-frame (A) will refer as absolute vector w.r.t. moving-frame (B) will be known as relative vector. The total vector distance between P and A is in Eq. 5.1.

$$r_{PA} = r_{BA} + r_{PB}. \tag{5.1}$$

The velocity (v_{PA}) of Eq. 5.1 represents in Eq. 5.2 between P in a moving rigid-body frame and A. Thus, P generates angular velocity. Finally, the acceleration of P w.r.t. A (a_{PA}) in Eq. 5.3.

$$
\begin{aligned}
\frac{d}{dt}(r_{PA}) &= \frac{d}{dt}(r_{BA}) + \frac{d}{dt}(r_{PB}), \\
v_{PA} &= v_{BA} + \omega \times r_{PB}.
\end{aligned}
\tag{5.2}
$$

Table 5.1: Inertial and Moving Axis Reference.

Parameter	Symbol
Fixed-frame Origin	A
Moving-frame Origin	B
A point on Moving Frame	P
Fixed-frame Axis	XYZ
Moving-frame Axis	xyz
Vector distance at B from A(absolute distance)	r_{BA}
Vector distance at P from B(relative distance)	r_{PB}
Vector distance at P from A(absolute and relative distance)	r_{PA}

where v_{BA} is the velocity between B and A.

$$
\begin{aligned}
\frac{d}{dt}(v_{PA}) &= \frac{d}{dt}(v_{BA}) + \frac{d}{dt}(\omega \times r_{PB}), \\
a_{PA} &= a_{BA} + \frac{d}{dt}(\omega \times r_{PB}) + \omega \times \frac{d}{dt}(r_{PB}).
\end{aligned}
\tag{5.3}
$$

where a_{BA} is the acceleration between B and A.

Lets, ω, the angular velocity vector, which points along the instantaneous axis of rotation and its direction is given by the right-hand rule below:

$$
\omega = \omega_x \hat{i} + \omega_y \hat{j} + \omega_z \hat{k}.
\tag{5.4}
$$

Hence, the derivative of the moving-frame in Eq. 5.4 as in Eq. 5.5.

$$
\begin{aligned}
\frac{d}{dt}(\omega) &= \frac{d}{dt}(\omega_x \hat{i}) + \frac{d}{dt}(\omega_y \hat{j}) + \frac{d}{dt}(\omega_z \hat{k}) \\
&\quad + \omega_x \frac{d}{dt}(\hat{i}) + \omega_y \frac{d}{dt}(\hat{j}) + \omega_z \frac{d}{dt}(\hat{k}).
\end{aligned}
\tag{5.5}
$$

But, the $\frac{d}{dt}(\hat{i})$, $\frac{d}{dt}(\hat{j})$ and $\frac{d}{dt}(\hat{k})$ are the derivative of moving-frame xyz. Hence, the results of these vectors are as in Eq. 5.6.

$$\omega_x \frac{d}{dt}(\hat{i}) = \Omega \times \omega_x \hat{i},$$

$$\omega_y \frac{d}{dt}(\hat{j}) = \Omega \times \omega_y \hat{j}, \tag{5.6}$$

$$\omega_z \frac{d}{dt}(\hat{k}) = \Omega \times \omega_z \hat{k}.$$

where Ω is the angular velocity of moving-frame xyz. Thus, Eq. 5.3 becomes

$$a_{PA} = a_{BA} + \alpha \times r_{PB} + \omega \times (\omega \times r_{PB}). \tag{5.7}$$

where $\alpha = \frac{d}{dt}(\omega) + (\omega \times \omega)$ is the angular acceleration of moving-frame.

5.2.1 Equations of Rotational Motion

Figure 5.2 illustrates the fundamental model to derive the equations of rotational motion (EORM) for a mass element position vectors from crucial several reference points. The purpose of the derivation is to obtain the moment about P (M_P)of the forces on a mass element (dm) as in Eq. 5.8. Later, the moment will act as inputs to the spacecraft.

$$dM_P = r \times dF_{net} + r \times df_{net}. \tag{5.8}$$

Hence, the total moment at P as in Eq. 5.9.

$$M_{Pnet} = \int_m (r \times \ddot{R})dm. \tag{5.9}$$

where $\int_m r \times df_{net} = 0$ since there is no force between the molecules within a rigid body and $dF_{net} = \ddot{R}dm$.
On the other hands,

$$\frac{d}{dt}(r \times \dot{R}) = \dot{r} \times \dot{R} + r \times \ddot{R},$$

$$r \times \ddot{R} = \frac{d}{dt}(r \times \dot{R}) - \dot{r} \times \dot{R}, \tag{5.10}$$
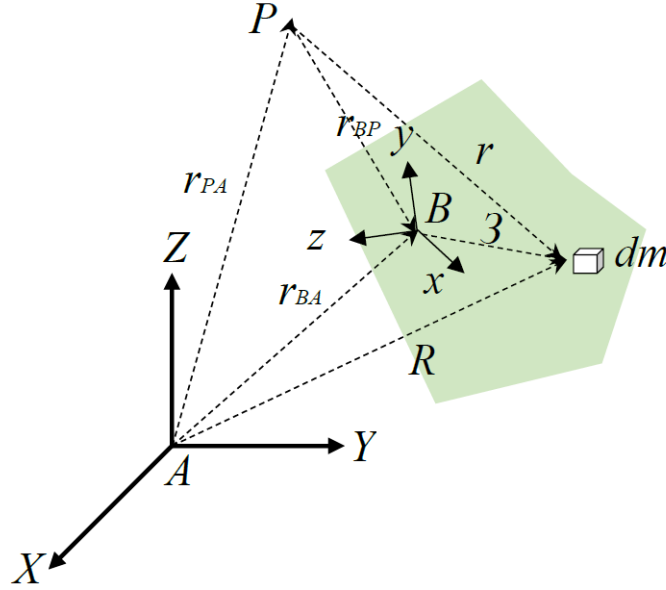
Figure 5.2: A Mass Element Position Vectors from Several Key Reference Points.

and

$$r = R - r_{PA},$$
$$\dot{r} = \dot{R} - r_{\dot{P}A},$$

(5.11)

But, from Eq. 5.10 and Eq. 5.11, thus,

$$\dot{r} \times \dot{R} = (\dot{R} - r_{\dot{P}A}) \times \dot{R},$$
$$= \dot{R} \times \dot{R} - r_{\dot{P}A} \times \dot{R},$$
$$= -r_{\dot{P}A} \times \dot{R},$$

(5.12)

Eq. 5.12 is replaced into Eq. 5.10 produces Eq. 5.13.

$$r \times \ddot{R} = \frac{d}{dt}(r \times \dot{R}) + r_{PA} \times \dot{R},$$

(5.13)

54

Hence, Eq. 5.13 is substitute in Eq. 5.8 and finally, the total moment about P in term of r_{PA} and R as in Eq. 5.14.

$$
\begin{aligned}
M_{Pnet} &= \int_m (\frac{d}{dt}(r \times \dot{R}) + r\dot{P}_A \times \dot{R})dm, \\
&= \frac{d}{dt}\int_m (r \times \dot{R}dm) + r\dot{P}_A \times \int_m \dot{R}dm.
\end{aligned}
\tag{5.14}
$$

The relationship between H_P and H_B can be derived as in Eq. 5.15 to Eq. 5.19. From Eq. 5.14,

$$
H_P = \int_m (r \times \dot{R}dm),
\tag{5.15}
$$

But,

$$
r = r_{BP} + \varsigma,
\tag{5.16}
$$

where ς is the distance between point B and P (see Figure 5.2). Eq. 5.16 replaced in Eq. 5.15 and produced Eq. 5.17.

$$
\begin{aligned}
H_P &= \int_m ((r_{BP} + \varsigma) \times \dot{R}dm), \\
&= r_{BP} \times \int_m \dot{R}dm + \int_m \varsigma \times \dot{R}dm,
\end{aligned}
\tag{5.17}
$$

From Eq. 5.17, the total moment about point B is

$$
\begin{aligned}
H_B &= \int_m \varsigma \times \dot{R}dm, \\
\int_m \dot{R}dm &= mv_a,
\end{aligned}
\tag{5.18}
$$

where $\dot{R} = v_B$. Replaced Eq. 5.18 to Eq. 5.17. Thus, angular momentum at any P point (Eq. 5.19) can be calculated using H_B (moment of inertia at the fixed-frame). For example, the inertia value of ISS (H_B) in Table 5.2 [6].

$$
H_P = H_B + r_{BP} \times mv_B.
\tag{5.19}
$$

Table 5.2: Moment of Inertia in ISS [6].

Parameter	Value	Unit
J_x	127538483.85	kgm^2
J_y	201272329.17	kgm^2
J_z	106892554.98	kgm^2

5.2.2 Euler's Angles and Euler's Equations

The spacecraft attitude and orientation have three rotation angles along roll, pitch and yaw (Figure 2.3) [6]. Hence, the relationship between the orientation of a rigid body relative to an inertial frame Figure 5.1) can be represented using Euler angles. Figure 5.3, 5.4 and 5.5 are the Euler's angle transformation from XYZ $(I'J'K')$ axis to xyz $(\hat{i}'\hat{j}'\hat{k}')$ axis. Eq. 5.20, 5.21 and 5.22 are the rotations along axis X (roll), Y (pitch) and Z (yaw) about ψ, θ and ϕ respectively according to Figure 5.3, 5.4 and 5.5.
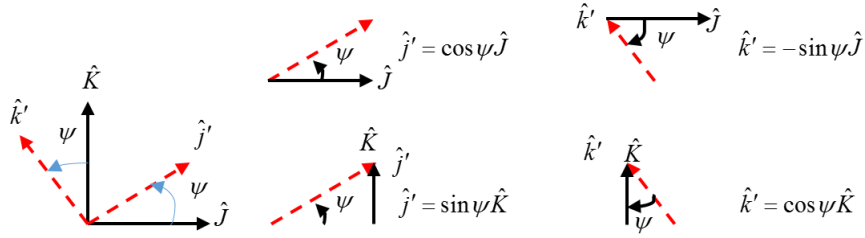
Figure 5.3: Rotation about ψ along X axis (roll).

$$R_X(\psi) = \begin{bmatrix} 1 & 0 & 0 \\ 0 & cos\psi & sin\psi \\ 0 & -sin\psi & cos\psi \end{bmatrix},$$ (5.20)

$$R_Y(\theta) = \begin{bmatrix} cos\theta & 0 & -sin\theta \\ 0 & 1 & 0 \\ sin\theta & 0 & cos\theta \end{bmatrix},$$ (5.21)

$$\hat{k}' = \cos\theta\hat{K} \qquad \hat{i}' = -\sin\theta\hat{K}$$

$$\hat{k}' = \sin\theta\hat{I} \qquad \hat{i}' = \cos\theta\hat{I}$$
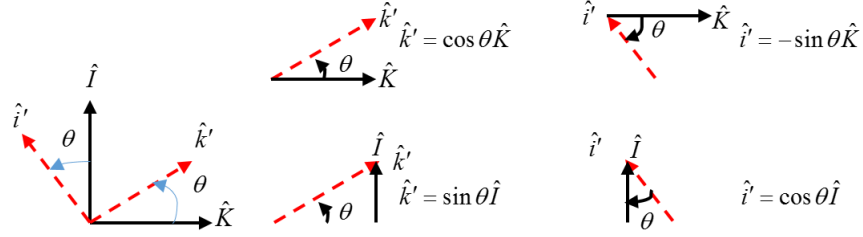
Figure 5.4: Rotation about θ along Y axis (pitch).

$$\hat{i}' = \cos\phi\hat{I} \qquad \hat{j}' = -\sin\phi I'$$

$$\hat{i}' = \sin\phi\hat{J} \qquad \hat{j}' = \cos\phi\hat{J}$$
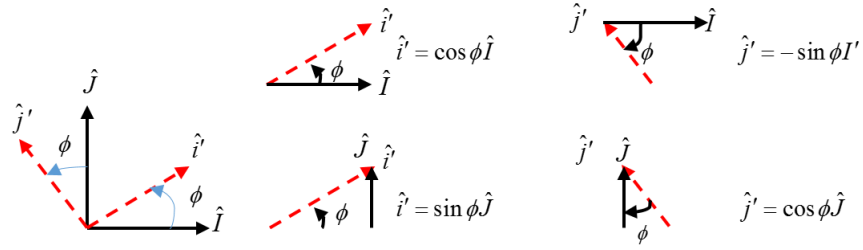
Figure 5.5: Rotation about ϕ along Z axis (yaw).

$$R_Z(\phi) = \begin{bmatrix} cos\phi & sin\phi & 0 \\ -sin\phi & cos\phi & 0 \\ 0 & 0 & 1 \end{bmatrix}. \tag{5.22}$$

Thus, the rotation matrix with sequence $R_X(\psi) - R_Y(\theta) - R_Z(\phi)$ denoted as Q as in Eq. 5.23.

57

$$
\begin{aligned}
Q &= R_Z(\phi) * R_Y(\theta) * R_X(\psi), \\
&= \begin{bmatrix} cos\phi cos\theta & cos\psi sin\phi + cos\phi sin\psi sin\theta & sin\psi sin\phi - cos\psi cos\phi sin\theta \\ -cos\theta sin\phi & cos\psi cos\phi - sin\psi sin\phi sin\theta & cos\phi sin\psi + cos\psi sin\phi sin\theta \\ sin\theta & -cos\theta sin\psi & cos\psi cos\theta \end{bmatrix}, \\
&= \begin{bmatrix} c\phi c\theta & c\psi s\phi + c\phi s\psi s\theta & s\psi s\phi - c\psi c\phi s\theta \\ -c\theta s\phi & c\psi c\phi - s\psi s\phi s\theta & c\phi s\psi + c\psi s\phi s\theta \\ s\theta & -c\theta s\psi & c\psi c\theta \end{bmatrix}.
\end{aligned}
$$

(5.23)

where c and s denoted as cos and sin respectively. Later, Eq. 5.23 used as the rotation sequence in SAOM design.

On the other hands, Euler's equations used to determine the inertia of a rigid body.

5.2.3   Spacecraft Attitude and Orientation Model Design

In this section, the angular velocity of spacecraft's attitude is modelled and presented in state space form. Figure 5.6 shows a rigid body spacecraft, orbiting the earth with respect to an ECI at an angular velocity, ω_o with three rotational degrees of freedom.
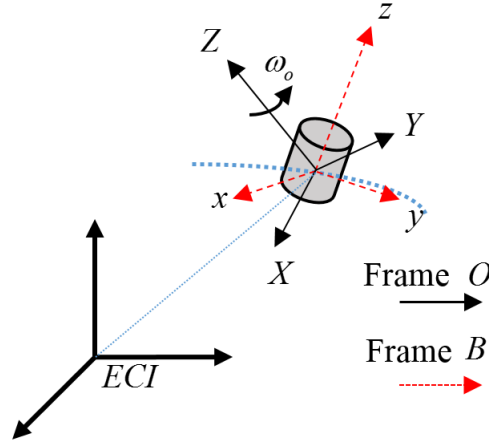
Figure 5.6: Spacecraft's attitude in moving frame B with respect to an orbiting reference frame O and both are moving in ECI.

The dynamic equations, concerning the effects of forces on the motion of the spacecraft [83], proven in section 5.2.2 as in Eq. 5.24.

$$J\dot{\omega} = J\omega \times \omega + \tau. \tag{5.24}$$

where $J = diag(J_x, J_y, J_z)$ is the constant inertia matrix in the body-fixed frame, ω is the spacecraft angular velocity orbiting around the Earth and $\tau = diag(\tau_x, \tau_y, \tau_z)$ is applied torque. The kinematics of the rigid body (Figure 5.6) using Euler's angles (Eq. 5.3, 5.4, 5.5), where the angular velocity of each axis is denoted by $\dot{\psi}$ (roll), $\dot{\theta}$ (pitch) and $\dot{\phi}$ (yaw) (see Figure 5.7).

59
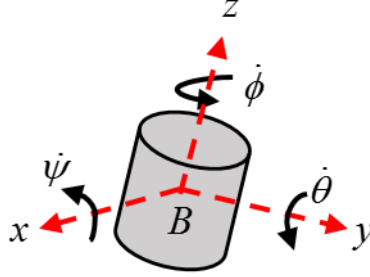
Figure 5.7: Sequence of Euler's angles, $(R_x(\psi) \rightarrow R_y(\theta) \rightarrow R_x(\psi))$, according moving frame B orientation relative to an orbiting frame O.

The absolute angular velocity, ω_B of mowing frame presented in Eq. 5.25.

$$\omega_B = \omega_{BOzyx} + \omega'_O, \tag{5.25}$$

where ω_{BO} is the angular velocity of B with respect to O, and ω_O is the velocity of O concerning ECI. ω_{BO} [17] depends on the sequence of rotations (Euler's angles sequence), wherein this case, the rotation follows Eq. 5.23. Thus, the ω_{BO} mathematical model as in 5.28 referred to frame B.

$$\omega_{BOx} = \begin{bmatrix} 1 & 0 & 0 \\ 0 & cos\psi & sin\psi \\ 0 & -sin\psi & cos\psi \end{bmatrix} = \begin{bmatrix} \dot{\psi} \\ 0 \\ 0 \end{bmatrix}, \tag{5.26}$$

$$\omega_{BOyx} = \begin{bmatrix} cos\theta & 0 & -sin\theta \\ 0 & 1 & 0 \\ sin\theta & 0 & cos\theta \end{bmatrix} \begin{bmatrix} \dot{\psi} \\ \dot{\theta} \\ 0 \end{bmatrix} = \begin{bmatrix} c\theta\dot{\psi} \\ \dot{\theta} \\ s\theta\dot{\psi} \end{bmatrix}, \tag{5.27}$$

$$\omega_{BOzyx} = \begin{bmatrix} cos\phi & sin\phi & 0 \\ -sin\phi & cos\phi & 0 \\ 0 & 0 & 1 \end{bmatrix} \begin{bmatrix} c\theta\dot{\psi} \\ \dot{\theta} \\ s\theta\dot{\psi} + \dot{\phi} \end{bmatrix} = \begin{bmatrix} s\phi\dot{\theta} + c\theta c\phi\dot{\psi} \\ c\phi\dot{\theta} - c\theta s\phi\dot{\psi} \\ \dot{\phi} + s\theta\dot{\psi} \end{bmatrix}, \tag{5.28}$$

However, ω_O is in frame O, thus must be expressed in body coordinates as in Eq. 5.29 using sequence in Eq. 5.23.

60

$$\omega_O' = Q \begin{bmatrix} 0 \\ 0 \\ \omega_O \end{bmatrix} = \begin{bmatrix} (s\psi s\phi - c\psi c\phi s\theta)\omega_O \\ (c\phi s\psi + c\psi s\phi s\theta)\omega_O \\ c\psi c\theta \omega_O \end{bmatrix}, \qquad (5.29)$$

With a small angle displacement assumption between B and O, the following parameters can be linearised into $c\psi = c\theta = c\phi \simeq 1$ and $s\psi = s\theta = s\phi \simeq 0$. Thus, Eq. 5.25 becomes

$$\omega_B = \begin{bmatrix} \dot{\psi} - \omega_O \theta \\ \dot{\theta} + \omega_O \psi \\ \dot{\phi} + \omega_O \end{bmatrix}, \qquad (5.30)$$

Finally, Eqn. 5.30 substituted into Eqn. 5.24 and produces Eq. 5.31.

$$J_x \ddot{\psi} = (J_y - Jz)\omega_O^2 \psi + (J_x + J_y - J_z)\omega_O \dot{\theta} + \tau_x,$$

$$J_y \ddot{\theta} = (J_z - J_y - J_x)\omega_O \dot{\psi} - (J_z - J_x)\omega_O^2 \theta + \tau_y, \qquad (5.31)$$

$$J_z \ddot{\phi} = \tau_z.$$

In conclusion, Eq. 5.31 can be represented in state space form as in Eq. 5.32.

$$\begin{bmatrix} \dot{x}_1(t) \\ \dot{x}_2(t) \\ \dot{x}_3(t) \\ \dot{x}_4(t) \\ \dot{x}_5(t) \\ \dot{x}_6(t) \end{bmatrix} = \begin{bmatrix} 0 & 1 & 0 & 0 & 0 & 0 \\ h & 0 & 0 & i & 0 & 0 \\ 0 & 0 & 0 & 1 & 0 & 0 \\ 0 & j & k & 0 & 0 & 0 \\ 0 & 0 & 0 & 0 & 0 & 1 \\ 0 & 0 & 0 & 0 & 0 & 0 \end{bmatrix} \begin{bmatrix} x_1(t) \\ x_2(t) \\ x_3(t) \\ x_4(t) \\ x_5(t) \\ x_6(t) \end{bmatrix} + \begin{bmatrix} 0 & 0 & 0 \\ \dfrac{\tau_x}{J_x} & 0 & 0 \\ 0 & 0 & 0 \\ 0 & \dfrac{\tau_y}{J_y} & 0 \\ 0 & 0 & 0 \\ 0 & 0 & \dfrac{\tau_z}{J_z} \end{bmatrix} \begin{bmatrix} u_{x_1} \\ u_{x_3} \\ u_{x_5} \end{bmatrix}, \qquad (5.32)$$

where

$$h = \left(\frac{J_y - J_z}{J_x}\right)\omega_O^2; \qquad i = \left(\frac{J_x + J_y - J_z}{J_x}\right)\omega_O;$$

$$j = \left(\frac{J_z - J_y - J_x}{J_y}\right)\omega_O; \quad k = -\left(\frac{J_z - J_x}{J_y}\right)\omega_O^2;$$

$$\begin{bmatrix} x_1(t) & x_2(t) & x_3(t) & x_4(t) & x_5(t) & x_6(t) \end{bmatrix}^T = \begin{bmatrix} \psi & \dot{\psi} & \theta & \dot{\theta} & \psi & \dot{\phi} \end{bmatrix}^T,$$

$$\begin{bmatrix} \dot{x}_1(t) & \dot{x}_2(t) & \dot{x}_3(t) & \dot{x}_4(t) & \dot{x}_5(t) & \dot{x}_6(t) \end{bmatrix}^T = \begin{bmatrix} \dot{\psi} & \ddot{\psi} & \dot{\theta} & \ddot{\theta} & \dot{\phi} & \ddot{\phi} \end{bmatrix}^T.$$

Converting the model in state-space form is importance before implementation of the SMC. There are three inputs supplied to the SAOM at $\dot{x}_2(t)$, $\dot{x}_4(t)$ and $\dot{x}_6(t)$ denote the roll, pitch and yaw angular velocity, respectively. Besides that, the angular outputs are measured at $x_1(t)$ (ψ), $x_3(t)$ (θ) and $x_5(t)$ (θ). Finally, futher analysis can be done on the SAOM.

5.3 Feasibility Study of Switching Function Approaches in LOSMC for a SAOM with State-variables and State-error Switching Surface

It is important to understand the range of limitations of SMC methods before further improvements can be made. Hence, the main novelty of this study is to design and investigate the LOSMC control law with a focus on the SFD characteristics and capabilities with two switching surface designs for a SAOM. In Chapter 3, the SFD can be designed using either state-variables or state-errors switching surface. Thus, this topic implementing the common SFD techniques on these switching surfaces for chattering attenuation produced by the classical SMC. A notable part of the chosen approach is that some of the gains can be manually tuned based on the designed characteristic equation while satisfying some mild conditions to ensure the existence of a sliding mode. This technique, however, did not produces an optimum output performances. Ideally, the discontinuous switching function must produce chattering due to a fast switching mechanism and discontinuous control accross the switching surface. Then, the characteristics such as chattering in the control inputs and transient reponse in the outputs are observed. The most common SFD methods are chosen for chattering elimination as per below:

1. Relay with state dependent gains (RSG).

2. Linear feedback with switched gains (LFSG).

5.3.1 State-variables Switching Surface Design on a SAOM (Continuous Control Law Design)

There are various approaches to design the continuous part (swicthing surface) using the state-variables such as regular form and reduced order dynamics, method of hierarchy and diagonilization methods [49] for a multi-input multi-output (MIMO) system. This design, however, will use the reduction of order method (ROOM). The rationale for this is that in the ROOM method, the switching surface coeeficients can be chosen flexibly and thus looser assumptions can be made as long as the characteristic equation of the compensated system is comparable to the design criteria.

The switching surface equation using state-variable $(\sigma_v(x))$ and its dynamics $(\dot{\sigma}_v(x))$ as in 5.33 and 5.34 where S is the switching surface coefficients.

$$\sigma_v(x) = Sx = 0, \tag{5.33}$$

$$\dot{\sigma}_v(x) = S\dot{x} = 0, \tag{5.34}$$

The spacecraft's attitude model is a multi-input (three inputs) and multi-output (three outputs) system. Hence, three set of switching surface coefficients $(S_1, S_2, \text{ and } S_3)$ are required for the SAOM:

$$S = \begin{bmatrix} S_1 \\ S_2 \\ S_3 \end{bmatrix} = \begin{bmatrix} s_{11} & s_{12} & s_{13} & s_{14} & s_{15} & s_{16} \\ s_{21} & s_{22} & s_{23} & s_{24} & s_{25} & s_{26} \\ s_{31} & s_{32} & s_{33} & s_{34} & s_{35} & s_{36} \end{bmatrix}. \tag{5.35}$$

It is appropriate to have the characteristic equation at $\lambda^3 + 6\lambda^2 + 11\lambda + 6$ with poles at -1, -2 and -3; the selection of the characteristic equation is made in order to allow the spacecraft's attitude converge to the zero less than 100 seconds [84]. Thus, some assumptions on the switching surface coefficients (s_{ij}) are needed to ensure this characteristic equation is achieved.

Consider the general form of a nonliner system in state-space as in 5.36.

$$\dot{x}(t) = f(t, x) + B(u(t) + d(t)), \tag{5.36}$$

64

where $x(t) \in R^n$ is a set of state variables, $f(t,x) \in R^n$ is a nonlinear function, $B \in R^{m \times n}$ matrix of system's inputs, $u(t) \in R^m$ is a set of inputs and $d(t) \in R^m$ is the disturbances.

The switching surface design using ROOM is as follows. Firstly, (5.36) is replaced in (5.34) and produces

$$S\dot{x}(t) = S(f(t,x) + B(u_{eq} + d(t))) = 0, \tag{5.37}$$

Now, $u(t)$ become control law U_{eq} (the continuous part). Hence:

$$u_{eq}(t) = -(SB)^{-1}(Sf(t,x) + SBd(t)), \tag{5.38}$$

Then, (5.38) is substituted into (5.36) and produces:

$$\dot{x}(t) = [I - B(SB)^{-1}S]f(t,x), \tag{5.39}$$

In ROOM, assumptions can be made on the s_{ij} values and can be chosen flexibly. Firstly, define SB.

$$SB = \begin{bmatrix} s_{12} & s_{14} & s_{16} \\ s_{22} & s_{24} & s_{26} \\ s_{32} & s_{34} & s_{36} \end{bmatrix}, \tag{5.40}$$

The determinant of SB can be set to any value as long as $|SB| \neq 0$ and $s_{ij} \geq 0$. To simplify the design process, assume $|SB| = 1$. One of the combinations to set $|SB| = 1$ is to let $s_{12} = s_{14} = s_{22} = s_{26} = s_{32} = s_{34} = s_{36} = 1$, $s_{24} = 2$ and $s_{16} = 0$. Thus, based on these selections, then:

$$(SB)^{-1} = \begin{bmatrix} 1 & -1 & 1 \\ 0 & 1 & -1 \\ -1 & 0 & 1 \end{bmatrix}, \tag{5.41}$$

Next, substitute Eqs. 5.32, 5.35 and 5.41 into 5.39 so the dynamic model is reduced to:

65

$$\begin{bmatrix} \dot{x}_1(t) \\ \dot{x}_2(t) \\ \dot{x}_3(t) \\ \dot{x}_4(t) \\ \dot{x}_5(t) \\ \dot{x}_6(t) \end{bmatrix} = \begin{bmatrix} 0 & 1 & 0 & 0 & 0 & 0 \\ 0 & a & 0 & b & 0 & c \\ 0 & 0 & 0 & 1 & 0 & 0 \\ 0 & d & 0 & e & 0 & f \\ 0 & 0 & 0 & 0 & 0 & 1 \\ 0 & 0 & 0 & h & 0 & i \end{bmatrix} \begin{bmatrix} x_1 \\ x_2 \\ x_3 \\ x_4 \\ x_5 \\ x_6 \end{bmatrix}, \qquad (5.42)$$

where

$$\begin{array}{llll} a & = & s_{21} - s_{11} - s_{31}; & \quad b & = & s_{23} - s_{13} - s_{33}; \\ c & = & s_{25} - s_{15} - s_{35}; & \quad d & = & s_{31} - s_{21}; \\ e & = & s_{33} - s_{23}; & \quad f & = & s_{35} - s_{25}; \\ g & = & s_{11} - s_{31}; & \quad h & = & s_{13} - s_{33}; \\ i & = & s_{15} - s_{35}; & & & \end{array}$$

Finally, using (5.34) and (5.42), the reduced order model of the spacecraft's attitude system is:

$$\dot{\hat{x}}(t) = \begin{bmatrix} \dot{\hat{x}}_1(t) \\ \dot{\hat{x}}_2(t) \\ \dot{\hat{x}}_3(t) \end{bmatrix} = \begin{bmatrix} a & b & c \\ d & e & f \\ g & h & i \end{bmatrix} \begin{bmatrix} \hat{x}_1(t) \\ \hat{x}_2(t) \\ \hat{x}_3(t) \end{bmatrix}, \qquad (5.43)$$

where $\dot{\hat{x}}_1(t) = \dot{x}_2(t)$, $\dot{\hat{x}}_2(t) = \dot{x}_4(t)$ and $\dot{\hat{x}}_3(t) = \dot{x}_6(t)$.

In this design, the characteristic equation of (5.43) is matched to $\lambda^3 + 6\lambda^2 + 11\lambda + 6$, in order to achieve zero steady state error less than 100 seconds [84]. Hence, the expanded characteristic equation of (5.43) is given as:

$$\begin{aligned} \Delta(\dot{\hat{x}}(t)) & = & \lambda^3 + (s_{11} - s_{15} - s_{21} + s_{23} + s_{31} - s_{33} + s_{35})\lambda^2 \\ && + (s_{11}s_{23} - s_{13}s_{21} - s_{11}s_{25} + s_{15}s_{21} + s_{13}s_{25} \\ && -s_{15}s_{23} - s_{11}s_{33} + s_{13}s_{31} + 2s_{11}s_{35} - 2s_{15}s_{31} \\ && -s_{13}s_{35} + s_{15}s_{33} - s_{21}s_{35} + s_{25}s_{31} + s_{23}s_{35} \\ && -s_{25}s_{33})\lambda + (s_{11}s_{23}s_{35} - s_{11}s_{25}s_{33} - s_{13}s_{21}s_{35} \\ && +s_{13}s_{25}s_{31} + s_{15}s_{21}s_{33} - s_{15}s_{23}s_{31}), \end{aligned} \qquad (5.44)$$

and the implied constraints on the values s_{ij} are given as:

$$s_{11} - s_{15} - s_{21} + s_{23} + s_{31} - s_{33} + s_{35} \quad = \quad 6,$$

$$\begin{aligned}
&s_{11}s_{23} - s_{13}s_{21} - s_{11}s_{25} + s_{15}s_{21} + s_{13}s_{25} \\
&-s_{15}s_{23} - s_{11}s_{33} + s_{13}s_{31} + 2s_{11}s_{35} - 2s_{15}s_{31} \\
&-s_{13}s_{35} + s_{15}s_{33} - s_{21}s_{35} + s_{25}s_{31} \\
&+s_{23}s_{35} - s_{25}s_{33} \quad = \quad 11,
\end{aligned} \tag{5.45}$$

$$\begin{aligned}
&s_{11}s_{23}s_{35} - s_{11}s_{25}s_{33} - s_{13}s_{21}s_{35} \\
&+s_{13}s_{25}s_{31} + s_{15}s_{21}s_{33} - s_{15}s_{23}s_{31} \quad = \quad 6,
\end{aligned}$$

Then, some of the coeeficients defined as $s_{13} = 0.5$, $s_{15} = 4$, $s_{23} = 3$, $s_{25} = 2$, $s_{31} = 1$ and $s_{35} = 2$ and then use these values in combination with (5.45) to solve for the remaining coefficients s_{ij}. Thus:

$$\begin{aligned}
s_{11} - s_{21} - s_{33} + 2 &= 6, \\
5s_{11} + 1.5s_{21} + 2s_{33} - s_{11}s_{33} - 11.5 &= 11, \\
6s_{11} - s_{21} - 2s_{11}s_{33} + 4s_{21}s_{33} - 11 &= 6,
\end{aligned} \tag{5.46}$$

Solving (5.46), then $s_{11} = 5.5303$, $s_{21} = 0.0623$ and $s_{33} = 1.468$. Finally, the switching surface design of (5.35) is given as follows:

$$S = \begin{bmatrix} s1 \\ s2 \\ s3 \end{bmatrix} = \begin{bmatrix} 5.5303 & 1 & 0.5 & 1 & 4 & 0 \\ 0.0623 & 1 & 3 & 2 & 2 & 1 \\ 1 & 1 & 1.468 & 1 & 2 & 1 \end{bmatrix}. \tag{5.47}$$

In conclusions, using the ROOM approach there are eighteen coefficients which have to be selected to define the switching surface design using state-variables, thus, gives flexibility to the designer. In principle one can meet the required dynamics for the sliding mode by choosing fifteen coefficients and then solving for the remaining three to ensure sure the compensated system meets the design criteria.

5.3.2 State-error Switching Surface on a SOAM (Continuous Control Law Design)

In this section, the switching surface designed refer to the SAOM model (5.32) using state-error as in Eq. 5.48 .

$$\sigma_e(t)_i = \frac{d}{dt}(e_i(t)) + \lambda_i e_i(t), \tag{5.48}$$

$$e_i(t) = x_n(t) - x_d(t)_n, \tag{5.49}$$

$$\frac{d}{dt}(e_i(t)) = \dot{x_n}(t) = x_{n+1}(t), \tag{5.50}$$

$$\frac{d^2}{dt^2}(e_i(t)) = \dot{x_{n+1}}(t). \tag{5.51}$$

with $i = 1, 2, 3$ and $n = 1, 3, 5$. $e_i(t)$ (5.49) is the deviation between the measured output $(x_n(t))$ and the input reference of the system $(x_d(t)_n)$ while $\frac{d}{dt}(e_i(t))$ (5.50) and $\frac{d^2}{dt^2}(e_i(t))$ (5.51) or later known as $\dot{e_i}(t)$ and $\ddot{e_i}(t)$ are the deviation dynamics. $\lambda_i > 0$ is the constant sliding slope. For the SAOM control input design, consider $(x_d(t)_n)$ is constant. Thus, $(\dot{x_d}(t)_n) = 0$. Taking the first dynamic of Eq. 5.48 produces Eq. 5.52. Hence,

$$\dot{\sigma_e}(t)_i = \ddot{e_i}(t) + \lambda_i \dot{e_i}(t). \tag{5.52}$$

Replaced (5.50) and (5.51) into (5.52) computes (5.53)

$$\dot{\sigma_e}(t)_i = \dot{x_{n+1}}(t) + \lambda_i x_{n+1}(t). \tag{5.53}$$

However, Eq. 5.32 can be presented into a general form (5.54). Furthermore, switching surface dynamics are set to zero $(\sigma_e(t)_i = \dot{\sigma_e}(t)_i = 0)$ to ensure the robustness can be achieved.

$$\dot{x}_n(t) = f(t, x_n) + B(u_n(t) + d_n(t)). \tag{5.54}$$

with $n = 1, 2, 3, 4, 5, 6$. Next, replaced (5.54) into (5.53) becomes (5.55) where $u_n(t) = u_{eq}(t)_i$.

$$f(t, x_{n+1}) + B(u_{eq}(t)_i + d_{n+1}(t)) + \lambda_i x_{n+1}(t) = 0. \qquad (5.55)$$

Hence, the SMC continuous control law as in Eq. 5.56.

$$u_{eq}(t)_i = -B^{-1}(f(t, x_{n+1}) + \lambda_i x_{n+1}(t)) - d_{n+1}(t). \qquad (5.56)$$

where $i = 1, 2, 3$ and $n = 1, 3, 5$.

5.3.3 Switching Function Design (SFD) Approaches for Discontinuous Control Law Design, $U_N(x)$

Classical SMC is well known for producing chattering in the control inputs. Hence, some modifications are required in the switching surface to eliminate the drawbacks. There are three popular modification techniques of low-order sliding mode control for SFD (relay with constant gains (RCG), RSG and LFSG) discussed in this section. The general form of RCG, RSG and LFSG are shown in Table 5.3.

Table 5.3: Existing Switching Function Control Algorithm.

SFD	Algorithm	Condition		
RCG	$U_{iN}(x) = \begin{cases} \alpha_i sgn(\sigma_i(x)), \\ 0 \end{cases}$	$\sigma_i(x)$ $\sigma_i(x)$	$\neq$ $=$	0 0
RSG	$U_{iN}(x) = \begin{cases} \alpha_i(x) sgn(\sigma_i(x)), \\ 0 \end{cases}$	$\sigma_i(x)$ $\sigma_i(x)$	$\neq$ $=$	0 0
LFSG	$U_N(x) = -L\sigma(x)$	L is symmetric positive definite constant matrix		

These variants must be proven stable by implementing the Lyapunov stability criterion before applying it to the SAOM.

5.3.3.1 Relays with constant gains (RCG)

The rules to meet the sufficiency condition for the designed SMC is $\sigma\dot{\sigma} = \alpha_i\sigma_i(x)sgn(\sigma_i(x)) < 0$, if $\sigma_i(x) \neq 0$. α_i is a constant tuning gain ($||\alpha_i|| \leq \bar{D}$, $\bar{D}$ is upper bound of matching uncertainties) where the value must be negative $\alpha_i < 0$. The stability condition for RCG is:

$$\begin{aligned} \sigma_i(x)\dot{\sigma}_i(x) &= \alpha_i\sigma_i(x)sgn(\sigma_i(x)) < 0, \\ &= \alpha_i\frac{\sigma_i^2(x)}{|\sigma_i(x)|}. \end{aligned}$$

$$\text{Let,} \quad \alpha_i \quad < \quad 0. \tag{5.57}$$

$$\begin{aligned} \text{Then,} \quad \sigma_i(x)\dot{\sigma}_i(x) &= -\alpha_i\frac{\sigma_i^2(x)}{|\sigma_i(x)|}. \\ &< \quad 0. \end{aligned}$$

Thus, the switching surface is meet the sufficiency conditions for the designed SMC.

5.3.3.2 Relays with state dependent gains (RSG)

The stability rules for the RSG controller are $\sigma\dot{\sigma} = \alpha_i(x)\sigma_i(x)sgn(\sigma_i(x)) < 0$, if $\sigma_i(x) \neq 0$. $\alpha_i(x)$ is a variable states function where $\alpha_i(x) = \beta_i(\sigma_i^{2k}(x) + \gamma_i)$ with $\beta_i < 0$, $\gamma_i > 0$ and k is an integer number.

$$\begin{aligned} \sigma_i(x)\dot{\sigma}_i(x) &= \alpha_i(x)\sigma_i(x)sgn(\sigma_i(x)) < 0, \\ \alpha_i(x) &= \beta_i(\sigma_i^{2k}(x) + \gamma_i). \end{aligned}$$

$$\text{Let,} \quad \beta_i(x) < 0, \gamma_i > 0, k = \text{positive integer.} \tag{5.58}$$

$$\begin{aligned} \text{Then,} \quad \sigma_i(x)\dot{\sigma}_i(x) &= -\beta_i(\sigma_i(x)^{2k} + \gamma_i)\frac{\sigma_i(x)^2}{|\sigma_i(x)|}. \\ &< \quad 0. \end{aligned}$$

Hence, the stability rules are fulfill in term of sliding mode existence.

5.3.3.3 Linear feedback with switched gains (LFSG)

The stability condition for LFSG is $\sigma^T(x)\dot{\sigma}(x) = -\sigma^T(x)L\sigma(x) < 0$, if $\sigma(x) \neq 0$, L is a symmetric positive definite constant matrix, $L \in R^{m \times m}$. Thus, the LFSG in the SAOM, L is a 3×3 matrix in (5.59).

$$L = \begin{bmatrix} w & y & z \\ y & w & y \\ z & y & w \end{bmatrix}. \tag{5.59}$$

5.3.4   Results

This topic presents the SAOM performances using SVSS and SESS design (continuous control law) with variants SFD approaches (discontinuous control law). The perfomance evaluations including the SAOM controlled outputs and inputs, and phase plane potrait between the outputs (angle) and its dynamics (angular velocity) where the results are compared to the ideal switching surface condition (Figure 3.3). The comparison between SVSS and SESS is a must before further improvements can be made where the appropriate method is chosen based on the performances. Table 5.4 shows summary of the SAOM evaluation criteria. There are three control inputs designed based on the compensated system where $u_{vsmc1}(t)$, $u_{vsmc2}(t)$, and $u_{vsmc3}(t)$ that are mapping to roll, pitch and yaw paramaters respectively. Then, Table 5.5 shows the parameter setup for the SAOM model (Eq. 5.32).

Table 5.4: Summary of the SAOM Evaluation Criteria.

Switching Surface	SFD	Control Inputs	Control Outputs	Phase Potrait
SVSS and SESS	Classical SMC	$u_{vsmc1}(t)$ $u_{vsmc2}(t)$ $u_{vsmc3}(t)$	$\phi(roll)$ $\theta(pitch)$ $\psi(yaw)$	$\dot{\phi}$ vs ϕ $\dot{\theta}$ vs θ $\dot{\psi}$ vs ψ
	RCG			
	RSG			
	LFSG			

Table 5.5: Numeric Parameters of the SAOM According to ISS [6].

Parameter	Value	Unit
ω_o	0.0011	$rads^{-1}$
J_x	127538483.85	kgm^2
J_y	201272329.17	kgm^2
J_z	106892554.98	kgm^2
τ_x, τ_y, τ_z	1×10^{-3}	N
$d(t)$	$sin(t)$	N

5.3.4.1 Classical SMC Control Input Results

In this section, the classical SMC control law is implemented on the SAOM where 5.60 and 5.61 referred to SVSS and SESS respectively. The numerical values for Eq. 5.60 as in Table 5.6 while Eq. 5.61 refered to Table 5.7.

Table 5.6: Classical SVSS-SMC: Numeric Parameters Setup.

Parameter	Value	
	Condition 1	Condition 2
$k_{1,2,3}$	0.1	0.5
s_1	5.5303 1 0.5 1 4 0	5.5303 1 0.5 1 4 0
s_2	0.0623 1 3 2 2 1	0.0623 1 3 2 2 1
s_3	1 1 1.468 1 2 1	1 1 1.468 1 2 1

$$u_{vsmc}(t) = -(SB)^{-1}(Sf(t,x) + SBd(t)) - k_i \frac{\sigma_v}{|\sigma_v|}, \tag{5.60}$$

$$u_{esmc}(t) = -B^{-1}(f(t,x_{n+1}) + \lambda_i x_{n+1}(t) - d(t)) - k_i \frac{\sigma_v}{|\sigma_v|}. \tag{5.61}$$

Table 5.7: Classical SESS-SMC: Numeric Parameters Setup.

Parameter	Value	
	Condition 1	Condition 2
$k_{1,2,3}$	0.1	0.5
$\lambda_{1,2,3}$	2.6 1 0.8	2.6 1 0.8

where $\rho_i > 0$ and $\gamma_i > 0$ are the gains, $||d(t)|| \leq \bar{D}$ and $||d(t)|| \leq \bar{D}$ are the bounded disturbances by a known constant $\bar{D}$ for the SAOM system.

The SAOM analysed using two k_i conditions to investigate the effect of the different gain values on the SAOM model with SVSS and SESS. Since the SAOM using classical SMC, hence the chattering phenomena is expected in the control inputs. Besides, the $\lambda_{1,2,3}$ (Table 5.7) are tuning manually by observing the output transient performances and s_1, s_2 and s_3 (Table 5.6) are based on Eq. 5.47.

Figure 5.8 and 5.9 illustrate the SAOM's performances with classical SVSS and SESS using $k_i = 0.1$ and $k_i = 0.5$ accordingly.

With $k_i = 0.1$, slightly chattering can be observed on both SVSS and SESS. The inputs are bounded within $1Nm$. However, SESS angular outputs converge to the desired outputs faster than SVSS (around $20s$ against around $70s$). Similar to the switching surface, all state-variables hitting switching surface at least at $15s$ for SESS compared to SVSS, which is $65s$. On the other hand, $k_i = 0.5$ shows SESS performed better than SVSS in term of control outputs performance. However, both control inputs produced chattering and bounded more than $1Nm$. In conclusion, the classical SESS-SMC on the SAOM performed better than SVSS-SMC with $k_i = 0.1$ is chosen. However, the chattering can be seen in the control inputs as expected.
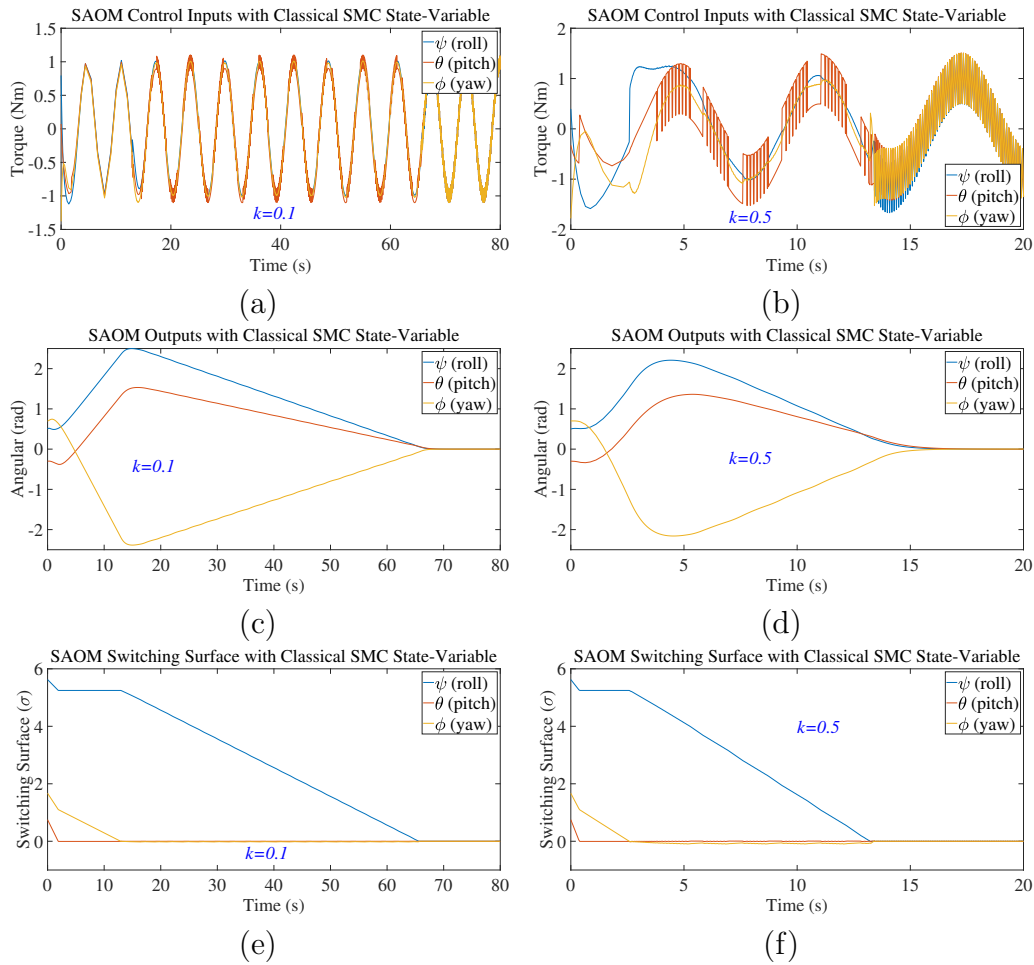
Figure 5.8: Classical SVSS-SMC: The SAOM's control inputs (a)(b), control outputs (c)(d) and switching surface (e)(f) with $k_i = 0.1$ and $k_i = 0.5$.
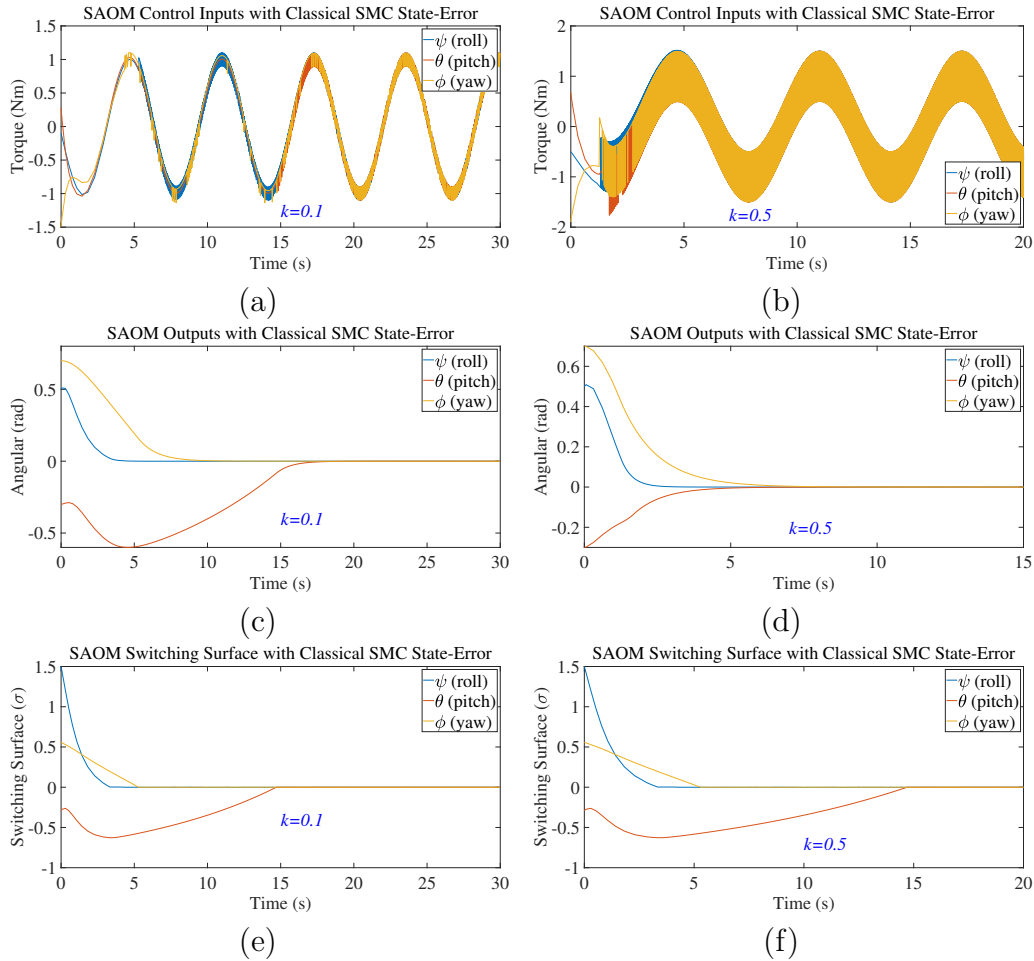
Figure 5.9: Classical SESS-SMC: The SAOM's control inputs (a)(b), control outputs (c)(d) and switching surface (e)(f) with $k_i = 0.1$ and $k_i = 0.5$.

5.3.4.2 Relays with State Dependent Gains

In this section, the RSG control law is implemented on the SAOM. RSG algorithm is shown in Table 5.3, and the details can be referred to in Eq. 5.58. Several conditions were selected for SVSS and SESS to investigate the effect of β_i and γ_i on the SAOM's transient performance in Table 5.16. For SVSS, the switching surface is in Eq. 5.33 while S coefficients in Eq. 5.47. On the other hand, SESS used Eq. 5.48 for the switching surface where the λ_i values in Table 5.9.

Table 5.8: SVSS-RSG and SESS-RSG: Numeric Parameters Setup.

Switching Surface	Condition	β_i	γ_i
SVSS	1		0.008
	2	5.000	0.009
	3		0.010
	4		0.008
	5	10.000	0.009
	6		0.010
	7		0.050
	8	10.000	0.100
	9		0.150
SESS	1	0.200	
	2	0.350	0.080
	3	0.500	
	4		0.050
	5	0.350	0.100
	6		0.150

Table 5.9: SESS-RSG: Parameters setup for λ_i.

λ_i	Value
1	2.60
2	1.00
3	0.80

Figure 5.10 (SVSS - condition 1, 2 and 3), 5.11 (SVSS - condition 4, 5 and 6) and 5.12 (SVSS - condition 7, 8 and 9) show the control inputs and outputs of the RSG implemented on SAOM using SVSS as the switching surface design. RSG ables to eliminate the chattering in the control inputs for condition 1 to 6 only, but the transient outputs are varying throughout the β_i and γ_i values where presented in Table 5.11. β_i value improved the settling time around $30s$ when increasing from 5 to 10 (refer to condition 1 to 6) but bounded input slightly arises around $0.04Nm$. On the other hand, the settling time recorded at most $15s$ for condition 7 to 9. However, the chattering can be observed in the controller input due to the large increment of γ_i value. Thus, according to the results, condition 4 shows the best setup for the RSG using SVSS method.
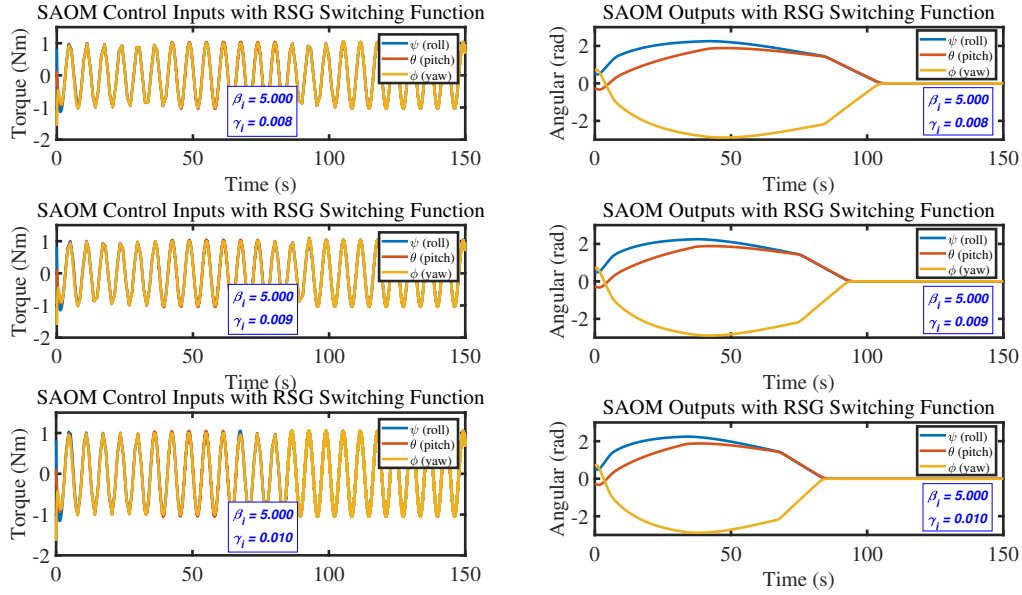
Figure 5.10: SVSS-RSG: SMC Outputs on the SAOM where $\beta_i = 5.000$ and variable γ_i.

Figure 5.13 (condition 1, 2 and 3) and 5.14 (condition 4, 5 and 6) illustrate the control outputs and inputs performance using SESS-RSG on the SAOM. The result shows similar findings in SVSS-RSG, where the arises of β_i and γ_i value improved the transient performance and increased the control torque. The minimum of the bounded input ($1.86Nm$) happens at condition 1, but the settling time is more than $100s$. Condition 4 produces $2.20Nm$ input and $45s$ settling time which is the best setup for SESS-RSG on the SAOM.

In conclusion, this topic implemented RSG on the SAOM using two types of switching surfaces; SVSS and SESS. Both methods capable of eliminating chattering in the control input when the RSG parameters (β_i and γ_i) are correctly tuned. In SVSS-RSG, condition 4 computes the best setup for the SAOM where the bounded input is $1.61Nm$ with the outputs settle around $63s$. For SESS-RSG, condition 4 recorded at most $2.20Nm$ and $45s$ for the control inputs and settle time respectively. Thus, the SVSS-RSG is performed better than SESS-RSG when considering the input torque values but differently on the outputs time convergence.
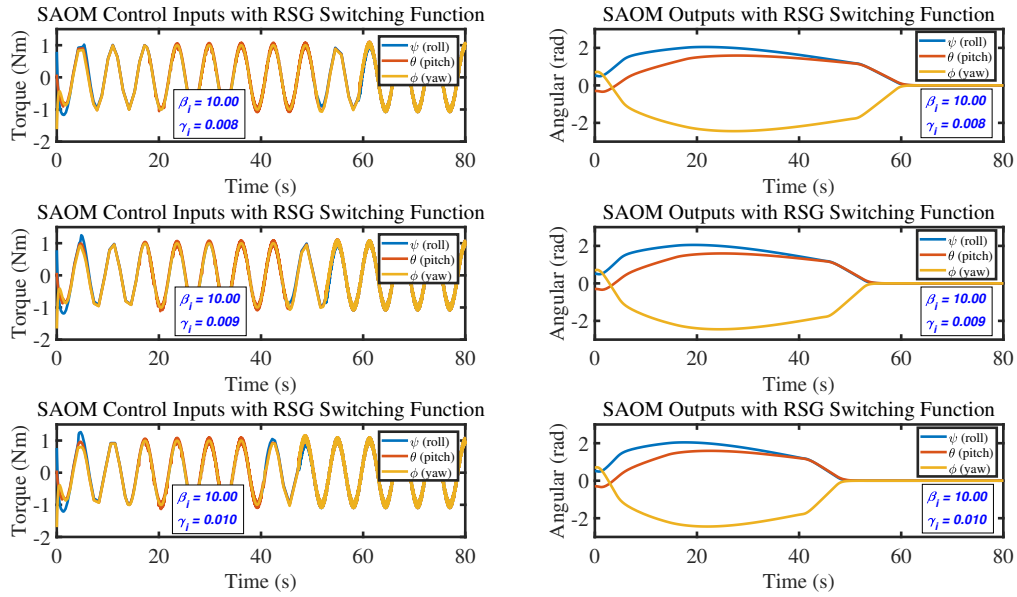
Figure 5.11: SVSS-RSG: SMC Outputs on the SAOM where $\beta_i = 10.00$ and variable γ_i.

5.3.4.3 Linear Feedback with Switched Gains

In this section, Linear Feedback with Switched Gains algorithm (Table 5.3) is applied on the SAOM where the algorithm explained in Eq. 5.59. The purpose of this evaluation is to investigate the performance of the LFSG on the SAOM with switching surface design using SVSS and SESS. The simulation setup is shown in Table 5.12.

Figure 5.16 presents the result for the SVSS-LFSG on the SAOM. The outcome of the analysis is summarised in Table 5.14.
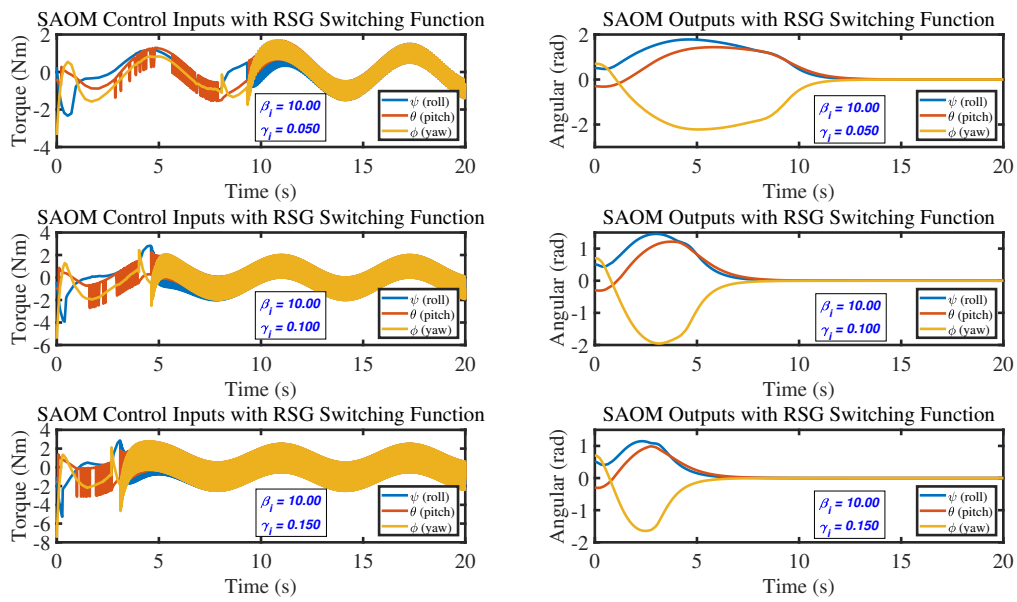
Figure 5.12: SVSS-RSG: SMC Outputs on the SAOM where $\beta_i = 10.00$ and variable γ_i.

Table 5.10: SVSS-RSG: Result Summary.

Switching Surface	Condition	β_i	γ_i	Chattering	Bounded Input (Nm)	Settling Time (s)
SVSS	1		0.008	No	1.57	105
	2	5	0.009	No	1.61	92
	3		0.010	No	1.65	85
	4		0.008	No	1.61	63
	5	10	0.009	No	1.65	58
	6		0.010	No	1.69	52
	7		0.050	Yes	3.36	15
	8	10	0.100	Yes	5.44	12
	9		0.150	Yes	7.52	9

Table 5.11: SESS-RSG: Result Summary.

Switching Surface	Condition	β_i	γ_i	Chattering	Bounded Input (Nm)	Settling Time (s)
SESS	1	0.200		No	1.86	> 100
	2	0.350	0.08	No	2.21	25
	3	0.500		No	2.56	18
	4		0.050	No	2.20	45
	5	0.350	0.100	No	2.21	22
	6		0.150	No	2.23	18
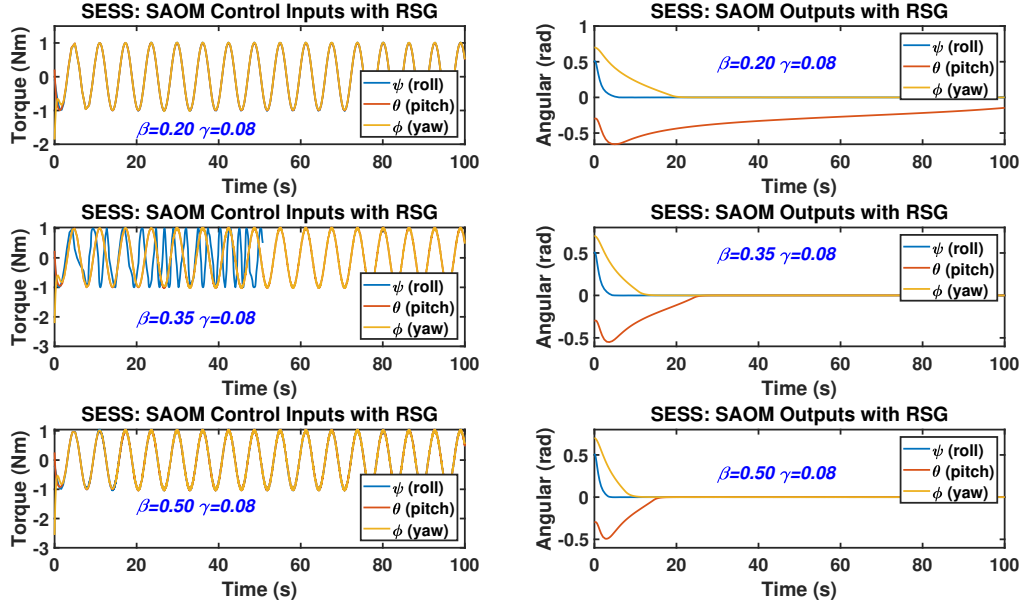
Figure 5.13: SESS-RSG: SAOM Inputs and Outputs with variable β_i and $\gamma_i = 0.08$.

Table 5.12: SVSS-LFSG and SESS-LFSG: Numeric Parameters Setup.

Switching Surface	Condition	w	y	z
SVSS	1	0.16	0.08	0.08
	2	0.32	0.16	0.16
	3	0.64	0.32	0.32
	4	1.00	0.50	0.50
SESS	1	1.00	0.50	0.50
	2	1.25	0.65	0.65
	3	2.00	1.00	1.00

84
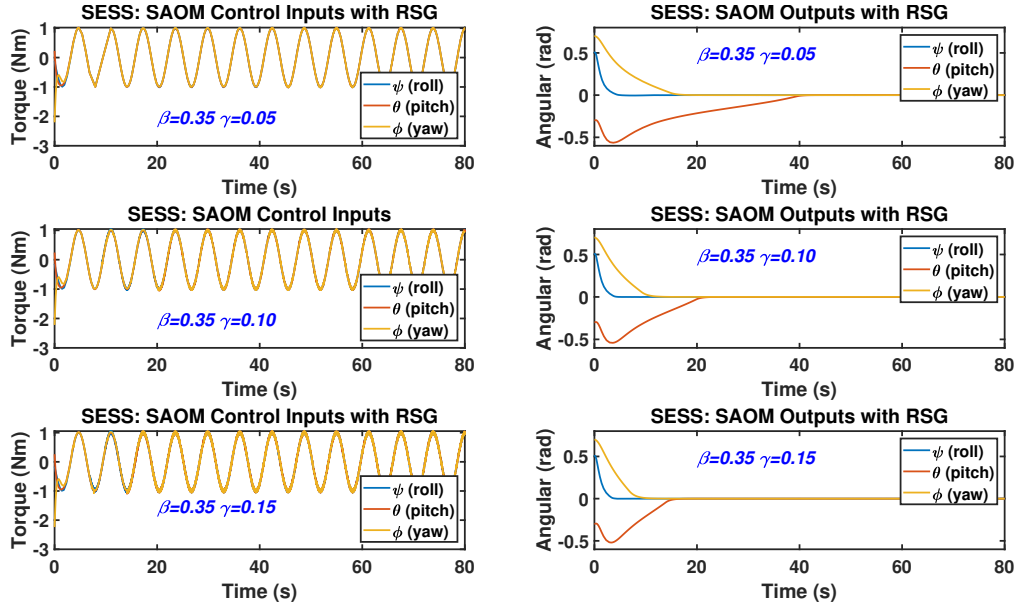
Figure 5.14: SESS-RSG: SAOM Inputs and Outputs with $\beta_i = 0.35$ and variable γ_i.

Table 5.13: SESS-LFSG: Parameters setup for λ_i.

λ_i	Value
1	0.002
2	1.000
3	0.800
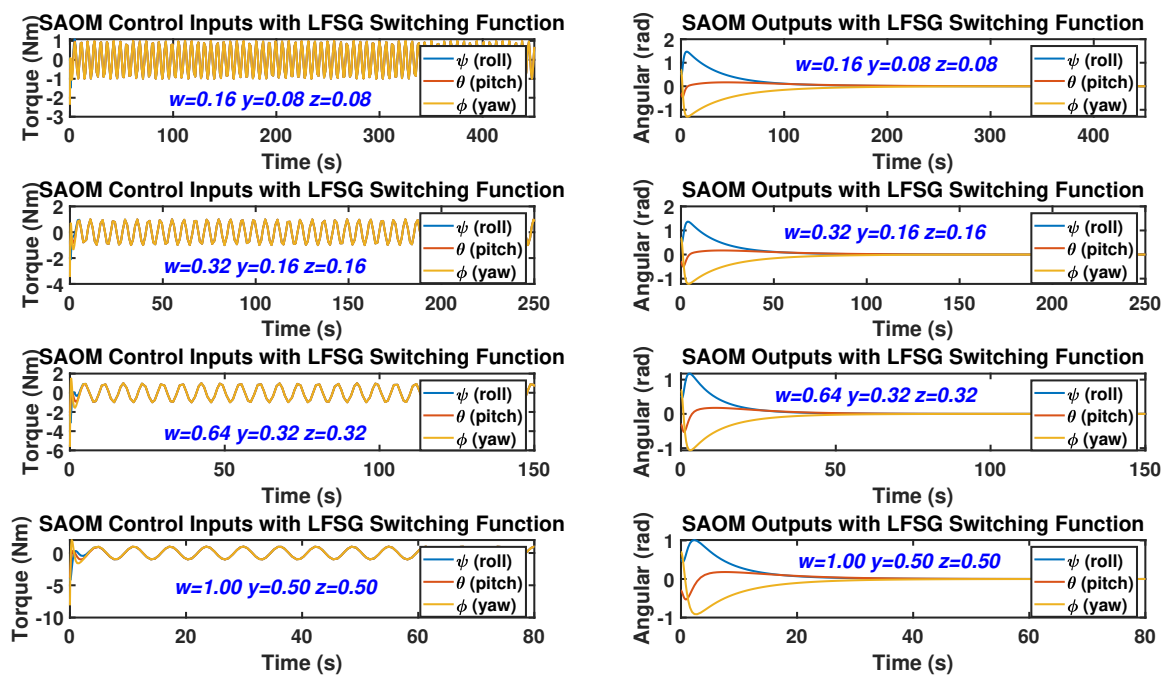
Figure 5.15: SVSS-LFSG: SAOM Inputs and Outputs with variable of w, y and z.

Table 5.14: SVSS-LFSG: Result Summary.

Switching Surface	Condition	w	y	z	Chattering	Bounded Input (Nm)	Settling Time (s)
SVSS	1	0.16	0.08	0.08	No	2.37	300
	2	0.32	0.16	0.16	No	3.46	150
	3	0.64	0.32	0.32	No	5.65	75
	4	1.00	0.50	0.50	No	8.11	50

Table 5.15: SESS-LFSG: Result Summary.

Switching Surface	Condition	w	y	z	Chattering	Bounded Input (Nm)	Settling Time (s)
SESS	1	1.00	0.50	0.50	No	1.21	60
	2	1.25	0.65	0.65	No	1.30	45
	3	2.00	1.00	1.00	No	1.54	25
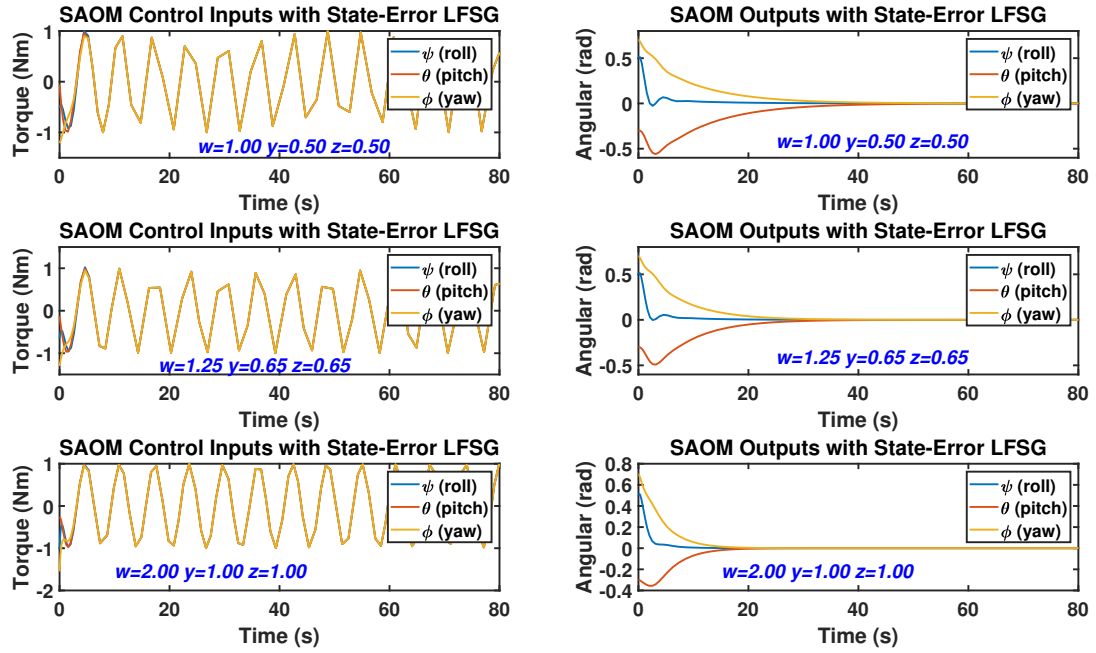
Figure 5.16: SESS-LFSG: SAOM Inputs and Outputs with variable of w, y and z.

Table 5.16: SVSS-LFSG and SESS-LFSG: Numeric Parameters Setup.

Switching Surface	Condition	w	y	z
SVSS	1		0.008	
	2	5.000	0.009	
	3		0.010	
	4		0.008	
	5	10.000	0.009	
	6		0.010	
	7		0.050	
	8	10.000	0.100	
	9		0.150	
SESS	1	0.200		
	2	0.350		0.080
	3	0.500		
	4		0.050	
	5	0.350	0.100	
	6		0.150	

5.3.5 Conclusion

In conclusion, SESS-SMC have advantages compared the SVSS-SMC. SESS-SMC requires only three parameters to determine the SAOM output characteristics. However, eighteen parameters are needed to develop the SVSS-SMC switching surface where increasing the algorithm complexity. Among the existing SFD, LFSG produced the best performances in term of the control torque range ($|1.21Nm|$) with the outputs settled at most around $63s$. Besides that, all SFD capable to force the state-variables to the desired value and also compressed the chattering drawbacks if the switching surface pa-

rameters are setted properly. Furthermore, the error of the controlled system is converged to zero in finite time. Based on this findings, therefore, a new LOSMC is proposed on the SAOM where the switching surface designed using SESS-SMC. In addition, the new algorithm used a boundary layer technique to eliminate the chattering in the control torque. Furthermore, the novelty of this technique is the new LOSMC method used errors information to auto-tuning the boundary layer width.

Chapter 6

A New Algorithm: Decaying Boundary Layer and Switching Function Method Thorough Error Feedback for Sliding Mode Control on Spacecraft's Attitude Model

A boundary layer technique is one of the most popular methods for chattering elimination in SMC. This technique strikes a trade off between invariance of system trajectories and smoothness of control [61]. The boundary layer is added inside $u(t)_n$ in $u(t)$. In [59], three boundary layer techniques around the sliding surface are introduced and discussed. The techniques are [19]:

- A constant boundary layer (CBL): CBL (Figure 6.1) is introduced to overcome the chattering problem but the control accuracy is dependent on the boundary layer width since the steady state error, $e_{ss} = 0$ if only if the state trajectory lies on $s = 0$.

- A decaying boundary layer (DBL): Subsequently, DBL (Figure 6.2) was developed and this method produced greater control accuracy when the state trajectory lies on $s = 0$ but the chattering is only eliminated for a short period.

- A state-dependent boundary layer design (SDBL): Finally, for further improvement of DBL, SDBL was proposed which produces chattering-free and high control accuracy. However, SDBL requires a high complexity algorithm.
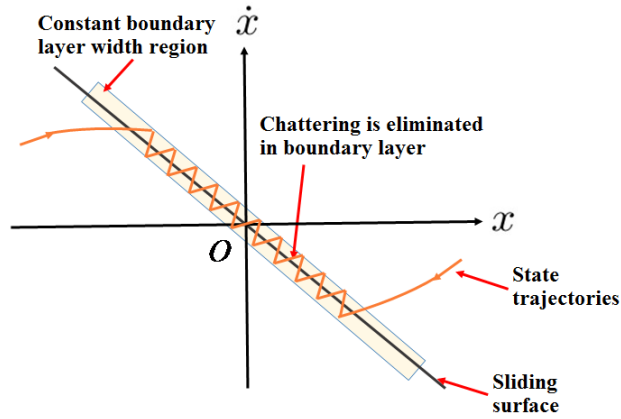
Figure 6.1: Constant boundary layer concept in SMC.
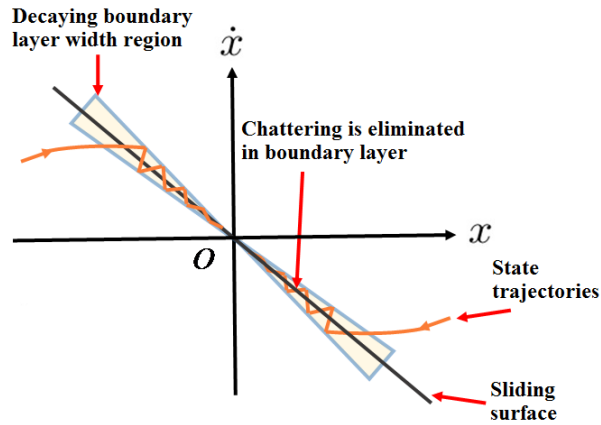
Figure 6.2: Decaying boundary layer concept in SMC.

Hence, this topic proposes an alternative improvement method to the DBL work in [59] on eliminating chattering using a DBLSF instead of using SDBL. DBLSF has less complexity compared to SDBL in [59] but produces

chattering-free and high control accuracy. The motivation to propose the DBLSF due to the conclusions obtained from section 5.3 which are:

- The best option to develop a basic SMC on the SAOM by using state-error switching surafce.

- The results show that the outputs error converge to zero throughout the time although disturbances exist in the SAOM.

Originally, in the DBL design [59], the boundary layer width varies with time. When the time approaches infinity, the boundary layer width becomes zero and hence the chattering reappears. Then, an initial improvement technique is proposed to the DBL, a decaying boundary layer thorough error feedback (DBLEF) [19]. DBLEF is proposed in order to introduce a boundary layer concept where the boundary layer width is not dependent on time. In this concept, boundary layer width will be generated every time when the error between the actual output and the required output, $|d_0| > 0$ to achieve high control accuracy.

Finally, DBLSF is introduced. DBLSF is a method where the boundary layer width and switching function are proportional to and depends upon the $|d_0|$. In DBLSF, the boundary layer width reappears every time $|d_0| > 0$. Hence, the control accuracy ($|d_0| = 0$) can be guaranteed when the disturbances and uncertainties reappear. Then, when $|d_0| = 0$, the switching function will be off in order to eliminate the chattering in the controller input.

6.1 Decaying Boundary Layer and Switching Function Thorough Error Feedback for Sliding Mode Control

Algorithm DBLSF: The boundary layer and switching function in control input will occur when $|d_0| > 0$ (Eq. 6.3). When $|d_0|$ approach to zero, the boundary layer will converge to zero (improving the control accuracy) while switching function will decaying off (eliminating the chattering). Thus, the DBLSF control development is presented in Eq. 6.1 to 6.2.

$$
\begin{aligned}
\sigma_{dblsf} &= \dot{e}_n + \lambda_n e_n, \\
\dot{\sigma}_{dblsf} &= \ddot{e}_n + \lambda_n \dot{e}_n,
\end{aligned}
\tag{6.1}
$$

$$
\begin{aligned}
u_{dblsfsmc} &= u_{dblsfeq} + u_{ndbslf}, \\
&= -B^{-1}(Ax + \lambda_n x_{n+1}) - \rho f_3,
\end{aligned}
\tag{6.2}
$$

where f_3 as in Eq. 6.3.

$$
f_3(s) = \frac{\sigma_{dblsf}(t)e^{\frac{-\pi}{|d_0|}}}{|\sigma_{dblsf}(t)| + \epsilon_0 e^{\frac{-\pi}{|d_0|}}}.
\tag{6.3}
$$

Table 6.1 shows the parametric setup for the SESS-DBLSF analysis on the SAOM model (Eq. 5.32).

Table 6.1: SESS-DBLSF: Numeric Parameter Setup.

Parameter	Value		
$\lambda_{1,2,3}$	2.6	1	0.8
$\pi_{1,2,3}$	0.05		
$\epsilon_{01,2,3}$	0.0001		
$\rho_{1,2,3}$	0.1		

Figure 6.3 illustrates the control torque and outputs of the SAOM using SESS-DBLSF. The chattering in the inputs is attenuated by the algorithm where bounded at $1.48Nm$. The outputs converged to the desired condition only around $25s$ while mantaining the control accuracy.
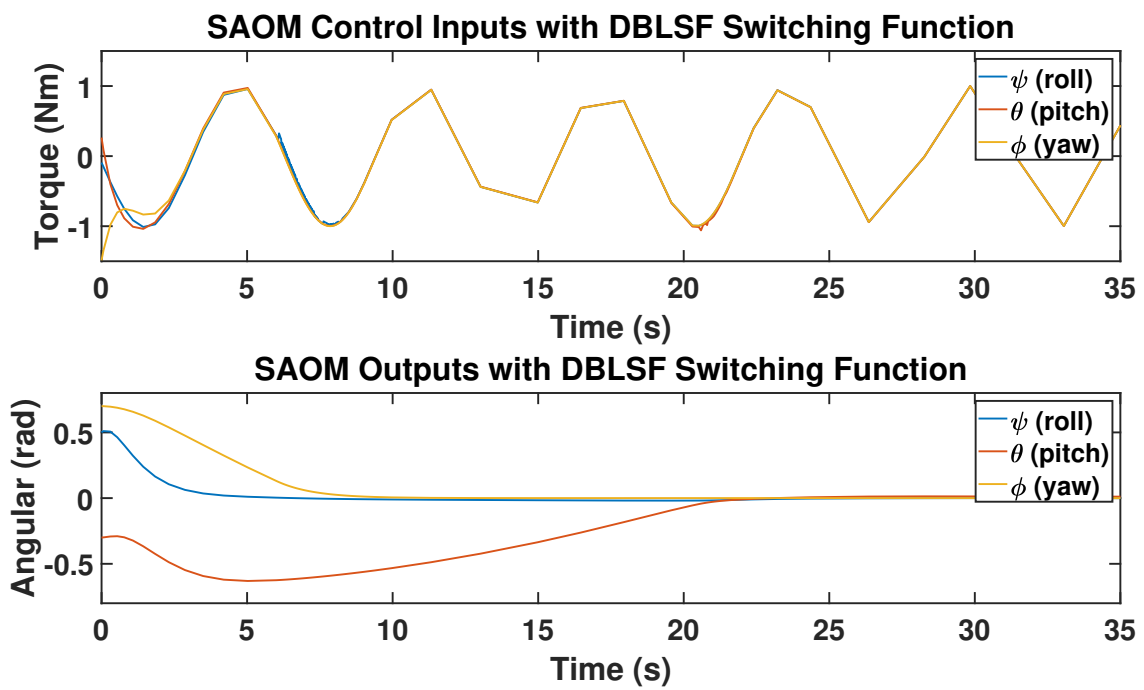
Figure 6.3: SESS-DBLSF: SAOM outputs and inputs.

6.2 Conclusion

In conclusion, the proposed DBLSF succeeded eliminate the chattering in the SMC and also able force the state-variables hitting the switching surface in finite time (fast response). However, the control torque is $1.48Nm$ which is not fulfill the actuator maximum specification, $|1Nm|$ (refer to Chapter 2, Table 2.6). Thus, the DBLSF requires an optimisation technique to make sure the SAOM's control inputs bounded at $|1Nm|$ and also-tuning the switching surface parameters using a cost function.

6.3 Optimisation in the Decaying Boundary Layer and Switching Function Thorough Error Feedback for Sliding Mode Control

In this chapter, there are several existing SMC methodologies (classical SMC, RSG, and LFSG) are evaluated on the SAOM. The techniques are designed using two switching function approaches; SVSS and SESS. The comparison results are simplified in Table 6.2 which focus on the chosen performance between SVSS and SESS. The findings concluded that SESS have the advantages compared to the SVSS. As result, a new LOSMC which is DBLSF is proposed and analysed on the ACS application using SESS switching surface. Based on the performances, the DBLSF is better than the existing SMC approaches (Table 6.3).

Table 6.2: The summary performance comparison between SVSS-SMC and SESS-SMC on the SAOM.

SMC Technique	SVSS	SESS
Classical SMC	-	✓
LFSG	-	✓

Table 6.3: The existing SMC and the DBLSF summary performance.

SMC Technique	Chattering	Bounded Input (Nm)	Settling Time (s)
Classical SMC	Yes	1.50	20
RSG	No	1.61	63
LFSG	No	1.21	60
DBLSF	No	1.48	23

On the other hand, throughout the simulation, the control torque using the classical SMC, RSG and LFSG are over than $1Nm$ and the sliding mode parameters are tuning using outputs observation technique. Thus, a cost function is required to optimize the outputs performance by adjusting

the SMC parameters automatically while let the control inputs within $1Nm$ range. Therefore, PSO is suggested to solve the drawbacks.

PSO is a straightforward concept, requires only primitive mathematical operators and needs less memory and speed of computational load where can be coded using only a few lines in the program code. Besides, PSO also suitable implements on nonlinear functions [85]. In PSO, there are two primary components used to determine the optimisation of the state, which is particle and swarm. Each particle updates their coordinates referred to the best solution (fitness) it has achieved so far, which known as *pbest*. On the other hands, the swarm keeps tracking the best value and location so far among all the particles in the population, known as (*gbest*).

Since SMC and PSO sharing similar important specifications (simple mathematical operators, required low computational load and inexpensive), thus, the combination of the PSO-DBLSF is suitable to implement on small spacecraft operation.

6.3.1 Particle Swarm Optimisation

In this topic, the PSO concept is elaborated, and the control strategies for PSO-DBLSF on SAOM is developed. In PSO, a swarm represents by a population while a particle denotes by an individual [86]. Each particle produces two parameters, which are position and velocity. The relationship between the current position and next iteration position, and velocity as in Eq. 6.4.

$$s_i(k+1) = s_i(k) + v_i(k+1), \tag{6.4}$$

where i is the particle number, k refers to the number of iteration, $s_i(k+1)$ and $v_i(k+1)$ represent the next iteration value for particle's position and velocity respectively and s_i is the current iteration for particle's position.

Then, the $v_i(k+1)$ term can be obtained using Eq. 6.5 [86].

$$v_i(k+1) = wv_i(k) + c_1r_1(pbest_i - s_i(k)) + c_2r_2(gbest_i - s_i(k)). \tag{6.5}$$

where w denotes the inertia weight for current particle's velocity, $v_i(k)$ represents the current iteration for velocity of particle, c_1, and c_2 are the cognitive

and social component which are known as learning factors and r_1 and r_2 are random number between 0 and 1.

In this study, the objective function in the SAOM model is to minimise the error value for each state (ψ, θ, ϕ). Hence, the PSO used the error values from the simulation to tuning the λ_n (Eq. 6.2), which act as the particle to improve the transient performance.

6.3.2   Results

In this topic, the spacecraft's position model (Eq. 5.32) is analysed using DBLSF and PSO-DBLSF [87]. Then, the transient performances and the outputs accuracy for both approaches are compared. The numeric parameters are set up for the SAOM, as shown in Table 6.4.

Table 6.4: Numeric parameters of the spacecraft's attitude system and PSO.

Parameter	Value	Unit
ω_O	0.0011	$rads^{-1}$
J_x	35	kgm^2
J_y	16	kgm^2
J_z	25	kgm^2
$\tau_{x,y,z}$	0.001	Nm
$d(t)$	$sin(t)$	$-$
c_1, c_2	1.42	$-$
w	0.9	$-$

Next, the λ_n values for all axis (ψ, θ and ϕ) using PSO (6.5) where the PSO coding is attached in Appendix 2 and output's observation technique are represent in Table 6.5. There are two periodic inputs given to each parameters with the state's initial condition as in Table 6.6.

Figure 6.4 shows the SAOM's outputs using the DBLSF (Figure 6.4a) and the PSO-DBLSF (Figure 6.4b) techniques. It clearly can be seen that the transient response of the PSO-DBLSF improved compared to the DBLSF. The rise time for the PSO-DBLSF's first periodic input ($0 \leq t < 75s$) are 2.746s, 3.912s and 3.207s for ψ, θ and ϕ respectively but the DBLSF shows

Table 6.5: The λ values using DBLSF and PSO-DBLSF.

	DBLSF	PSO-DBLSF
λ_ψ	0.2500	2.4567
λ_θ	0.2500	2.1442
λ_ϕ	0.2500	1.6229

Table 6.6: Inputs characteristics on the SAOM with states initial condition.

	Initial Condition	Targeted Outputs	
		$0 \leq t < 75s$	$75 \leq t \leq 150s$
Roll (ψ)	-0.50	0.50	1.00
Pitch (θ)	-0.87	1.05	0.25
Yaw (ϕ)	0.35	-1.57	-0.25

over than $8s$ for all states. In term of accuracy, the outputs error compared to the desired inputs are slightly comparable for both methods. The PSO-DBLSF recorded less maximum-error among the states (0.2095%) compared to the DBLSF (2.0200%) algorithm. On the other hand, both methods effectively eliminate the chattering in the control inputs (Figure 6.5b and Figure 6.5c) compared to the classical SMC algorithm (Figure 6.5a). Besides that, the control inputs are bounded within $1Nm$ for DBLSF and PSO-DBLSF. The detailed summary for all observations in term of the outputs accuracy comparison, control torque results and transient characteristics between the DBLSF and the PSO-DBLSF is shown in Table 6.7, Table 6.9 and Table 6.8.
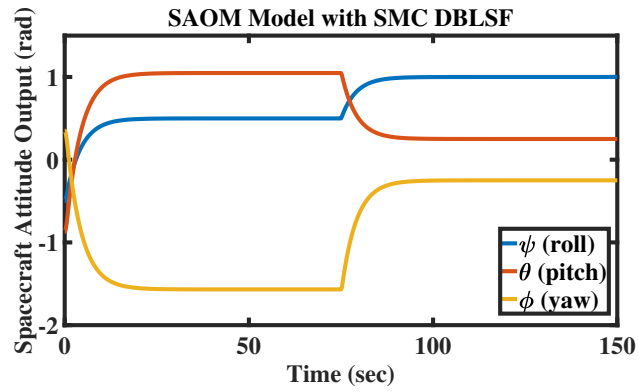
(a) DBLSF: SAOM's outputs
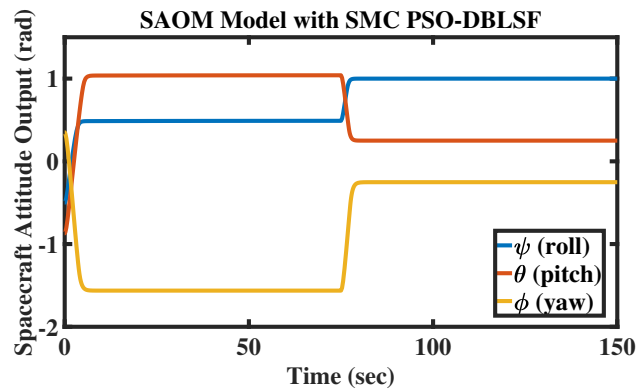
(b) PSO-DBLSF: SAOM's outputs

Figure 6.4: DBLSF and PSO-DBLSF: SAOM's outputs with pattern control torque inputs.
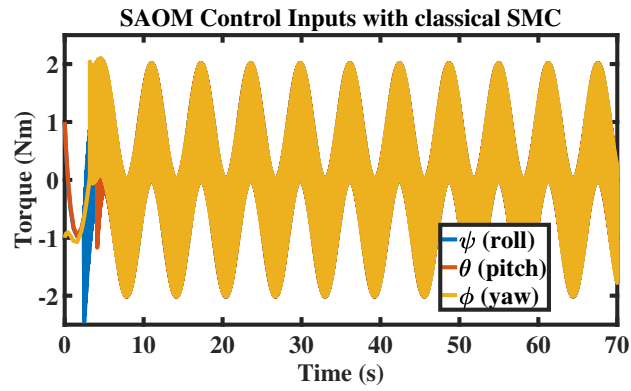
(a) Classical SMC: SAOM's control torque.
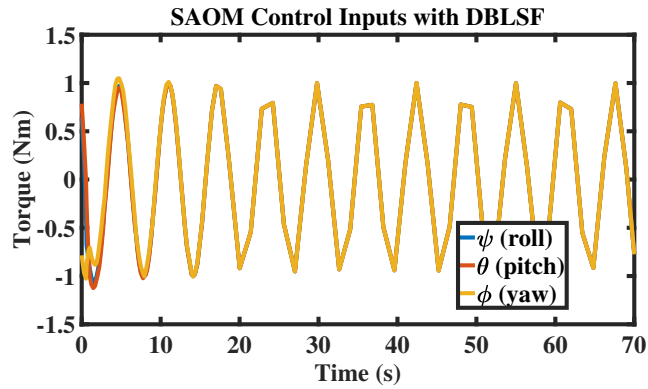
(b) DBLSF: SAOM's control torque.
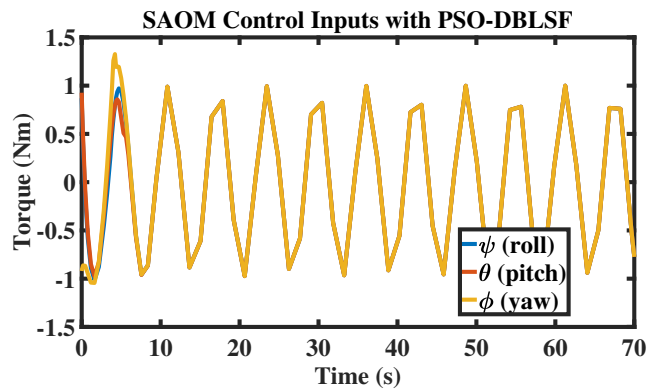
(c) PSO-DBLSF: SAOM's control torque.

Figure 6.5: The SAOM's control inputs using the classical SMC, DBLSF and PSO-DBLSF.

Table 6.7: The outputs accuracy comparison between the DBLSF and the PSO-DBLSF compared to the target output.

Output Parameters	Time (s)	Desired Output (rad)	DBLSF		PSO-DBLSF	
			Output (rad)	Error (%)	Output (rad)	Error (%)
Roll (ψ)	75	0.5000	0.4899	2.0200	0.4991	0.1800
	150	1.000	0.9997	0.0300	0.9999	0.0100
Pitch (θ)	75	1.0500	1.0402	0.9333	1.0478	0.2095
	150	0.2500	0.2503	0.1200	0.2504	0.1600
Yaw (ϕ)	75	-1.5700	-1.5628	0.4586	-1.5678	0.1401
	150	-0.2500	-0.2521	0.8400	-0.2496	0.1600

Table 6.8: DBLSF and PSO-DBLSF: The SAOM's transient comparison.

	Rise Time / Fall Time (s)	
	$0 \leq t < 75s$	
SMC Approaches	DBLSF	PSO-DBLSF
Roll (ψ)	8.713	2.746
Pitch (θ)	8.753	3.912
Yaw (ϕ)	8.753	3.207

Table 6.9: Classical SMC, DBLSF and PSO-DBLSF: The control torque performance.

SMC Technique	Chattering	Bounded Input (Nm)
Classical SMC	Yes	2.40
DBLSF	No	1.00
PSO-DBLSF	No	1.00

6.3.3 Conclusion

SMC approaches can produce high control accuracy, but the occurrence of chattering phenomena is a significant drawback. The proposed DBLSF

method in [19] can eliminate chattering; however, did not offer optimisation in the transient characteristics. Implementing a PSO on a DBLSF, then, capable of optimizing the performance of the output while maintaining the accuracy and eliminate the chattering in the control input. Besides that, the PSO algorithm also can contain the control inputs within the acceptance range for an application, which in this case is $1Nm$.

6.4　Higher-order Sliding Mode Control: Supertwisting Sliding Mode Control

STSMC is one of the HOSMC family. The STSMC formulation can be reffered in section 4.3. In this section, the STSMC and PSO-STSMC are applied on the SAOM. The objective of this study to investigate the DBLSF method compared to the STSMC for the SAOM application.

6.4.1　STSMC and PSO-STSMC

Consider a sliding variable and its dynamics in Eq. 6.6 and 6.7.

$$\sigma_i = \dot{e}_i + \lambda_{stri}, \tag{6.6}$$

$$\dot{\sigma} = \phi(\sigma, t) + \gamma(\sigma, t)u_{st}. \tag{6.7}$$

where $|\phi| \leq \Phi$, $0 \leq \Gamma_m \leq \gamma(\sigma, t) \leq \Gamma_M$ and $i = 1, 2, 3$. The STSMC controller algorithm as in Eq. 6.8 to 6.11.

$$u_{st} = u_{1ss} + u_{2ss}, \tag{6.8}$$

with

$$\dot{u_{1ss}} = \begin{cases} -u_{stri}, & \text{if } |u_{stri}| > U_{ss}, \\ -W_{stri}sgn(\sigma_i), & \text{if } |u_{stri}| \leq U_{ss}, \end{cases} \tag{6.9}$$

and

$$u_{2ss} = \begin{cases} -L_{stri}|s_{0tri}|^{0.5}sgn(\sigma_i), & \text{if } |s_{tri}| > s_{0tri}, \\ -L_{stri}|s_{tri}|^{0.5}sgn(\sigma_i), & \text{if } |s_{tri}| \leq s_{0tri}. \end{cases} \tag{6.10}$$

with s_0 is boundary layer width around the sliding surface and U_{ss} is the maximum control input. In (6.9) and (6.10), the W_{stri} and L_{stri} are constant and can be computed based on Eq. 6.11.

$$
\begin{aligned}
W_{stri} &= \frac{\Phi}{\Gamma_m}, \\
L_{stri} &= \frac{4\Phi}{\Gamma_m^2} \frac{\Gamma_M(W_{stri} + \Phi)}{\Gamma_m(W_{stri} - \Phi)}.
\end{aligned}
\tag{6.11}
$$

Then, the STSMC and PSO-STSMC numeric parameters setup as in Table 6.10. The STSMC parameters are tuning manually using output observation technique while PSO-STSMC values are auto-adjusted using PSO code (Appendix 2). Table 6.11 shows the desired outputs with the state-variables initial condition.

Table 6.10: The super twisting parameter values for STSMC and PSO-STSMC on the SAOM.

		STSMC	PSO-STSMC
λ_{str}	λ_{str1}	0.2500	0.2620
	λ_{str2}	0.2500	0.5955
	λ_{str3}	0.2500	0.3039
W_{str}	W_{str1}	44001.0	18566.0
	W_{str2}	18334.0	30478.0
	W_{str3}	31429.0	4269.6
L_{str}	L_{str1}	91915.0	97086.0
	L_{str2}	36390.0	92533.0
	L_{str3}	67959.0	70670.0
s_{0tr}	s_{0tr1}	0.01	0.1
	s_{0tr2}	0.01	0.2
	s_{0tr3}	0.01	0.01

Table 6.11: STSMC and PSO-STSMC: States desired outputs with initial conditions.

	Initial Condition	Targeted Outputs
Roll (ψ)	-0.50	0.50
Pitch (θ)	-0.87	1.05
Yaw (ϕ)	0.35	-1.57

6.4.2 Results

Figure 6.6 and Figure 6.7 present the SAOM's control outputs and inputs accordingly, with STSMC and PSO-STSMC techniques. The PSO-STSMC drives the states to the desired outputs faster than STSMC. However, the STSMC method is not appropriate for the SAOM due to the control torque performance. The STSMC and PSO-STSMC recorded the maximum control torque at least $7000Nm$ which is inlogical for the SAOM operation. Thus, the STSMC in not suitable for the SAOM.
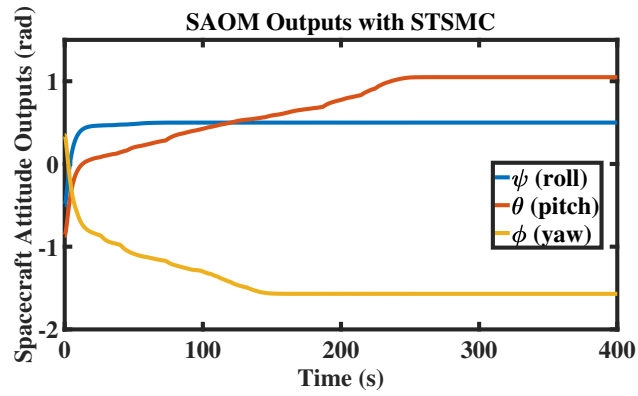
(a) SAOM outputs using STSMC method.
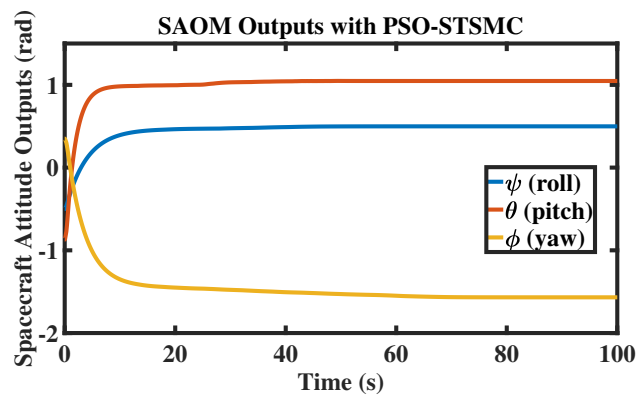
(b) SAOM outputs using PSO-STSMC method.

Figure 6.6: SAOM outputs with STSMC and PSO-STSMC.
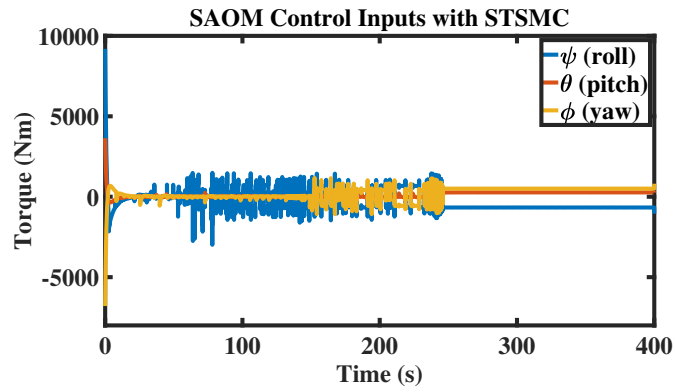
(a) SAOM control inputs using STSMC method.
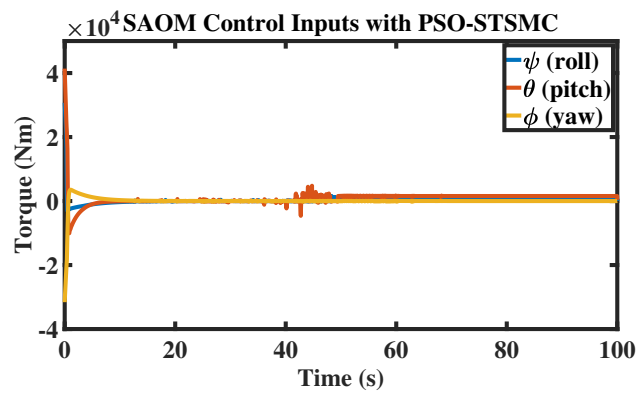
(b) SAOM control inputs using PSO-STSMC method.

Figure 6.7: SAOM control inputs with STSMC and PSO-STSMC.

6.5   Conclusion

This chapter introduced, designed and analysed the SMC approaches (LOSMC and HOSMC) to eliminate the chattering drawbacks in SMC. The conventional SMC and the LOSMC (RSG and LFSG) switching surface are developed using SESS-SMC and SVSS-SMC. SESS-SMC, however, performed better than SVSS-SMC subjected to the control torque and outputs transient. Furthermore, SESS-SMC needs only three parameters to construct the swicthing surface algorithm while SVSS-SMC requires eighteen parameters. Then, a new LOSMC boundary layer technique (DBSLF) is proposed and designed using SESS-SMC switching surface. The algorithm used error to control the boundary layer width to suppress the chattering and produced high-accuracy outputs. However, a cost function is required to contain the DBLSF on the SAOM control torque within $|1Nm|$ and improved the transient trajectory. Hence, a PSO is introduced to the system. As the results, the PSO able to enhance the DBLSF weakness. For comparison, a STSMC (HOSMC) is applied on the SAOM. The results show that the STSMC and PSO-STSMC is unsuitable for the SAOM application due to the control torque performance. In conclusion, the new DBLSF computes the best results compared to the classical SMC, RSG, LFSG and STSMC with PSO existance.

Chapter 7

Spacecraft's Rendezvous and Docking Manoeuvres with Sliding Mode Control Methods Formulation and Results

7.1   Introduction

A rendezvous and docking manoeuvres involved a passive (target) and active (chaser) vehicles [3]. International space station (ISS) is one of the non-maneuvring (passive) vehicles where the space shuttle is the nominal chaser. Then, an insensitive control approach with high-accuracy and fast response is a must for this attitude control subsystem (ACS) application. Hence, this chapter is organised as per below:

1. Spacecraft's rendezvous and docking manoeuvres (SRDM) formulation begin with the model developement using the equations of motion between the target and chaser vehicles. Then, the relative acceleration formula between the chaser (moving-frame) and ECI (fixed-frame) is constructed. Then, the outcomes of the formulation is translated to a state-space form for further investigation and analysis.

2. Based on Chapter 4, the DBLSF performed better than other SMC approaches on the SAOM. Thus, the DBLSF is chosen for the SRDM control design. However, the STSMC also is injected to the SRDM to

investigate the effect of HOSMC to the application. Then, the comparison of the methods are compared. Moreover, the PSO is applied on both methodologies to enhance the SRDM performance.

7.2 Spacecraft's Rendezvous and Docking Manoeuvres Formulation

The SRDM formulation is divided into three stages. In the end, a sixth-order of SRDM system is expected due to the spacecraft's direction in x, y and z-axis. Then, the modeling system's converted to the state-space form for the controller implementation and analysis.

7.2.1 First Stage

The equations of relative motion between B and C can be derived based on Fig. 7.1. Using Newton's first law, the total forces between B and C as in Eq. 7.1.
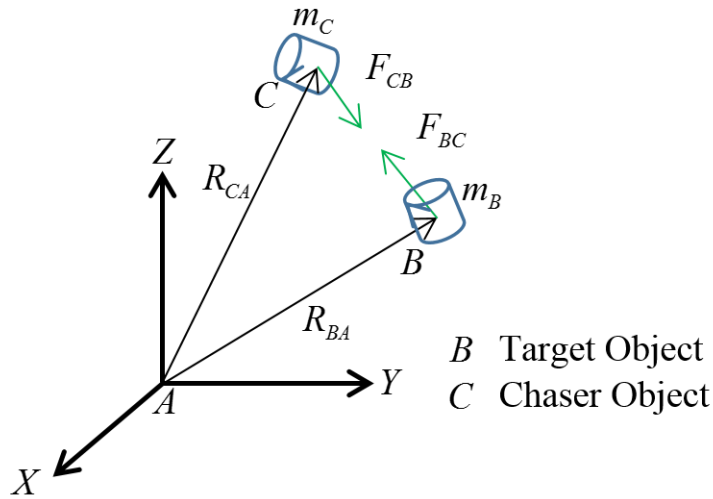
Figure 7.1: The forces act between two vehicles.

$$F_{BC} = -F_{CB}, \tag{7.1}$$

However, according to Newton's gravitational law,

$$F_{BC} \quad = \quad m_B \ddot{R}_{BA} \quad = \quad G\frac{m_B m_C}{r^2}\hat{u}_R, \tag{7.2}$$

113

$$F_{CB} = m_C \ddot{R}_{CA} = G\frac{m_C m_B}{r^2}(-\hat{u}_r,)$$
$$= -G\frac{m_C m_B}{r^2}\hat{u}_r, \tag{7.3}$$

where $r = R_{BA} - R_{CA}$, m_B is mass of vehicle B and m_C is mass of vehicle C. Next, multiply Eq. 7.2 with m_C and Eq. 7.3 with m_B and get Eq. 7.4 and Eq. 7.5 respectively with $\hat{u}_r = \dfrac{\mathrm{r}}{r}$.

$$m_B m_C \ddot{R}_{BA} = G\frac{m_B m_C^2 r}{r^2}\frac{\mathrm{r}}{r},$$
$$= G\frac{m_B m_C^2}{r^3}\mathrm{r}, \tag{7.4}$$

$$m_C m_B \ddot{R}_{CA} = -G\frac{m_B^2 m_C}{r^2}\frac{\mathrm{r}}{r},$$
$$= -G\frac{m_B^2 m_C}{r^3}\mathrm{r}, \tag{7.5}$$

Then, subtracting Eq. 7.4 and Eq. 7.5 to get Eq. 7.6.

$$m_B m_C(\ddot{R}_{BA} - \ddot{R}_{CA}) = -G m_B m_C\frac{(m_B + m_C)}{r^3}\mathrm{r}, \tag{7.6}$$

Hence, cancelling m_B and m_C on both sides and attain the equations of motion as in Eq. 7.7.

$$\ddot{\mathrm{r}} = -G\frac{(m_B + m_C)}{r^3}\mathrm{r},$$
$$= -\frac{\mu}{r^3}\mathrm{r}, \tag{7.7}$$

where $\mu = G(m_B + m_C)$ which is gravitational parameter.

According to Fig. 7.2, the position of vehicle C as in Eq. 7.8, the acceleration as in Eq. 7.9 and the forces per unit mass acted on chaser as in Eq. 7.10.

$$R_{CA} = R_{BA} + \delta R_{CB}, \tag{7.8}$$

$$\delta \ddot{R}_{CA} = \ddot{R}_{BA} + \delta \ddot{R}_{CB}, \tag{7.9}$$

$$F_C = F_{\delta R_{CB}} + F_{R_{CA}},$$

$$m_C \ddot{R}_{CA} = F_{\delta R_{CB}} - \mu m_C \frac{R_{CA}}{R_{CA}^3}, \tag{7.10}$$

$$\ddot{R}_{CA} = \frac{F_{\delta R_{CB}}}{m_C} - \mu \frac{R_{CA}}{R_{CA}^3},$$

Replaced Eq. 7.9 and 7.8 into Eq. 7.10 to get the acceleration between chaser and target as in Eq. 7.11.

$$\ddot{R}_{BA} + \delta \ddot{R}_{CB} = \frac{F_{\delta R_{CB}}}{m_C} - \mu \frac{(R_{BA} + \delta R_{CB})}{R_{CA}^3},$$

$$\delta \ddot{R}_{CB} = \frac{F_{\delta R_{CB}}}{m_C} - \mu \frac{(R_{BA} + \delta R_{CB})}{R_{CA}^3} - \ddot{R}_{BA}, \tag{7.11}$$

However, Eq. 7.11 can be simplified by using the properties as in Eq. 7.12.

$$R_{CA}^2 = R_{CA}.R_{CA} = (R_{BA} + \delta R_{CB}).(R_{BA} + \delta R_{CB}),$$

$$= R_{BA}^2 + 2R_{BA}.\delta R_{BC} + \delta R_{CB}^2,$$

$$= R_{BA}^2 \left(1 + \frac{2R_{BA}.\delta R_{BC}}{R_{BA}^2} + \frac{\delta R_{CB}^2}{R_{BA}^2} \right), \tag{7.12}$$

However, the distance between B and C (δR_{CB}) is too small compared to R_{BA} and R_{CA}. Hence $\dfrac{\delta R_{CB}}{R_{BA}} <<< 1$. Then, Eq. 7.12 becomes Eq. 7.13
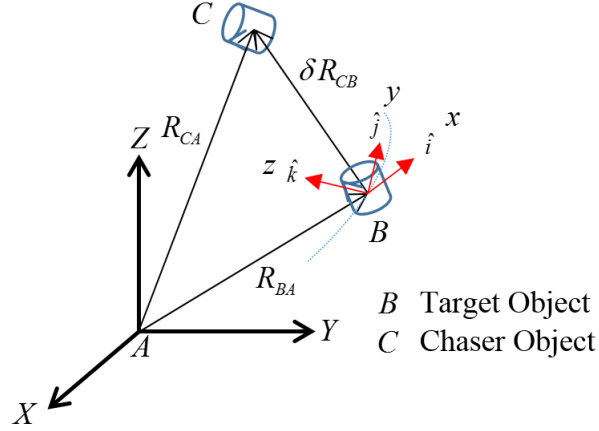
Figure 7.2: Trajectory of target and chaser object using Clohessy-Wiltshire frame.

$$R_{CA}^2 = R_{BA}^2 \left(1 + \frac{2R_{BA}.\delta R_{CB}}{R_{BA}^2} \right), \quad (7.13)$$

In order to make Eq. 7.13 comparable to Eq. 7.11, thus, Eq. 7.13 becomes Eq. 7.14.

$$R_{CA}^2 R_{CA}^{-3/2} = R_{BA}^2 \left(1 + \frac{2R_{BA}.\delta R_{CB}}{R_{BA}^2} \right) R_{CA}^{-3/2},$$

$$R_{CA}^{-3} = R_{BA}^{-3} \left(1 + \frac{2R_{BA}.\delta R_{CB}}{R_{BA}^2} \right)^{-3/2}, \quad (7.14)$$

Applying binomial theorem on Eq. 7.14, hence becomes Eq. 7.15.

$$\left(1 + \frac{2R_{BA}.\delta R_{CB}}{R_{BA}^2} \right)^{-3/2} = \left(1 + \left(-\frac{3}{2} \right) \left(\frac{2R_{BA}.\delta R_{CB}}{R_{BA}^2} \right) \right),$$

$$= 1 - 3 \left(\frac{R_{BA}.\delta R_{CB}}{R_{BA}^2} \right), \quad (7.15)$$

Replaced Eq. 7.15 into Eq. 7.14 and produces Eq. 7.16.

$$
\begin{aligned}
R_{CA}^{-3} &= R_{BA}^{-3}\left(1 - 3\left(\frac{R_{BA}.\delta R_{CB}}{R_{BA}^2}\right)\right), \\
\frac{1}{R_{CA}^3} &= \frac{1}{R_{BA}^3} - \frac{3R_{BA}.\delta R_{CB}}{R_{BA}^5},
\end{aligned}
\tag{7.16}
$$

Substituted Eq. 7.16 into Eq. 7.11 and get Eq. 7.17.

$$
\begin{aligned}
\delta \ddot{R}_{CB} &= -\ddot{R}_{BA} - \mu\left(\frac{1}{R_{BA}^3} - \frac{3R_{BA}.\delta R_{CB}}{R_{BA}^5}\right).(R_{BA} + \delta R_{CB}) + \frac{F_{\delta R_{CB}}}{m_C}, \\
&= -\ddot{R}_{BA} - \mu\frac{R_{BA}}{R_{BA}^3} - \mu\frac{\delta R_{CB}}{R_{BA}^3} - \mu\frac{3R_{BA}.\delta R_{CB}}{R_{BA}^5}.(R_{BA} + \delta R_{CB}) + \frac{F_{\delta R_{CB}}}{m_C}, \\
&= -\ddot{R}_{BA} - \mu\frac{R_{BA}}{R_{BA}^3} - \mu\frac{\delta R_{CB}}{R_{BA}^3} - \mu\frac{3(R_{BA}.\delta R_{CB}).R_{BA}}{R_{BA}^5} + \frac{F_{\delta R_{CB}}}{m_C},
\end{aligned}
\tag{7.17}
$$

with $(R_{BA}.\delta R_{CB})\delta R_{CB}$ can be neglected because of $\delta R_{CB}{}^2$. On the other hands, $\ddot{R}_{BA} = -\mu\dfrac{R_{BA}}{R_{BA}^3}$. Finally, Eq. 7.17 becomes Eq. 7.18.

$$
\delta \ddot{R}_{CB} = -\frac{\mu}{R_{BA}^3}\left(\delta R_{CB} + 3\frac{(R_{BA}.\delta R_{CB})R_{BA}}{R_{BA}^2}\right) + \frac{F_{\delta R_{CB}}}{m_C}.
\tag{7.18}
$$

7.2.2   Second Stage

The second stage begin with finding the relative acceleration formula between point C with respect to point A as in Eq. 7.19 to Eq. 7.25. The position of C relatives to A as in Eq. 7.19.

$$R_{CA} = R_{BA} + \delta R_{CB}, \tag{7.19}$$

where $\delta R_{CB} = x\hat{i} + y\hat{j} + z\hat{k}$. Next, Eq. 7.20 shows the dynamic of Eq. 7.19 in term of velocity.

$$\dot{R}_{CA} = \dot{R}_{BA} + \delta \dot{R}_{CB}, \tag{7.20}$$

But,

$$\begin{aligned} \delta \dot{R}_{CB} &= \dot{x}\hat{i} + \dot{y}\hat{j} + \dot{z}\hat{k} + x\dot{\hat{i}} + y\dot{\hat{j}} + z\dot{\hat{k}}, \\ &= \delta v_{CB} + \Omega{\times}\delta R_{BC}, \end{aligned} \tag{7.21}$$

Replaced Eq. 7.21 into Eq. 7.20 and becomes Eq. 7.22.

$$v_{R_{CA}} = v_{BA} + \delta v_{CB} + \Omega{\times}\delta R_{CB}, \tag{7.22}$$

The acceleration between point C and A is given in Eq. 7.23.

$$\begin{aligned} \dot{v_{R_{CA}}} &= \dot{v_{BA}} + \delta\dot{v_{CB}} + \frac{d}{dt}(\Omega{\times}\delta R_{CB}), \\ a_{R_{CA}} &= a_{BA} + \delta\dot{v_{CB}} + \dot{\Omega} \times \delta R_{CB} + \Omega{\times}\delta \dot{R}_{CB}, \end{aligned} \tag{7.23}$$

However, from Eq. 7.21, $\delta v_{CB} = \dot{x}\hat{i} + \dot{y}\hat{j} + \dot{z}\hat{k}$. Hence, the dynamic of this term as in Eq. 7.24.

$$\begin{aligned} \delta\dot{v_{CB}} &= \ddot{x}\hat{i} + \ddot{y}\hat{j} + \ddot{z}\hat{k} + \dot{x}\dot{\hat{i}} + \dot{y}\dot{\hat{j}} + \dot{z}\dot{\hat{k}}, \\ &= \delta a_{CB} + \Omega{\times}\delta v_{CB}, \end{aligned} \tag{7.24}$$

Substituted Eq. 7.21 and Eq. 7.24 into Eq. 7.23 and produces Eq. 7.25, the relative acceleration formula between C with respect to A.

$$
\begin{aligned}
a_{R_{CA}} &= a_{BA} + \delta a_{CB} + \Omega \times \delta v_{CB} + \dot{\Omega} \times \delta R_{CB} + \Omega \times (\delta v_{CB} + \Omega \times \delta R_{CB}), \\
&= a_{BA} + \delta a_{CB} + 2\Omega \times \delta v_{CB} + \dot{\Omega} \times \delta R_{CB} + \Omega \times \Omega \times \delta R_{CB}.
\end{aligned}
$$

$$(7.25)$$

The next stage is to obtain the relationship between kinematics and equations of motion based on Eq. 7.25 which refer to δR_{CB}. The orbit of the target (A) is assumed in circular which is a good assumption for a space station in LEO [3]. Thus, the angular velocity of target vehicle as in Eq. 7.26.

$$\Omega \;=\; n\hat{k} \;=\; \sqrt{\frac{\mu}{R_{BA}^3}}\hat{k} \;=\; \text{constant,}$$
$$\dot{\Omega} \;=\; 0,$$

(7.26)

Previously,

$$\delta R_{CB} \;=\; \delta x\hat{i} + \delta y\hat{j} + \delta z\hat{k},$$
$$\delta v_{CB} \;=\; \delta\dot{x}\hat{i} + \delta\dot{y}\hat{j} + \delta\dot{z}\hat{k},$$
$$\delta a_{CB} \;=\; \delta\ddot{x}\hat{i} + \delta\ddot{y}\hat{j} + \delta\ddot{z}\hat{k},$$

(7.27)

Then, Eq. 7.26 and Eq. 7.27 are replaced in Eq. 7.25 and produces Eq. 7.28.

$$\delta\ddot{R}_{CB} \;=\; \delta\ddot{x}\hat{i} + \delta\ddot{y}\hat{j} + \delta\ddot{z}\hat{k} + 2n\hat{k} \times (\delta\dot{x}\hat{i} + \delta\dot{y}\hat{j} + \delta\dot{z}\hat{k})$$
$$+ n\hat{k} \times n\hat{k} \times (\delta x\hat{i} + \delta y\hat{j} + \delta z\hat{k}),$$

(7.28)

From Eq. 7.28, thus

$$2n\hat{k} \times (\delta\dot{x}\hat{i} + \delta\dot{y}\hat{j} + \delta\dot{z}\hat{k}) \;=\; -2n\delta\dot{y}\hat{i} + 2n\delta\dot{x}\hat{j},$$

(7.29)

$$n\hat{k} \times n\hat{k} \times (\delta x\hat{i} + \delta y\hat{j} + \delta z\hat{k}) \;=\; -n^2\delta x\hat{i} - n^2\delta y\hat{j},$$

(7.30)

Replaced Eq. 7.29 and Eq. 7.30 into Eq. 7.28, generates Eq. 7.31 where the equations of motion based on Eq. 7.25.

$$\delta\ddot{R}_{CB} \;=\; \delta\ddot{x}\hat{i} + \delta\ddot{y}\hat{j} + \delta\ddot{z}\hat{k} - 2n\delta\dot{y}\hat{i} + 2n\delta\dot{x}\hat{j} - n^2\delta x\hat{i} - n^2\delta y\hat{j},$$
$$=\; (\delta\ddot{x} - 2n\delta\dot{y} - n^2\delta x)\hat{i} + (\delta\ddot{y} + 2n\delta\dot{x} - n^2\delta y)\hat{j} + (\delta\ddot{z})\hat{k}.$$

(7.31)

7.2.3　Third Stage

Replaced Eq. 7.27 into Eq. 7.18 with

$$R_{BA} = R_{BA}\hat{i},$$

$$R_{BA}.\delta R_{CB} = (R_{BA}\hat{i}).(\delta x\hat{i} + \delta y\hat{j} + \delta z\hat{k}) = R_{BA}\delta x,$$

$$\frac{\mu}{R_{BA}^3} = n^2,$$

$$F_{\delta R_{CB}} = F_{\delta x}\hat{i} + F_{\delta y}\hat{j} + F_{\delta z}\hat{k},$$

to get Eq. 7.32.

$$
\begin{aligned}
\delta \ddot{R}_{CB} &= -n^2((\delta x\hat{i} + \delta y\hat{j} + \delta z\hat{k}) - \frac{3}{R_{BA}^2}(R_{BA}\delta_x).(R_{BA}\hat{i})) + \frac{(F_{\delta x}\hat{i} + F_{\delta y}\hat{j} + F_{\delta z}\hat{k})}{m_C}, \\
&= -n^2((\delta x\hat{i} + \delta y\hat{j} + \delta z\hat{k}) - 3\delta x\hat{i})) + \frac{(F_{\delta x}\hat{i} + F_{\delta y}\hat{j} + F_{\delta z}\hat{k})}{m_C}, \\
&= \left(2n^2\delta_x + \frac{F_{\delta x}}{m_C}\right)\hat{i} + \left(\frac{F_{\delta y}}{m_C} - n^2\delta_y\right)\hat{j} + \left(\frac{F_{\delta z}}{m_C} - n^2\delta_z\right)\hat{k},
\end{aligned}
$$

$$(7.32)$$

Lets combine Eq. 7.31 (equations of motion) and Eq. 7.32 (a kinematic relationship) to produce Eq. 7.33.

$$
\begin{aligned}
\delta\ddot{x} - 2n\delta\dot{y} - n^2\delta x)\hat{i} + (\delta\ddot{y} + 2n\delta\dot{x} - n^2\delta y)\hat{j} + (\delta\ddot{z})\hat{k} &= \\
\left(2n^2\delta_x + \frac{F_{\delta x}}{m_C}\right)\hat{i} + \left(\frac{F_{\delta y}}{m_C} - n^2\delta_y\right)\hat{j} + \left(\frac{F_{\delta z}}{m_C} - n^2\delta_z\right)\hat{k},&
\end{aligned}
$$

$$(7.33)$$

Finally, the relative dynamic model of SRDM by following Clohessy-Wiltshire based on Eq. 7.33 as in Eq. 7.34.

$$\delta\ddot{x} - 2n\delta\dot{y} - 3n^2\delta x = \frac{F_{\delta x}}{m_C},$$

$$\delta\ddot{y} + 2n\delta\dot{x} = \frac{F_{\delta y}}{m_C}, \qquad (7.34)$$

$$\delta\ddot{z} + n^2\delta z = \frac{F_{\delta z}}{m_C}.$$

For control algorithm implementation and further analysis, Eq. 7.34 can be represented in state-space form below.

$$
\begin{bmatrix} \dot{x}_1 \\ \dot{x}_2 \\ \dot{x}_3 \\ \dot{x}_4 \\ \dot{x}_5 \\ \dot{x}_6 \end{bmatrix}
=
\begin{bmatrix}
0 & 1 & 0 & 0 & 0 & 0 \\
3n^2 & 0 & 0 & 2n & 0 & 0 \\
0 & 0 & 0 & 1 & 0 & 0 \\
0 & -2n & 0 & 0 & 0 & 0 \\
0 & 0 & 0 & 0 & 0 & 1 \\
0 & 0 & 0 & 0 & -n^2 & 0
\end{bmatrix}
\begin{bmatrix} x_1 \\ x_2 \\ x_3 \\ x_4 \\ x_5 \\ x_6 \end{bmatrix}
+
\begin{bmatrix}
0 & 0 & 0 \\
\dfrac{1}{m_C} & 0 & 0 \\
0 & 0 & 0 \\
0 & \dfrac{1}{m_C} & 0 \\
0 & 0 & 0 \\
0 & 0 & \dfrac{1}{m_C}
\end{bmatrix}
\begin{bmatrix} u_x + w_x \\ u_y + w_y \\ u_z + w_z \end{bmatrix}
$$

$$(7.35)$$

where

$$\begin{bmatrix} \delta_x & \dot{\delta}_x & \delta_y & \dot{\delta}_y & \delta_z & \dot{\delta}_z \end{bmatrix}^T = \begin{bmatrix} x_1 & x_2 & x_3 & x_4 & x_5 & x_6 \end{bmatrix}^T$$

$$\begin{bmatrix} \dot{\delta}_x & \ddot{\delta}_x & \dot{\delta}_y & \ddot{\delta}_y & \dot{\delta}_z & \ddot{\delta}_z \end{bmatrix}^T = \begin{bmatrix} \dot{x}_1 & \dot{x}_2 & \dot{x}_3 & \dot{x}_4 & \dot{x}_5 & \dot{x}_6 \end{bmatrix}^T$$

$$(u_x, u_y, u_z) = (F_{\delta x}, F_{\delta y}, F_{\delta z})$$

(w_x, w_y, w_z) are the component of the external disturbances.

122

7.3 Decaying Boundary Layer and Switching Function Thorough Error Feedback on the SRDM

SMC is one of the established tools to deal with the uncertain system while robust insensitive towards unmatched uncertainties [75]. SMC manipulates the inputs of a system by introducing a control input $(u_{smc}(t))$ comprises two important basis, sliding surface $(u_{eq}(t))$ and switching surface $(u_n(t))$, as in Eq. 7.36 [88].

$$u_{smc}(t) = u_{eq}(t) + u_n(t). \tag{7.36}$$

The SMC control input algorithm is developed using the DBLSF due to the advantages obtained from Chapter 4 where SESS-SMC is basis for the switching surface design. Therefore, the DBLSF and PSO-DBLSF strengths and weakness are obtained and presented at the end of this topic. Moreover, the SRDM requires force input to move the chaser to the target. Thus, a different SRDM outcomes contrast to the SAOM are predicted.

7.3.1 The DBLSF Parameter Setup on the SRDM

The DBLSF algorithm is introduced and explained in section 5.4. The SRDM model (Eq. 7.35) parameters are set as in Table 7.1. Table 7.2 presents the λ_{sfm} values for the SESS-DBLSF-SMC switching surface design and its dynamic (Eq. 7.37). The λ_{sfm} values for the DBLSF and PSO-DBLSF are chosen using output observation technique and PSO respectively.

$$
\begin{aligned}
\sigma(t) &= \dot{e}(t) + \lambda_{sfm}e(t), \\
\dot{\sigma}(t) &= \ddot{e}(t) + \lambda_{sfm}\dot{e}(t).
\end{aligned}
\tag{7.37}
$$

Table 7.1: Numeric Paramater of the Spacecraft Rendezvous and Docking Manoeuvres System [7].

Parameter	Value	Unit
n	7.2722×10^{-5}	$rads^{-1}$
m_C	300	kg
$[x_1(0), x_2(0), x_3(0)]$	[800,600,500]	m
$[x_2(0), x_4(0), x_6(0)]$	[0,0,0]	m
$W_{x,y,x}$	$10 sint(t)$	$0 < t < 30s$
U_{max}	4000	N

Table 7.2: The λ_{sfm} values for DBLSF and PSO-DBLSF on SRDM.

	DBLSF	PSO-DBLSF
λ_{sfm1}	0.0100	0.0035
λ_{sfm2}	0.0100	0.0052
λ_{sfm3}	0.0100	0.0043

7.3.2 Results

Figure 7.3 and 7.4 illustrate the DBLSF and PSO-DBLSF control outputs and inputs on the SRDM. The PSO-DBLSF converge the chaser to the target faster than DBLSF improved at least almost 40%. There is no chattering observed in the control force where less than $|2N|$ recorded for both methods. Besides that, the phase plane potrait for the PSO-DBLSF (Figure 7.5b) compared to the DBLSF (Figure 7.5b) is almost identical to the ideal switching surface trajectory (Figure 7.6).
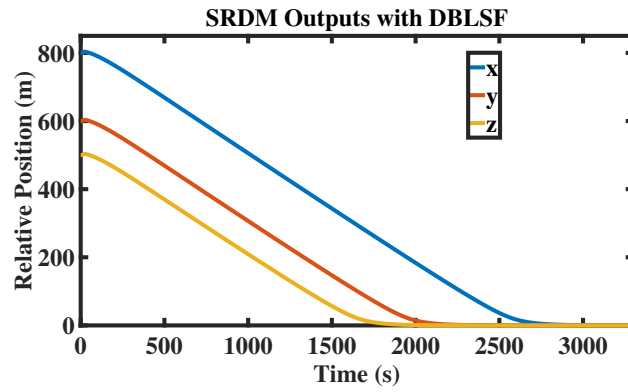
(a) SRDM outputs using DBLSF method.
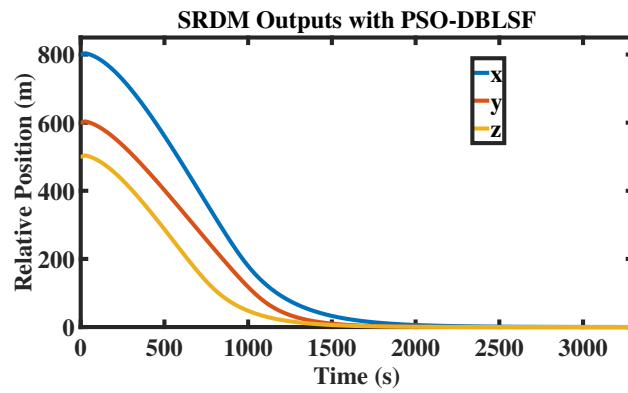
(b) SRDM outputs using PSO-DBLSF method.

Figure 7.3: SRDM outputs with DBLSF and PSO-DBLSF approaches.
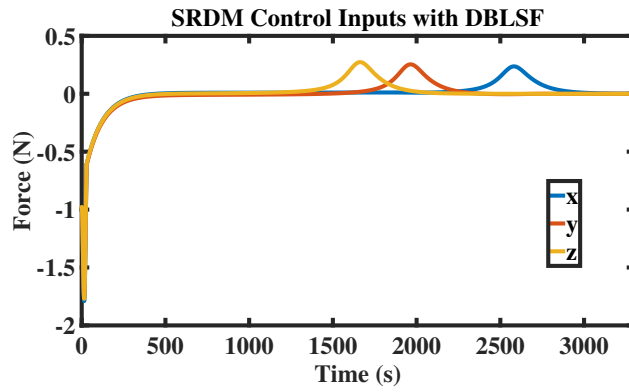
(a) SRDM control inputs using DBLSF technique.
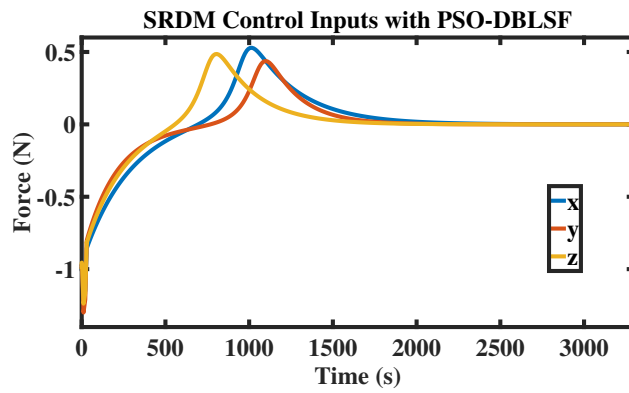
(b) SRDM control inputs using PSO-DBLSF technique.

Figure 7.4: SRDM control inputs with DBLSF and PSO-DBLSF algorithms.

Table 7.3: The transient comparison between DBLSF and PSO-DBLSF on SRDM.

	Rise Time / Fall Time (s)		
	DBLSF	PSO-DBLSF	Improvement (%)
Relative Position, x	1985.000	961.977	51.54
Relative Position, y	1505.000	898.384	40.31
Relative Position, z	1273.000	770.299	39.49

7.4 STSMC and PSO-STSMC

This topic presents the analysis results for the STSMC and PSO-STSMC on the SRDM with SRDM numeric parameters as in Table 7.1. Then, the STSMC and PSO-STSMC parameters are setup as in Table 7.4.

Table 7.4: The super twisting parameter values for STSMC and PSO-STSMC on the SRDM.

		STSMC	PSO-STSMC
λ_{str}	λ_{str1}	0.7500	0.3834
	λ_{str2}	0.7500	0.5449
	λ_{str3}	0.7500	0.7500
W_{str}	W_{str1}	3000.5	2644.5
	W_{str2}	3000.5	3229.5
	W_{str3}	3000.5	3000.5
L_{str}	L_{str1}	2166.7	4458.9
	L_{str2}	2166.7	3575.9
	L_{str3}	2166.7	2166.7
s_{0tr}	s_{0tr1}	0.01	0.05
	s_{0tr2}	0.01	0.10
	s_{0tr3}	0.01	0.15
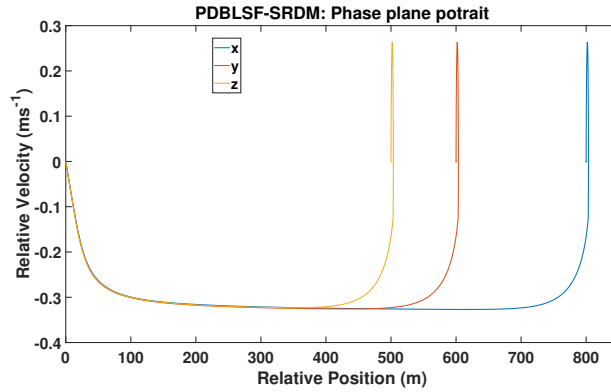
(a) DBLSF-SRDM: Phase plane potrait.
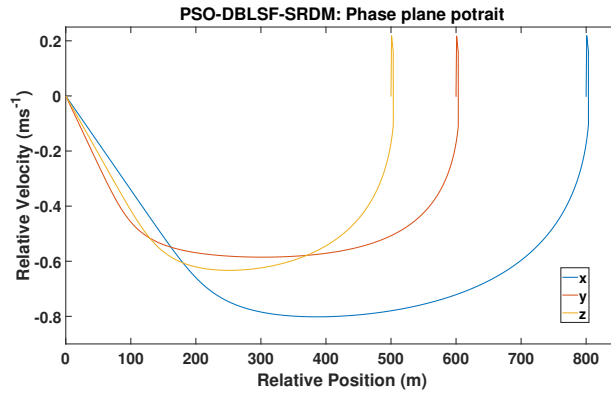
(b) PSO-DBLSF-SRDM: Phase plane potrait.

Figure 7.5: Phase plane potrait for the DBLSF and PSO-DBLSF on the SRDM.

7.4.1 Results

In this topic, the SRDM results using STSMC and PSO-STSMC are presented. The analysis is referred to the control force, control outputs and phase-plane trajectory performance. Figure 7.7 shows that both methods produced similar control outputs settling time, at least $55s$. The PSO-STSMC keeps the states maintained at their targeted output, but STSMC computes an oscillating output at the finite time. Besides that, the PSO-STSMC (Figure 7.8a) needs at most $3262.27N$ to enforce the states to achieve
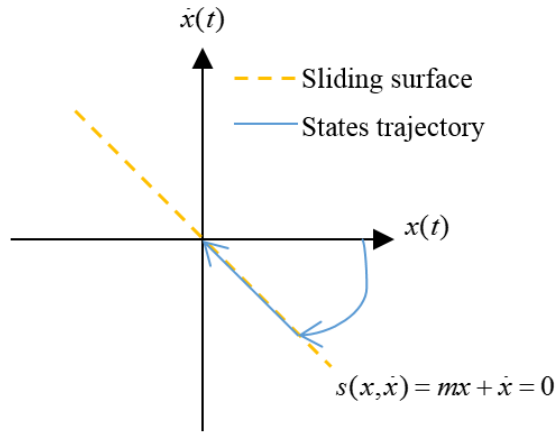
Figure 7.6: Phase portrait when $m|\dot{x}| < 1$ and $\sigma(x, \dot{x}) = 0$.

the desired outputs. However, STSMC requires (Figure 7.8b) $3595.28N$ but both control inputs are within the SRDM input range specification (Table 7.4). Furthermore, the SRDM states slide on the switching surface for PSO-STSMC compared but not for the STSMC after $30s$.

Figure 7.9 presents the phase-plane portrait for both approaches. The PSO helps in tuning the STSMC parameters where the trajectory of the state travel smoothly from the initial condition to the desired outputs (Figure 7.9b). For the STSMC-SRDM, a spiral pattern can be observed in Figure 7.9a where the relative position at $0m$ and the relative velocity between $-10ms^{-1}$ and $10ms^{-1}$.
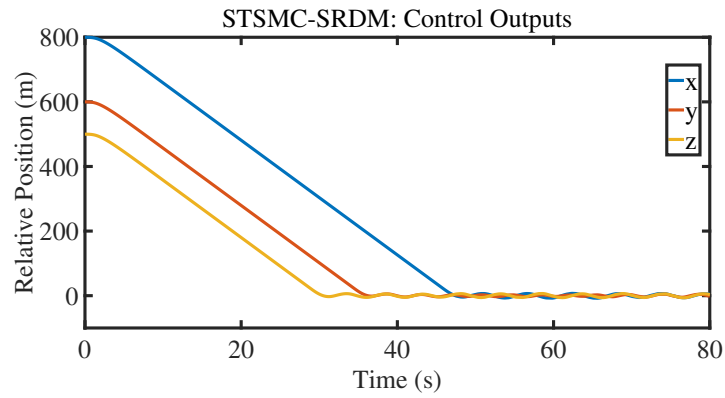
(a) SRDM outputs using STSMC method.
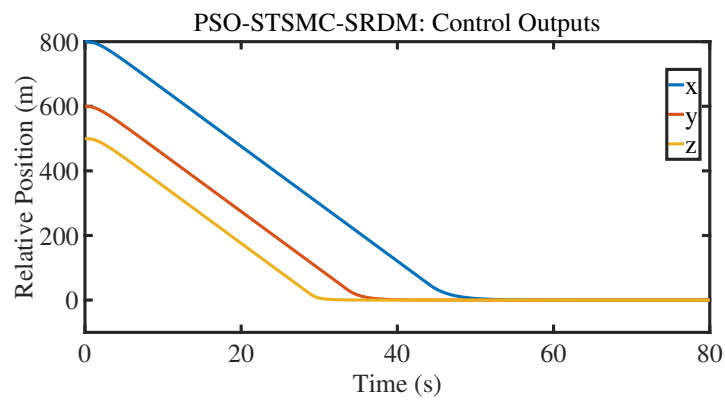
(b) SRDM outputs using PSO-STSMC method.

Figure 7.7: SRDM outputs with STSMC and PSO-STSMC approaches.
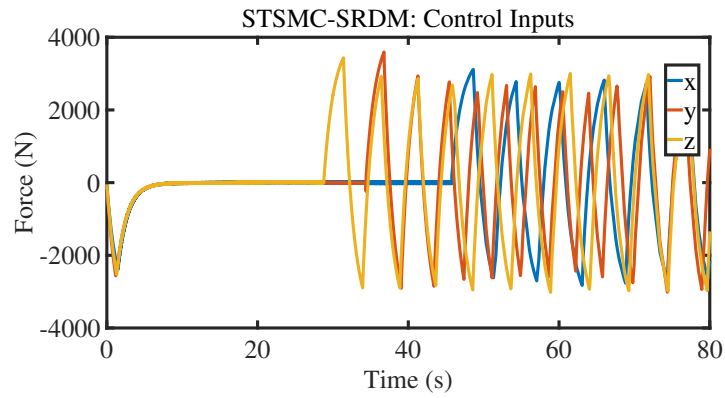
(a) SRDM control inputs using STSMC technique.
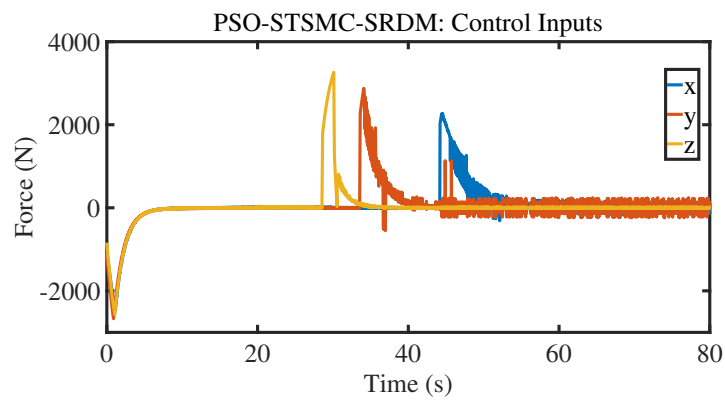
(b) SRDM control inputs using PSO-STSMC technique.

Figure 7.8: SRDM control inputs with DBLSF and PSO-STSMC algorithms.
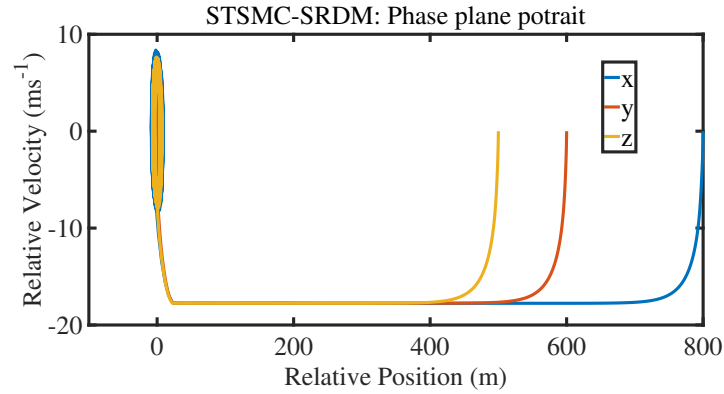
(a) STSMC-SRDM: Phase plane potrait.
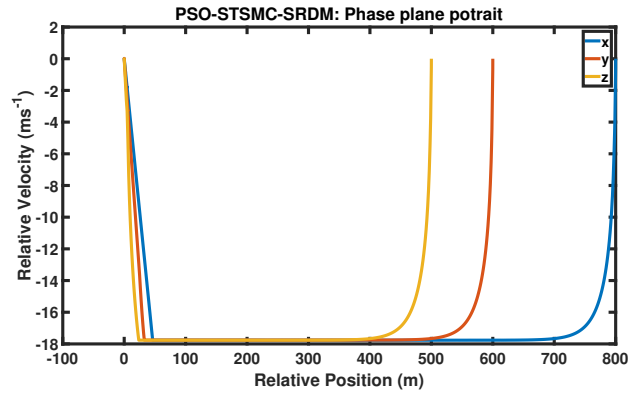
(b) PSO-STSMC-SRDM: Phase plane potrait.

Figure 7.9: Phase plane potrait for the STSMC and PSO-STSMC on the SRDM.

7.5 Conclusion

The DBLSF and STSMC can drive the SRDM outputs to achieve the desired position infinite time. However, DBLSF requires high rise time (961.977) compared to the STSMC $(40s)$ with the existence of the PSO algorithm. In contrast, DBLSF needs low input force (less than $2N$) while STSMC requires $(3595.28N)$. Moreover, the DBLSF produces a clear control inputs trajectory. In conclusion, the DBLSF generates a useful control inputs reference while the STSMC produces a fast response system.

Chapter 8

Conclusions and Future Works

8.1 Conclusions

A spacecraft's position is essential to make sure the missions are successful, although there exist challenges in space, such as uncertainties and disturbances produced by either internal of the spacecraft or space phenomena. Hence, a robust attitude and orientation control must complete the spacecraft missions and benefit human needs.

ACS, one of the spacecraft subsystems, consists of actuators, helps about maintaining or obtaining the spacecraft at a target orbit. However, the actuators could suffer damage, such as LOE, LIUT and FFPT. As one of the solutions, SMC introduced to the ACS to minimise the possible implications.

The SMC comes with benefits. For instance, low sensitivity towards perturbations, low cost, low computational burden, energy efficiency and low complexity were suitable for small spacecraft operation. Classical SMC's control law structure developed from two important parts, which are $u_{eq}(t)$ and $u_n(t)$. The $u_{eq}(t)$ can be constructed using either SVSS or SESS. On the other hand, although SMC has these major contributions, the switching function in the conventional SMC's control inputs generate chattering that can cause damage to the mechanical parts. Thus, many modification techniques in the switching function have been introduced to tackle this drawback, using LOSMC or HOSMC.

LOSMC is a low complexity algorithm that only produces a robust controller when the state variables hit the sliding surface. For improvement, HOSMC is replaced with the LOSMC, but the techniques require high com-

plexity algorithm. Thus, a new LOSMC (DBLSF) is developed and compared to LOSMC and HOSMC techniques. These controllers are designed and implemented on two ACS applications, SAOM and SRDM, considered both SVSS and SESS for the $u_{eq}(t)$ development.

For the SAOM, SESS have advantages compared to SVSS in term of the sliding surface coefficients complexity, and the output's error converged to zero in finite time. Then, the DBLSF controller used SESS for $u_{eq}(t)$ design and well-performed compared to the existing LOSMC, but the system's control input exceeded the allowable value, $|1Nm|$. However, PSO able to enhance the DBLSF weakness. In contrast, the STSMC (HOSMC) is unsuitable for the SAOM application due to the control input's performance. Hence, DBSLF with PSO existence computes the best results compared to the conventional SMC, LOSMC and HOSMC approaches investigated in the thesis.

Next, the DBLSF and STSMC can converge the SRDM's output to achieve the desired position in finite time with or without PSO tuning. Though, the DBLSF generates a useful control inputs reference while the STSMC produces a fast response time.

In conclusion, the DBLSF performed well compared to other LOSMC and HOSMC methods discussed in the thesis on SAOM. However, in SRDM, the DBLSF performance is better in control inputs reference, but not the response time criteria, compared to STSMC.

8.2   Direction for Future Works

In the thesis, the SMC algorithms only explored and validated the space applications using simulation-based. Thus, for future works, the DBLSF technique is suggested to be implemented on the actual system (experiment), and the results are contrasted with the existing SMC approaches. In this case, a gimbal system (Figure 8.1) holds the specification of rotation along x (roll), y (pitch) and z (yaw) axis, which can be used to almost mimicking the spacecraft's characteristics. Thus, use a gimbal system for the experiment purpose.
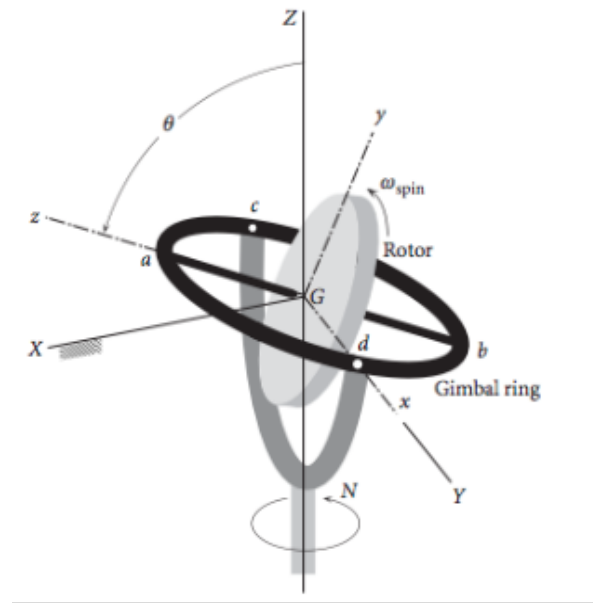
Figure 8.1: A gimbal system: rotating, precessing, and nutating gyro [3].

Beforehand, a simulation validation can be checked on the gimbal model. As an alternative, quaternion (Eq. 8.1) [89] suggested being used to determine the rotational motion of the rigid body instead of Euler's equations.

$$q_1 = \ell_1 \frac{\beta}{2}$$

$$q_2 = \ell_2 \frac{\beta}{2}$$

$$q_3 = \ell_3 \frac{\beta}{2} \tag{8.1}$$

$$q_4 = \cos \frac{\beta}{2}$$

where $q \in \Re^4$, $\ell = \begin{bmatrix} \ell_1 & \ell_2 & \ell_3 \end{bmatrix}$ denotes a unit vector called the Euler axis, and β is the magnitude of the Euler axis rotation.

Literatures show that the quaternion-based tecniques have been widely use for SMC on space applications [90–93]. Furthermore, the quaternion's information also proposed to develop a new LOSMC. In details, the DBLSF used $e(t)$ value to control the boundary layer width in SMC. The newly proposed technique can use the magnitude value in the quaternion to determine the boundary layer size. Finally, this will provide useful technical information to researchers about the possible control strategies with their performances on the gimbal system.

Bibliography

[1] M. Schmidhuber, S. Löw, K. Müller, S. Scholz, F. Chatel, R. Faller, and J. Letschnik, "Spacecraft subsystem operations," in *Spacecraft Operations.* Springer, 2015, pp. 213–323.

[2] S. Spurgeon, "Sliding mode control: a tutorial," in *2014 European Control Conference (ECC).* IEEE, 2014, pp. 2272–2277.

[3] H. Curtis, *Orbital mechanics for engineering students.* Butterworth-Heinemann, 2013.

[4] S. R. Starin and J. Eterno, "Attitude determination and control systems," 2011.

[5] A. J. Koshkouei, K. J. Burnham, and A. S. Zinober, "Dynamic sliding mode control design," *IEE Proceedings-Control Theory and Applications*, vol. 152, no. 4, pp. 392–396, 2005.

[6] A. Tewari, *Advanced control of aircraft, spacecraft and rockets.* John Wiley & Sons, 2011, vol. 37.

[7] L. Zhao, Y. Jia, and F. Matsuno, "Adaptive time-varying sliding mode control for autonomous spacecraft rendezvous," in *Decision and Control (CDC), 2013 IEEE 52nd Annual Conference on.* IEEE, 2013, pp. 5504–5509.

[8] J. N. Pelton, S. Madry, and S. Camacho-Lara, *Handbook of satellite applications.* Springer New York, 2017.

[9] T. Kawanishi, T. Sezai, Y. Ito, K. Imaoka, T. Takeshima, Y. Ishido, A. Shibata, M. Miura, H. Inahata, and R. W. Spencer, "The advanced

microwave scanning radiometer for the earth observing system (amsr-e), nasda's contribution to the eos for global energy and water cycle studies," *IEEE Transactions on Geoscience and Remote Sensing*, vol. 41, no. 2, pp. 184–194, 2003.

[10] J. R. Wertz, "Autonomous spacecraft navigation system," Apr. 28 1992, uS Patent 5,109,346.

[11] P. Fortescue, G. Swinerd, and J. Stark, *Spacecraft systems engineering*. John Wiley & Sons, 2011.

[12] L. Trevino, "Spacex dragon re-entry vehicle: Aerodynamics and aerothermodynamics with application to base heat-shield design." Georgia Institute of Technology, 2008.

[13] P. Kansakar and F. Hossain, "A review of applications of satellite earth observation data for global societal benefit and stewardship of planet earth," *Space Policy*, vol. 36, pp. 46–54, 2016.

[14] S. Rybak, G. Willen, W. Follett, G. Hanna, E. Cady, E. DiStefano, and J. Meserole, "Feasibility study for a cryogenic on-orbit liquid depot-storage, acquisition and transfer (cold-sat) satellite," 1990.

[15] D. K. Oi, A. Ling, G. Vallone, P. Villoresi, S. Greenland, E. Kerr, M. Macdonald, H. Weinfurter, H. Kuiper, E. Charbon *et al.*, "Cubesat quantum communications mission," *EPJ Quantum Technology*, vol. 4, no. 1, p. 6, 2017.

[16] H. N. Shou, "Micro-satellite attitude determination and control subsystem design and implementation: Software-in-the-loop approach," in *2014 International Symposium on Computer, Consumer and Control*. IEEE, 2014, pp. 1283–1286.

[17] M. Schmidhuber, S. Löw, K. Müller, S. Scholz, F. Chatel, R. Faller, and J. Letschnik, "Flight dynamics operations," in *Spacecraft Operations*. Springer, 2015, pp. 124–126.

[18] E. Agasid, R. Burton, A. Goktug Karacalioglu, R. Carlino *et al.*, "Small spacecraft technology state of the art nasa," TP–2014–216648/REV1 (Mission Design Division Staff, Ames Research Center . . . , Tech. Rep., 2014.

[19] H. B. Hassrizal and J. A. Rossiter, "Application of decaying boundary layer and switching function method thorough error feedback for sliding mode control on spacecraft's attitude," in *Control and Automation (MED), 2017 25th Mediterranean Conference on*. IEEE, 2017, pp. 1250–1256.

[20] M. Jin, J. Lee, P. H. Chang, and C. Choi, "Practical nonsingular terminal sliding-mode control of robot manipulators for high-accuracy tracking control," *IEEE Transactions on Industrial Electronics*, vol. 56, no. 9, pp. 3593–3601, 2009.

[21] C. Batur, T. Sreeramreddy, and Q. Khasawneh, "Sliding mode control of a simulated mems gyroscope," *ISA transactions*, vol. 45, no. 1, pp. 99–108, 2006.

[22] C. Edwards and S. Spurgeon, *Sliding mode control: theory and applications*. Crc Press, 1998.

[23] Y. Wang, Y. Xia, H. Shen, and P. Zhou, "Smc design for robust stabilization of nonlinear markovian jump singular systems," *IEEE Transactions on Automatic Control*, vol. 63, no. 1, pp. 219–224, 2017.

[24] Y. Shtessel, C. Edwards, L. Fridman, and A. Levant, *Sliding mode control and observation*. Springer, 2014.

[25] V. Utkin, "Discussion aspects of high-order sliding mode control," *IEEE Transactions on Automatic Control*, vol. 61, no. 3, pp. 829–833, 2015.

[26] F. Plestan, A. Glumineau, and S. Laghrouche, "A new algorithm for high-order sliding mode control," *International Journal of Robust and Nonlinear Control: IFAC-Affiliated Journal*, vol. 18, no. 4-5, pp. 441–453, 2008.

[27] H. B. Hassrizal and J. A. Rossiter, "A survey of control strategies for spacecraft attitude and orientation," in *Control (CONTROL), 2016 UKACC 11th International Conference on*. IEEE, 2016, pp. 1–6.

[28] S. Odenwald, "Space weather," http://www.solarstorms.org/Sscope.html.

[29] A. J. Weiss, C. Möstl, T. Amerstorfer, R. L. Bailey, M. A. Reiss, J. Hinterreiter, U. A. Amerstorfer, and M. Bauer, "Analysis of coronal mass

ejection flux rope signatures using 3dcore and approximate bayesian computation," *The Astrophysical Journal Supplement Series*, vol. 252, no. 1, p. 9, 2021.

[30] Materialscientist, "Micro-g environment," https://en.wikipedia.org/wiki/Micro-g-environment, 2015.

[31] J. Gosling, E. Hildner, R. MacQueen, R. Munro, A. Poland, and C. Ross, "The speeds of coronal mass ejection events," *Solar Physics*, vol. 48, no. 2, pp. 389–397, 1976.

[32] D. N. Baker, "The occurrence of operational anomalies in spacecraft and their relationship to space weather," *IEEE Transactions on Plasma Science*, vol. 28, no. 6, pp. 2007–2016, 2000.

[33] T. K. Brown and J. A. Donaldson, "Fault protection architecture for the command and data subsystem on the cassini spacecraft," in *Proceedings of 14th Digital Avionics Systems Conference*. IEEE, 1995, pp. 158–163.

[34] C. Greenwood, S. Lenhart, B. Inenaga, C. Jennings, A. Mendelsohn, M. Staley, and R. Vaughan, "Ss/l's super power subsystem development and application on the 1300 family of spacecraft," in *20th AIAA International Communication Satellite Systems Conference and Exhibit*, 2002, p. 1979.

[35] M. Navabi and H. Rangraz, "Comparing optimum operation of pulse width-pulse frequency and pseudo-rate modulators in spacecraft attitude control subsystem employing thruster," in *2013 6th International Conference on Recent Advances in Space Technologies (RAST)*. IEEE, 2013, pp. 625–630.

[36] M. Schmidhuber, S. Löw, K. Müller, S. Scholz, F. Chatel, R. Faller, and J. Letschnik, "Flight dynamics operations," in *Spacecraft Operations*. Springer, 2015, pp. 291–292.

[37] B. Lawson, "Satellite technologies," http://www.mpoweruk.com/satellites.htm, 2005.

[38] A. University, "Air university space primer," Air University, 2003.

[39] L. Cao, X. Chen, and T. Sheng, "Fault tolerant small satellite attitude control using adaptive non-singular terminal sliding mode," *Advances in Space Research*, vol. 51, no. 12, pp. 2374–2393, 2013.

[40] M. Schmidhuber, S. Löw, K. Müller, S. Scholz, F. Chatel, R. Faller, and J. Letschnik, "Attitude and orbit control subsystem operations," in *Spacecraft Operations*. Springer, 2015, p. 291.

[41] O. L. de Weck, "Attitude determination and control (adcs)," 2001.

[42] R. Burton, S. Rock, J. Springmann, and J. Cutler, "Dual attitude and parameter estimation of passively magnetically stabilized nano satellites," *Acta Astronautica*, vol. 94, no. 1, pp. 145–158, 2014.

[43] R. Wisniewski, "Linear time-varying approach to satellite attitude control using only electromagnetic actuation," *Journal of Guidance, Control, and Dynamics*, vol. 23, no. 4, pp. 640–647, 2000.

[44] L. Cao, X. Li, X. Chen, and Y. Zhao, "Minimum sliding mode error feedback control for fault tolerant small satellite attitude control," *Advances in Space Research*, vol. 53, no. 2, pp. 309–324, 2014.

[45] S. Emelyanov, "Variable structure control systems," *Moscow, Nouka*, 1967.

[46] U. Itkis, *Control systems of variable structure*. Halsted Press, 1976.

[47] V. Utkin, "Variable structure systems with sliding modes," *IEEE Transactions on Automatic control*, vol. 22, no. 2, pp. 212–222, 1977.

[48] J. Y. Hung, W. Gao, and J. C. Hung, "Variable structure control: A survey," *IEEE transactions on industrial electronics*, vol. 40, no. 1, pp. 2–22, 1993.

[49] R. A. DeCarlo, S. H. Zak, and G. P. Matthews, "Variable structure control of nonlinear multivariable systems: a tutorial," *Proceedings of the IEEE*, vol. 76, no. 3, pp. 212–232, 1988.

[50] H. Alwi, C. Edwards, O. Stroosma, and J. Mulder, "Fault tolerant sliding mode control design with piloted simulator evaluation," *Journal of Guidance, Control, and Dynamics*, vol. 31, no. 5, pp. 1186–1201, 2008.

[51] T. Wang, W. Xie, and Y. Zhang, "Sliding mode fault tolerant control dealing with modeling uncertainties and actuator faults," *ISA transactions*, vol. 51, no. 3, pp. 386–392, 2012.

[52] J. Zhao, B. Jiang, P. Shi, and Z. He, "Fault tolerant control for damaged aircraft based on sliding mode control scheme," *International Journal of Innovative Computing, Information and Control*, vol. 10, no. 1, pp. 293–302, 2014.

[53] J. Guldner and V. I. Utkin, "Sliding mode control for an obstacle avoidance strategy based on an harmonic potential field," in *Proceedings of 32nd IEEE Conference on Decision and Control*. IEEE, 1993, pp. 424–429.

[54] T. Nguyen, J. Leavitt, F. Jabbari, and J. Bobrow, "Accurate sliding-mode control of pneumatic systems using low-cost solenoid valves," *IEEE/ASME Transactions on mechatronics*, vol. 12, no. 2, pp. 216–219, 2007.

[55] A. Sofyalı and E. M. Jafarov, "Integral sliding mode control of small satellite attitude motion by purely magnetic actuation," *IFAC Proceedings Volumes*, vol. 47, no. 3, pp. 7947–7953, 2014.

[56] H. Lee and V. I. Utkin, "Chattering suppression methods in sliding mode control systems," *Annual reviews in control*, vol. 31, no. 2, pp. 179–188, 2007.

[57] V. Utkin, "Chattering problem," *IFAC Proceedings Volumes*, vol. 44, no. 1, pp. 13 374–13 379, 2011.

[58] V. Utkin and H. Lee, "Chattering problem in sliding mode control systems," in *International Workshop on Variable Structure Systems, 2006. VSS'06*. IEEE, 2006, pp. 346–350.

[59] M. S. Chen, Y. R. Hwang, and M. Tomizuka, "A state-dependent boundary layer design for sliding mode control," *Automatic Control, IEEE Transactions on*, vol. 47, no. 10, pp. 1677–1681, 2002.

[60] N. S. Hussain, H. H. Basri, and S. Yaacob, "State-dependent boundary layer method for attitude control of satellite," *Jurnal Teknologi*, vol. 76, no. 12, 2015.

[61] P. V. Suryawanshi, P. D. Shendge, and S. B. Phadke, "A boundary layer sliding mode control design for chatter reduction using uncertainty and disturbance estimator," *International Journal of Dynamics and Control*, pp. 1–10, 2015.

[62] M. C. VanDyke, J. L. Schwartz, and C. D. Hall, "Unscented kalman filtering for spacecraft attitude state and parameter estimation," *Department of Aerospace & Ocean Engineering, Virginia Polytechnic Institute & State University, Blacksburg, Virginia*, 2004.

[63] S. J. Julier and J. K. Uhlmann, "New extension of the kalman filter to nonlinear systems," in *AeroSense'97*. International Society for Optics and Photonics, 1997, pp. 182–193.

[64] H. Song, Y. Yu, M. Yang, and D. Xu, "A novel smc-fuzzy speed controller for permanent magnet brushless dc motor," in *Applied Power Electronics Conference and Exposition, 2003. APEC'03. Eighteenth Annual IEEE*, vol. 1. IEEE, 2003, pp. 281–285.

[65] X. Liu, P. Guan, and J. Liu, "Fuzzy sliding mode attitude control of satellite," in *Decision and Control, 2005 and 2005 European Control Conference. CDC-ECC'05. 44th IEEE Conference on*. IEEE, 2005, pp. 1970–1975.

[66] T. Gonzalez, J. A. Moreno, and L. Fridman, "Variable gain supertwisting sliding mode control," *IEEE Transactions on Automatic Control*, vol. 57, no. 8, pp. 2100–2105, 2012.

[67] C. T. Heng, Z. Jamaludin, A. Y. B. Hashim, L. Abdullah, and N. A. Rafan, "Design of super twisting algorithm for chattering suppression in machine tools," *International Journal of Control, Automation and Systems*, vol. 15, no. 3, pp. 1259–1266, 2017.

[68] S. Kempf, F. K. Schäfer, T. Cardone, I. Ferreira, S. Gerené, R. Destefanis, and L. Grassi, "Simplified spacecraft vulnerability assessments at component level in early design phase at the european space agency's concurrent design facility," *Acta Astronautica*, vol. 129, pp. 291–298, 2016.

[69] C. McManus and T. D. Barfoot, "A serial approach to handling high-dimensional measurements in the sigma-point kalman filter," *Robotics: Science and Systems VII*, p. 209, 2012.

[70] L. Perea, J. How, L. Breger, and P. Elosegui, "Nonlinearity in sensor fusion: Divergence issues in ekf, modified truncated sof, and ukf," in *AIAA Guidance, Navigation and Control Conference and Exhibit*, vol. 6514, 2007.

[71] V. I. Utkin, "Sliding mode control design principles and applications to electric drives," *IEEE transactions on industrial electronics*, vol. 40, no. 1, pp. 23–36, 1993.

[72] M. Rubagotti and A. Ferrara, "Second order sliding mode control of a perturbed double integrator with state constraints," in *Proceedings of the 2010 American control conference.* IEEE, 2010, pp. 985–990.

[73] C. Edwards, A. Akoachere, and S. K. Spurgeon, "Sliding-mode output feedback controller design using linear matrix inequalities," *IEEE Transactions on Automatic Control*, vol. 46, no. 1, pp. 115–119, 2001.

[74] S.-C. Lin and Y.-Y. Chen, "Rbf-network-based sliding mode control," in *Systems, Man, and Cybernetics, 1994. Humans, Information and Technology., 1994 IEEE International Conference on*, vol. 2. IEEE, 1994, pp. 1957–1961.

[75] M. T. Hamayun, C. Edwards, H. Alwi *et al.*, *Fault tolerant control schemes using integral sliding modes.* Springer, 2016.

[76] J.-J. E. Slotine, W. Li *et al.*, *Applied nonlinear control.* Prentice hall Englewood Cliffs, NJ, 1991, vol. 199, no. 1.

[77] A. Ibraheem, A. Bahgat, and M. A. Motelb, "Fuzzy logic sliding mode controller for dc drive," in *Current Advances in Mechanical Design and Production VII.* Elsevier, 2000, pp. 75–83.

[78] Y. B. Shtessel, L. Fridman, and A. Zinober, "Higher order sliding modes," *International Journal of Robust and Nonlinear Control: IFAC-Affiliated Journal*, vol. 18, no. 4-5, pp. 381–384, 2008.

[79] L. Fridman and A. Levant, "Higher order sliding modes as a natural phenomenon in control theory," in *Robust Control via variable structure and Lyapunov techniques.* Springer, 1996, pp. 107–133.

[80] I. A. Shkolnikov and Y. B. Shtessel, "Tracking in a class of nonminimum-phase systems with nonlinear internal dynamics via sliding mode control using method of system center," *Automatica*, vol. 38, no. 5, pp. 837–842, 2002.

[81] Y. Shtessel, C. Edwards, L. Fridman, and A. Levant, "Introduction: Intuitive theory of sliding mode control," in *Sliding Mode Control and Observation.* Springer, 2014, pp. 1–42.

[82] A. Swikir and V. Utkin, "Chattering analysis of conventional and super twisting sliding mode control algorithm," in *2016 14th international workshop on variable structure systems (VSS).* IEEE, 2016, pp. 98–102.

[83] F. Bacconi, "Spacecraft attitude dynamics and control," *Florence: Florence university*, vol. 2006, pp. 1–0, 2005.

[84] R. Stengal, "Spacecraft attitude control," http://www.princeton.edu/ stengel/MAE342.html, 2016.

[85] R. Eberhart and J. Kennedy, "A new optimizer using particle swarm theory," in *MHS'95. Proceedings of the Sixth International Symposium on Micro Machine and Human Science.* IEEE, 1995, pp. 39–43.

[86] M. N. Ayob, Z. M. Yusof, A. Adam, A. F. Z. Abidin, I. Ibrahim, Z. Ibrahim, S. Sudin, N. Shaikh-Husin, and M. K. Hani, "A particle swarm optimization approach for routing in vlsi," in *2010 2nd International Conference on Computational Intelligence, Communication Systems and Networks.* IEEE, 2010, pp. 49–53.

[87] H. Hassrizal, J. Rossiter, S. M. Othman, and M. Ayob, "Particle swarm algorithm sliding mode control on spacecraft's attitude with switching function method thorough error feedback," in *IOP Conference Series: Materials Science and Engineering*, vol. 705, no. 1. IOP Publishing, 2019, p. 012039.

[88] H. B. Hassrizal, J. A. Rossiter, and A. R. Firdaus, "Feasibility study of switching function approaches in sliding mode control for a spacecraft's attitude control system," in *Proceedings of CoDIT'18*. IEEE, 2018.

[89] F. Terui, "Position and attitude control of a spacecraft by sliding mode control," in *Proceedings of the 1998 American Control Conference. ACC (IEEE Cat. No. 98CH36207)*, vol. 1. IEEE, 1998, pp. 217–221.

[90] J. Yang and E. Stoll, "Adaptive sliding mode control for spacecraft proximity operations based on dual quaternions," *Journal of Guidance, Control, and Dynamics*, vol. 42, no. 11, pp. 2356–2368, 2019.

[91] H. Bang, C.-K. Ha, and J. H. Kim, "Flexible spacecraft attitude maneuver by application of sliding mode control," *Acta Astronautica*, vol. 57, no. 11, pp. 841–850, 2005.

[92] J. E. Stott and Y. B. Shtessel, "Launch vehicle attitude control using sliding mode control and observation techniques," *Journal of the Franklin Institute*, vol. 349, no. 2, pp. 397–412, 2012.

[93] J. Sanwale, P. Trivedi, M. Kothari, and A. Malagaudanavar, "Quaternion-based position control of a quadrotor unmanned aerial vehicle using robust nonlinear third-order sliding mode control with disturbance cancellation," *Proceedings of the Institution of Mechanical Engineers, Part G: Journal of Aerospace Engineering*, vol. 234, no. 4, pp. 997–1013, 2020.

Appendix 1

PSO Source Code

```matlab
% Symbols directory
% A/G/Pe - Agent (or Particle in PSO)/Global Best/Personal Best
% F/P/V  - Fitness/Position/Velocity
% s/c    - Social Coefficient/Congnitive Coefficient
% iw     - Inertia Weight
% i      - Iteration
% p      - Particle
% d      - Dimension
% N      - Number of

% 4 Tempat Perlu Di Ubah

clc;
clear all;
close all;
for Np = 5:5:10
    for Ni = 20:10:20
        for computation = 1:1:1

            save('memoryindahdaunpisang.mat','Np','Ni','computation');

            % Clear previous data
            clc;
            clear;
            rand('twister',sum(100*clock))
            % Problem Parameters/Information

             load('memoryindahdaunpisang.mat')

            Np
            Ni
            computation

%             m=0.33;
%             S=10;
%             f=27.5;
%             k=1000;
%             w=0.05;
%             Pa=2100;
%             rho=8.8665e-6;
%             cd=0.63;
%             Kl=2.381e-3;
%             Kc=2.5e-4;
%             c=cd*w*sqrt(2/rho);
%             Kv=0.017;
%             Fo=10000;

            LS1=0.01;
            LS2=0.01;
            LS3=0.01;
%             Q =1000;
%             k1 =1000;
%             c1 =5000;
%             c2 =5000;
```

```matlab
            % Particle Swarm Optimization (PSO) Parameters
            % Model PSO: A = [k1, k2, k3, rho1, rho2, rho3];

            tic;%start stopwatch
            s = 1.42;
            c0 = 1.42;
            iw = 0.9;
            %Np = 5;
            Nd = 3;
            %Ni = 100;

            uP = [10 10 10];
            lP = [0 0 0];

            AP = zeros(Np,Nd);
            AV = zeros(Np,Nd);
            GP = zeros(Ni,Nd);
            PeP = zeros(Np,Nd);

            % Initialize PSO Algorithm
            GF(1) = 9999;
            for p = 1:Np
                for d = 1:Nd
                    AP(p,d) = lP(d) + (uP(d) - lP(d)) * rand();
                    AV(p,d) = rand();
                end
                PeF(p) = 9999;
            end

            % AP(1,1) = 200;
            % AP(1,2) = 80;
            % AP(1,3) = 1.5;
            % AP(1,4) = 400;
            % AP(1,5) = 0.033;
            % AP(1,6) = 1;

            % Start Iteartion of PSO Algorithm
            for i=1:Ni
                i

                iw = 0.4 + 0.5 * (Ni - i)/Ni;

                for p = 1:Np
                    p;
                    GF(i);
                    % Calculate Particle Fitness
                      LS1=AP(p,1);
                      LS2=AP(p,2);
                      LS3=AP(p,3);
%                     Q=AP(p,1);
%                     k1=AP(p,2);
%                     c1=AP(p,3);
%                     c2=AP(p,4);
%
                      sim('srdmmodeldblsfpso.slx');
```

```matlab
            v1=open('psodblsfsrdm1.mat');
            v2=open('psodblsfsrdm2.mat');
            v3=open('psodblsfsrdm3.mat');
%
            [row1 col1]=size(v1.ans1)
            [row2 col2]=size(v2.ans2)
            [row3 col3]=size(v3.ans3)

            tempsum1=0;
            tempsum2=0;
            tempsum3=0;

                for r1=1:col1
                    tempsum1=0.00001*(tempsum1+v1.ans1(2,r1));
                end

            tempsum2=tempsum1;
                for r2=1:col2
                    tempsum2=0.00001*(tempsum2+v2.ans2(2,r2));
                end

            tempsum3=tempsum2;
                for r3=1:col3
                    tempsum3=0.00001*(tempsum3+v3.ans3(2,r3));
                end

            tempsum3;

            AF(p) = tempsum3;

            % Update Personal Best Record
            if AF(p) < PeF(p)
                PeF(p) = AF(p);
                for d=1:Nd
                    PeP(p,d) = AP(p,d);
                end
            end

        end

        for p = 1:Np
            % Update Global Best Record
            if AF(p) < GF(i)
                GF(i) = AF(p);
                for d=1:Nd
                    GP(i,d) = AP(p,d);
                end
            end
        end

        for p = 1:Np
            for d = 1:Nd
                % Update Particle Velocity
                AV(p,d) = iw * AV(p,d) + c0 * rand() * (PeP(p,d) - AP(p,d)) +↙
```

```matlab
s * rand() * (GP(i,d) - AP(p,d)); %%%

                    % Update Particle Position
                    AP(p,d) = AP(p,d) + AV(p,d);

                    % Check For Constraints
                    % if AP(p,d) > uP(d)
                    %     AP(p,d) = uP(d)-rand (100,1000);
                    % end
                     if AP(p,d) < lP(d)
                        AP(p,d) = -AP(p,d);
                     end

                end
            end

            % Check For Constraints

            % Update Information Of Global Best
            GF(i+1) = GF(i);
            GF(i)
            for d=1:Nd
                GP(i+1,d) = GP(i,d);
            end
        end

        elapsed_time=toc; % time taken for this algorithm


        % Display Best Found Result %%%%% UBAH DI SINI %%%%%%%%%
        plot(1:Ni,GF(1:Ni));
        save('data.mat');
          LS1=GP(Ni,1);
          LS2=GP(Ni,2);
          LS3=GP(Ni,3);
%         Q=GP(Ni,1);
%         k1=GP(Ni,2);
%         c1=GP(Ni,3);
%         c2=GP(Ni,4);

                sim('srdmmodeldblsfpso.slx');
                v1=open('psodblsfsrdm1.mat');
                v2=open('psodblsfsrdm2.mat');
                v3=open('psodblsfsrdm3.mat');
            savename = sprintf('Ni %d, Np %d, Com %d.mat',Ni,Np,computation);
        save(savename);
    end
  end
end
```

Appendix 2

Author's Publications

A Survey of Control Strategies for Spacecraft Attitude and Orientation

Hassrizal H. B.* and J. A. Rossiter[†]

* [†] Department of Automatic Control and Systems Engineering, The University of Sheffield,
Mappin Street, Sheffield, S1 3JD, UK
* School of Mechatronic Engineering, Universiti Malaysia Perlis, Malaysia
Email: * hbhassanbasri1@sheffield.ac.uk, [†] j.a.rossiter@sheffield.ac.uk

Abstract—This paper presents a survey of different control methods deployed for spacecraft attitude control with a focus on strengths, weaknesses and opportunities for improvement. Common methods discussed include Sliding Mode Control (SMC), Unscented Kalman Filter (UKF) and Adaptive Control. Common challenges are the disturbances and uncertainties in space and produced by the spacecraft. This overview is used as a foundation for proposing useful research directions for developing improved control methods for the spacecraft attitude and orientation, with core requirements being low cost, robustness, precision, high efficiency and low computational load. The paper also summarises key actuation types used for satellite orientation, magnetics actuator and reaction wheels actuator, as the control strategy deployed, robustness and performance have strong links to the actuation.

Keywords: SMC, spacecraft attitude control, actuator, robustness, disturbances and uncertainties

I. INTRODUCTION

A spacecraft is a vehicle which travels in outer space in order to accomplish a variety of missions and purposes such as communications, earth observation, meteorology, navigation, space colonization, planetary exploration and transportation of humans and cargo. The development of manned or auto manoeuvring spacecraft has and continues to have a huge impact on human civilisation. One of the criteria to make sure spacecraft are capable of completing their missions is the ability to control precisely the spacecraft orientation and attitude. The orientation of a defined spacecraft body uses system coordinates with respect to a defined frame of Geocentric Inertial System (GCI) and Heliocentric Inertial System (HCI). Attitude control is the maintenance of desired, specified attitude within a given tolerance [1]. The location and position of a spacecraft is linked to the choice of orbit which in turn depends on their mission. Based on these requirements, effective control of satellite attitude is one of the critical parts to make sure these missions are accomplished successfully.

Many researchers have proposed various controllers to achieve the precision and optimisation of satellite attitude. A few common specifications for assessing these strategies have been robustness, energy efficiency, minimum maintenance and weight reduction.

Attitude control can be categorized into two parts. The first part is the orientation of the spacecraft with respect to selected reference objects or directions, e.g., earth, sun, stars, and flight directions. The second is the dynamics of the spacecraft where some parts of the spacecraft need to change their orientation over time, for example to rotate about a dedicated axes or to stabilise the orientation after separation from a launcher. Besides that, the orbit control consists of all aspects of maintaining or acquiring a target orbit [2].

Common control strategies include Sliding Mode Control (SMC), Kalman Filter (KF), Extended Kalman Filter (EKF), Unscented Kalman Filter (UKF), Adaptive Fuzzy Control; all these methods are elaborated on in this paper. A key aim is to evaluate their effectiveness in meeting mission criteria alongside other requirements. In order to test the robustness of the designed attitude satellite system, various types of disturbances and uncertainties are introduced to the system where these problems are based on real case scenarios which can have origins either internal or external to the spacecraft.

The paper is organised as follows. Section 2 describes the orbits relative to the earth and the spacecraft challenges in maintaining the orientation and attitude in the presence of uncertainties and disturbances in space. Section 3 describes different types of spacecraft actuators and the reliability, capability and expense of these actuators. Section 4 elaborates the development of the control strategies for spacecraft orientation and attitude along with a discussion of strengths and weaknesses. In Section 5, brief conclusions are given along with proposals for future work, that is where improvements of the control strategies are possible.

II. EARTH'S ORBITS AND CHALLENGES

Across space, there are 3 orbit classifications relative to earth; Lower Earth Orbit (LEO), Medium Earth Orbit (MEO) and High Earth Orbit (HEO). For each of these Kepler's Law can be used to explain the planetary or object motion. The definition of these orbits is shown in Table I.

Table I
ORBITS DISTANCE FROM THE EARTH

Orbit	Distance from the Earth's surface
Low Earth Orbit (LEO)	2 000 km
Medium Earth Orbit (MEO)	2 000 km to 20 350 km
High Earth Orbit (HEO)	over 20 350 km

A. Earth's Orbits

Weather forecasts, communication, broadcasting, earth imaging, surveillance of a pre-selected region, military purposes, global positioning satellite (GPS) are all common uses of satellites which gather and distribute information. To accomplish these tasks, the satellites must be in their correct orbit region.

Objects inside the LEO, orbit the Earth as fast as 50 times a day. Most satellites such as the International Space Station (ISS), the space shuttle and Hubble space telescope are located in this orbit. The object must travel at more than 8 km/s to avoid being dragged back to the earth by gravity. Unfortunately, there is also atmospheric drag inside this region. Although the amount is very small, it will cause a slow movement of the object towards the earth if not counteracted effectively. Also, since the satellite speed is very fast, it cannot maintain its position long enough in any pre-specified region to be used for surveillance tasks, earth imaging and military missions.

An object orbiting the earth twice a day will be in a MEO. The information from GPS navigation, which is widely used in society is provided by satellites inside the MEO. The GPS navigation requires 4 satellites to give an accurate position.

Weather forecast, communication and broadcasting are suitable tasks for satellites inside a HEO also known as the High Altitude Geostationary region since the satellite orbits the earth once a day. These satellites maintain their location relative to a point on the earth all the time. For instance, a television antenna can always point in the same direction since the satellite location does not change relative to the television antenna.

Table II [3] shows the relationship between gravitational acceleration and the distance from the earth's surface and also compares this with gravitational forces due to the sun (which do not change on this scale). The greater the distance from the earth's surface the lower the gravity acceleration. In LEO, the gravity is $9ms^{-2}$ while for a distance over 200,000 km from earth this is as low as $10mms^{-2}$.

Table II
GRAVITATIONAL ACCELERATION DUE TO THE EARTH AND THE SUN

Location	Earth	Sun
Earth's Surface	$9.81ms^{-2}$	$6mms^{-2}$
LEO	$9ms^{-2}$	$6mms^{-2}$
200 000 km from the Earth	$10mms^{-2}$	$6mms^{-2}$
6 million km from the Earth	$10\mu ms^{-2}$	$6mms^{-2}$

B. Orbital Manoeuvres

Sometimes, the spacecraft need to change its altitude from one orbit to another due to the different circumstances. The orbital transfer can be dramatic, such as transfer from an initial parking orbit to the final mission orbit, rendezvous with or intercept another spacecraft or correct the orbital elements in order to adjust the for the perturbations. There are two ways to maneuver the orbital either by changing the spacecraft velocity vector or the spacecraft direction. The Hohmann transfer method, impulsive maneuvers method, bi-elliptic Hohmann transfer method, phasing maneuvers method and apse line rotation method are common transfer techniques have been used to accomplish this task [4]. Minimum energy consumption must be considered when designing the orbital transfer. It is important to maintain the spacecraft have enough energy to perform the manoeuvring.

C. Spacecraft Challenges in Space

When spacecraft are orbiting the earth, there are external disturbances and uncertainties impacting on the spacecraft [5] as shown in Table III. International Space Station (ISS) operating in LEO requires re-boosting several times every year because of the atmospheric drag is constantly decreasing ISS attitude by a kilometer every 12 days. The solar storms heat the upper atmosphere which increases the ISS drag and accelerates the orbit decay [6]. This symptom makes the spacecraft experience inadequate aerodynamic torque indeed.

Solar storm happens when particles that are thrown out from the sun under solar activity (the sum of all variable and short-lived disturbances on the sun, as sunspots, prominences and solar flares) [7]. Besides that, the chosen position in space can change the behaviour away from a pure Keplerian orbit because not only of the gravitational field of the earth but also the influence of the gravity of the Sun and the Moon [5]. Therefore, robust control strategies are required to make sure the spacecraft position and attitude is insensitive towards these influences.

Table III
DISTURBANCES AND UNCERTAINTIES IN SPACE

Disturbances/Uncertainties	Affect to the Spacecraft
Sun UV	Ultra violet light from the sun will darken the solar panel and ultimately reduce the efficiency and thus power output produced by the solar panel. Hence, the satellites must be energy efficient to counter this degradation.
Solar Storm	The solar wind consists of high speed particles of protons and electrons. The particles put the pressure on spacecraft (this phenomenon also creates the aurora). However in the South Atlantic, the magnetic field is anomalously low and thus spacecraft in this area are exposed to more energy particles and hence suffer more damage.
Atmosphere Drag in LEO	The spacecraft altitude will change because of atmospheric drag slowing the speed. Thus in LEO, the spacecraft consumes high power to counter the earth gravitational field in order to maintain altitude by using their thrusters to maintain the speed.
Sun and Moon Gravitational Force	The gravitational forces of the sun and the moon cause periodic variations in all of the orbital elements, but only the right ascension of the ascending node, argument of perigee, and mean anomaly experience secular variations.

III. SPACECRAFT ACTUATORS AND CHALLENGES

Generally, there are 6 subsystems in a satellite structure; a structural subsystem, a telemetry subsystem, a power subsys-

tem, a thermal control subsystem, a communication payload and attitude/orbit control subsystem. The attitude and orbit subsystem is used to determine and control the orientation of the satellite in order to accomplish the missions. One of the components to determine the attitude and orbit control of the spacecraft is actuator. The actuator will apply the necessary forces to re-orient the spacecraft to the desired attitude according to the deviation between desired orientation and current position, as detected by sensors, until the deviation is equal to zero [8]. There are two common types of actuator to be discussed in this paper; reaction wheels and magnetic torquers. Researchers model the linear and non-linear satellite systems and design the controller based on these actuators. A common challenge for researchers is the effective consideration and rejection of the disturbances and uncertainties which exist in space and on the spacecraft as shown in Table III and Table IV.

A. Reaction Wheels

Reaction wheels, also known and operated as a momentum wheel, consist of a rotating mass attached to an electric motor; devices on a spacecraft are aligned on X (pitch), Y (roll) and Z (yaw) axis as shown in Figure 1. Sometimes, the reaction wheels have the fourth device which is used for redundancy purpose. The pointing accuracy of reaction wheels can achieve up to 0.001^0 precision [9]. Unfortunately, reaction wheels suffer from degradation, for example, loss of effectiveness (LOE), stuck fault (lock in unknown time or LIUT) and failure for a period time (FFPT) [10]. One of the malfunctions to a reaction wheel happened to the Mars Odyssey Spacecraft in 2012. The Mars Odyssey detected one of its three reaction wheels, which are used to control orbiter orientation in space produced unusual readings. It makes the spacecraft gone into safe mode before the recovery actions are taken. The orbiter carries a spare reaction wheel onboard, in case one of the three in use fails. Besides that, reaction wheels are heavy and thus require substantial space inside the spacecraft. Moreover, they have low power efficiency, require high energy to operate and also are unsuitable for small satellites. Furthermore, flywheels or batteries are required to supply the power to reaction wheels during an eclipse. Nevertheless, researchers have developed spacecraft using reaction wheels as the main actuator in MEO and HEO since, in these orbits, the interaction between a spacecraft and the earth magnetic field is very low.

B. Magnetic Torquer

Magnetic torquers, also known as magnetorquers, utilise an electrical current run around a piece of metal (torque rods with an iron core or air coils [2]); this creates an electromagnet. Within space in LEO, this electromagnet will be subject to a force causing it to align itself along the Earths magnetic field and thus generate a torque on the spacecraft. These magnetic controls are relatively light but low accuracy (1^0) [1]. They also can be used to compensate for the natural magnetic effects of satellite components [9]. A magnetic torquer is available as long as sufficient electric power is
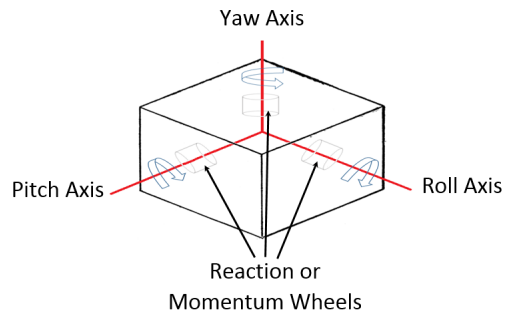
Figure 1. Reaction Wheels Direction

available. With the advantages of smaller size, less weight and energy and negligible degradation due to no moving parts, magnetorquers are widely used for small satellites in LEO. Nevertheless, magnetorquers require more complex control design since various uncertainties exist such as non-clean magnetic fields inside the spacecraft that interfere with the magnetic interaction between the spacecraft and the earth [11]. The use of magnetorquers also introduces challenges, for example the system is only controllable in two axes at any time; the axes being perpendicular to the local geomagnetic field vector [12].

C. Summary of between Reaction Wheels and Magnetic Torquer Actuator

Based on the description of both actuators, it can be said these actuators have advantages and disadvantages. The selection of actuator type when designing the spacecraft is dependent on their missions, for example considering the reliability, accuracy and location in space. A summary of spacecraft actuator characteristics is shown in Table IV.

D. Actuators Challenges in Space

There are several issues which from challenges for an attitude controller. Some actuators are made from mechanical moving parts and one main component is a motor. A motor will degrade in time thus affecting spacecraft attitude performance. Fault-tolerant strategies to cope with scenarios such as LOE, LIUT and FFPT may come at the price of a significant disruption to a satellite's performance [13]. Besides that, internal noise from sources within a satellite will have impact similar to a disturbance torque form.

For magnetic actuators, the magnetic field generated by the coil will be affected by the material within the magnetorquers since non-clean magnetics exists where the currents flowing in the harness, solar panels, permanent magnets, solenoid valves etc. can lead to unwanted disturbances to the spacecraft's attitude [14]. This problem will be a huge challenge for spacecraft to maintain their attitude and orientation.

IV. CONTROL STRATEGIES

A lot of criteria must be taken into account when designing an attitude control system: computational time, control power consumption, the robustness of the designed control towards

Table IV
CHARACTERISTICS SUMMARY OF REACTION WHEELS AND MAGNETIC
TORQUER ACTUATORS

Actuator	Reaction Wheels (RW)	Magnetics
Characteristics	The RW has a high pointing accuracy of 0.001^0. However, the RW requires high energy consumption, large size and requires a separate power source (flywheel or battery) during an eclipse.	The Magnetic actuator is small, low weight and consumes low power but low accuracy (1^0). It also free of degradation due to having no moving parts. However, the control design for the Magnetics actuator is complex.
Orbit	The RW have been implemented on spacecraft in LEO, MEO and HEO but is unsuitable for small spacecraft due to the size requirement.	The Magnetics actuator is only suitable for spacecraft in LEO since near to the earth there is a large magnetic field compared to MEO and HEO.
Challenges	The RW degrades over time (LOE, LIUT, FFPT) since it uses moving parts.	The magnetic actuator produces non-clean magnetic fields generated by current flowing inside the actuator that can cause interference.

internal and external disturbances and uncertainties, accuracy of the output, improvements from previously compensated attitude control systems and capability of the spacecraft to process the designed controller. Figure 2 shows the block diagram for an attitude control subsystem which tackles these objectives. By considering all these criteria it is possible to ensure the spacecraft can accomplish its mission for long periods and also to ensure the appropriateness of the designed attitude control systems for specific spacecraft characteristics.

Sliding Mode Control (SMC), Fuzzy SMC, Unscented Kalman Filter (UKF) (improvement of Kalman Filter and Extended Kalman Filter) and Adaptive Control are examples of spacecraft attitude controllers. The performances and capability of these controllers are reviewed here in order to compare and contrast their efficacy. These controllers are tested with linear and non-linear spacecraft models and various types of disturbances and uncertainties.
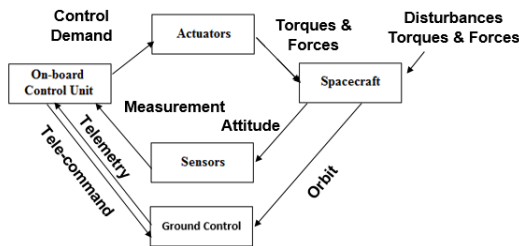
Figure 2. Attitude Control Subsystem Components and Cycles

A. Adaptive Sliding Mode Control

Sliding Mode Control (SMC) is a robust control strategy known to be relatively insensitive towards disturbances and uncertainties. Besides that, SMC is easy to implement and has low computational costs. Due to these advantages, SMC

is convenient for small spacecraft in LEO but it suffers from a chattering phenomena which is a drawback. The chattering causes wear and tear on the actuator. In response, researchers proposed Fuzzy SMC, Minimum Sliding Mode Error Feedback, Adaptive Non-Singular Terminal SMC, Adaptive Fuzzy SMC and Integral SMC as alternatives to suppress this chattering phenomenon and improved overall performance, including the transient response, effectiveness and accuracy. The modified SMC approaches have been implemented on reaction wheels [10], [13], [15] and magnetic actuators [16]. Adaptive SMC has been shown to give good precision, effectiveness and convergence to the desired position in finite time, in the presence of various disturbances and modelling uncertainties.

1) Adaptive Fuzzy Sliding Mode Control: The Adaptive Fuzzy Sliding Mode Control (AFSMC) [15] was introduced because fixed fuzzy rules contribute to a non-robust system. Hence, Adaptive Fuzzy was integrated inside SMC to improve robustness for less disturbances and uncertainties. However, this method requires a high computing burden which limits the on-line spacecraft application. As such, the AFSMC is unsuitable to be implemented inside small spacecraft. The AFSMC is divided into two components where equivalent control terms are used to deal with the uncertainties while hitting control is used to achieve the attitude precision. The equivalent control term is the approximation of the control law to achieve zero steady-state value. Furthermore, hitting control functions are the chattering remover. Finally, based on the result, the AFSMC is able produced precise attitude control subject to less disturbances and uncertainties. The AFSMC is unsuitable for huge disturbances and uncertainties challenge.

2) Minimum Sliding Mode Error Feedback Control: The Adaptive Non-Singular Terminal SMC [10] produced robustly and high-efficiency attitude control of the spacecraft but this control method also required a heavy computational burden since it used more fuzzy parameters. In order to overcome this effect, researchers developed the Minimum Sliding Mode Error Feedback Control (MSMEFC) [13]. The uncertain disturbances are offset by an equivalent control error in order to improve the control performance. A cost function contains all the information of sliding mode error and the equivalent control error is derived in order to estimate the optimal equivalent control error where this estimation will feedback to the conventional SMC to produce the MSMEFC result. As result, the MSMEFC not only results in energy efficiency but also is robust towards faults (LOE, LIUT and FFPT inside the actuator) and perturbations. The MSMEFC have not considered the orbital manoeuvres inside the analysis because sometimes orbital manoeuvres is required due to the serious perturbations.

3) Integral Sliding Mode Control: Small satellites due to their small size and weight require less energy consumption. Most researchers considered magnetic actuation to fulfil these criteria. Integral Sliding Mode Control [16] used purely magnetic attitude control with realistic non-linear parameters. The control torque vector at the output of the controller acts on the spacecraft after successive manipulations. As the result, the

disturbances can't be fully eliminated because of the difference between the control torque vector generated by the controller and the applied control torque vector.

B. Unscented Kalman Filter

Some researchers introduced an Unscented Kalman Filtering (UKF) controller [17] as an improvement on a Kalman Filter (KF) and Extended Kalman Filter (EKF) [18] for spacecraft attitude state and parameter estimation. The improvement has been made since KF is used for estimating a linear system while EKF limited estimating up to first-order terms for nonlinear systems by neglecting higher-order terms. Neglecting the higher-order terms can lead to the instability. Based on the result, UKF was able to converge, despite poor initial estimates of the parameters, through numeric simulation; using simulated noisy measurements brings better convergenc characteristics and greater accuracy than the EKF [17]. Furthermore, UKF is also easier to implement because this control method is derivative-free [19]. EKF computes the output by using a Jacobian; the Jacobian leads to more complexity and computational demand. Compared to UKF, this method approximates the state/measurement estimate and the associated uncertainty by a statistical linear regression through a well-chosen set of a set of samples determined from the apriori mean and covariance of the state known as "sigma points" and thus is less complex [20].

C. Proposed Control Method (A State-Dependent Boundary Layer Method for SMC

Since the SMC effectively can be implemented on both magnetics and reaction wheels actuator, insensitivity towards to perturbation in space and the spacecraft and fast response controller, hence, the modification inside the SMC switching function is proposed as proven by MSMEFC. The modification must eliminate the chattering drawback and also produce the precise and effective spacecraft attitude and at the same time maintaining the minimum energy consumption. Furthermore, the low computational burden is required and as an example, the spacecraft capable perform the orbital maneuver in order to withstand the serious perturbation. One of the modification methods in order to accomplish these targets is the implementation of the state-dependent boundary layer method. The boundary layer in the SMC is used to remove the chattering phenomena. In the principle, a constant boundary layer around sliding surface, $s = 0$ (ideal case for control input of SMC where along of this surface,the steady state error of the output, $e_{ss} = 0$) as in Figure 3 is used to remove the chattering phenomena but it leads to the imprecise output. Therefore, variable or decaying boundary layer width is required in order to overcome the problem. As the result, the boundary layer width is determined by the states of the system where this boundary layer is decaying towards to the sliding surface, $s = 0$. When the states lie on this surface, the preciseness of the output is guaranteed where $e_{ss} = 0$. The state-dependent boundary layer design is proven to eliminate the chattering

phenomenon while ensuring almost perfect control accuracy at the same time [21].
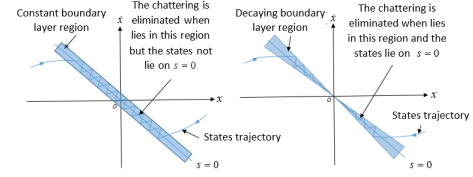
Figure 3. SMC with Constant and Decaying/Variable Boundary Layer

V. CONCLUSIONS AND FUTURE RECOMMENDATIONS

Table V summarises the strengthens and weaknesses of common approaches to spacecraft attitude control and hence gives insight to where improvements would be beneficial.

SMC is robust but it has chattering as the drawback. One proposed alternative of Adaptive Fuzzy requires an additional cost function inside the SMC thus increasing complexity and computational load more than is allowable. Integral SMC cannot adequately eliminate disturbances and uncertainties which bring to the impreciseness output of the spacecraft attitude. According to the MSMEFC advantages, this method is suitable to be implemented for both small and huge spacecraft due to the energy efficiency and high robustness. This can be achieved because the MSMEFC do modification inside the SMC algorithm by adding cost function without compound with another type of controllers. As such, in order to minimize the size, low the complexity and optimize the small spacecraft performance with greater accuracy, modification in SMC algorithm is one of the ways to achieve the objectives while implement on magnetics actuator.

Overall, some of the control strategies discussed in Section IV manage to control the linear and non-linear attitude and orientation of spacecraft systems. The controllers must be robust against the disturbances and uncertainties which exist in space and the spacecraft. Besides that, the spacecraft attitude and orientation outputs must be precise, effective and can converge to the desired position in finite time, while being efficient with the spacecraft's power consumption. A low computational process load, small size, and ease of implementation must also be taken into account when designing a controller, especially for the small spacecraft. Based on Table V, the MSMEFC and UKF demonstrate these criteria better than the alternative controllers. Nevertheless, although the results shown by both methods give precise attitude output, these methods also can consider serious perturbations and how to maintain the desired attitude and orientation in space. Hence, one of the possible methods to resist the serious perturbations by using the orbital manoeuvre. The orbital manoeuvre required a control method in order to achieve precise new desired attitude by using the minimum energy consumption. One of the solutions is using state-dependent boundary layer method of SMC.

VI. ACKNOWLEDGEMENTS

Table V
COMPARISON BETWEEN SPACECRAFT ATTITUDE CONTROLLER

Controller	Advantages	Disadvantages	Improvement
Sliding Mode Control (SMC)	The SMC is a low complexity, low computational burden, less weight and low cost control method. The SMC also a robust control method where the output can converge in finite time with sufficient precision. Hence, the SMC is suitable for various type of the attitude and orientation spacecraft control.	The SMC produces a chattering effect to the system. It caused wear and tear to the actuator.	A modification in the SMC switching function is required in order to remove the chattering drawback.
Adaptive Fuzzy Sliding Mode Control (AFSMC)	Fixed fuzzy rules lead to limited robustness which makes the system become unstable. However, it solved the chattering phenomena caused by the SMC. Then, adaptive fuzzy rules are introduced not only to counter instability but also produced the precise attitude of the spacecraft.	The AFSMC is a complex fuzzy parameter which leads to a high computational load. As such, the AFSMC is unsuitable to use in small spacecraft. Besides that, it also only robust towards to minimum disturbances and uncertainties in space and the spacecraft.	To use in small spacecraft, a modification inside switching function of SMC is proposed instead of combine the SMC with the other controller methods, such as Fuzzy. The modification can minimize the computational burden of the spacecraft.
Minimum Sliding Mode Error Feedback Control (MSMEFC)	The MSMEFC is an energy efficiency and robust control method suitable for realistic disturbances and uncertainties generated by the spacecraft and in space. The MSMEFC contains a cost function which is used to offset the disturbances and uncertainties to improve the control performance. Hence, the MSMEFC is suitable for small spacecraft.	The MSMEFC considered fault actuator as uncertainties but sometimes there are serious perturbations happens in space.	One of the ways to reject the serious perturbations effect is introducing orbital manoeuvres with minimum energy consumption to the spacecraft.
Integral Sliding Mode Control (ISMC)	The ISMC is implemented on a magnetic actuator. This controller has small size and weight and low energy consumption, thus is suitable for small spacecraft.	The ISMC is influenced by the disturbances and uncertainties because the difference of the control torque (the ideal case, sliding surface, $s = 0$) and the applied control torque vector which resulting impreciseness output.	More research on fundamental problem specific to the purely magnetic attitude control problem is required in order to overcome the disadvantages.
Unscented Kalman Filter (UKF)	The UKF is able to converge and estimate higher order non-linear parameter which bring better converge characteristics and greater accuracy than the the EKF with poor initial estimates. Furthermore, the UKF is easy to implement since it uses no derivatives. This control method has low computational requirements and low complexity.	The UKF have not been tested with real case perturbations in space and the spacecraft.	The UKF can be tested with the real case of disturbances and uncertainties such as fault-tolerant in actuator.

REFERENCES

[1] O. L. de Weck, "Attitude determination and control (adcs)," 2001.
[2] M. Schmidhuber, S. Löw, K. Müller, S. Scholz, F. Chatel, R. Faller, and J. Letschnik, "Attitude and orbit control subsystem operations," in *Spacecraft Operations*. Springer, 2015, p. 291.
[3] Materialscientist, "Micro-g environment," https://en.wikipedia.org/wiki/Micro-g-environment, 2015.
[4] H. Curtis, *Orbital mechanics for engineering students*. Butterworth-Heinemann, 2013.
[5] M. Schmidhuber, S. Löw, K. Müller, S. Scholz, F. Chatel, R. Faller, and J. Letschnik, "Flight dynamics operations," in *Spacecraft Operations*. Springer, 2015, pp. 124–126.
[6] S. Odenwald, "Space weather," http://www.solarstorms.org/Sscope.html.
[7] E. J. Overby, "Attitude control for the norwegian student satellite ncube," *Norwegian University of Science and Technology. Department of Engineering Cybernetics*, 2004.
[8] B. Lawson, "Satellite technologies," http://www.mpoweruk.com/satellites.htm, 2005.
[9] A. University, "Air university space primer," Air University, 2003.
[10] L. Cao, X. Chen, and T. Sheng, "Fault tolerant small satellite attitude control using adaptive non-singular terminal sliding mode," *Advances in Space Research*, vol. 51, no. 12, pp. 2374–2393, 2013.
[11] R. Burton, S. Rock, J. Springmann, and J. Cutler, "Dual attitude and parameter estimation of passively magnetically stabilized nano satellites," *Acta Astronautica*, vol. 94, no. 1, pp. 145–158, 2014.
[12] R. Wisniewski, "Linear time-varying approach to satellite attitude control using only electromagnetic actuation," *Journal of Guidance, Control, and Dynamics*, vol. 23, no. 4, pp. 640–647, 2000.
[13] L. Cao, X. Li, X. Chen, and Y. Zhao, "Minimum sliding mode error feedback control for fault tolerant small satellite attitude control," *Advances in Space Research*, vol. 53, no. 2, pp. 309–324, 2014.
[14] W. Steyn, "Magnetic attitude determination and control for low earth orbiting small satellites," *Power (milli-W)*, vol. 250, p. 150, 2001.
[15] X. Liu, P. Guan, and J. Liu, "Fuzzy sliding mode attitude control of satellite," in *Decision and Control, 2005 and 2005 European Control Conference. CDC-ECC'05. 44th IEEE Conference on*. IEEE, 2005, pp. 1970–1975.
[16] A. Sofyalı and E. M. Jafarov, "Integral sliding mode control of small satellite attitude motion by purely magnetic actuation," 2014.
[17] M. C. VanDyke, J. L. Schwartz, and C. D. Hall, "Unscented kalman filtering for spacecraft attitude state and parameter estimation," *Department of Aerospace & Ocean Engineering, Virginia Polytechnic Institute & State University, Blacksburg, Virginia*, 2004.
[18] S. J. Julier and J. K. Uhlmann, "New extension of the kalman filter to nonlinear systems," in *AeroSense'97*. International Society for Optics and Photonics, 1997, pp. 182–193.
[19] C. McManus and T. D. Barfoot, "A serial approach to handling high-dimensional measurements in the sigma-point kalman filter," *Robotics: Science and Systems VII*, p. 209, 2012.
[20] L. Perea, J. How, L. Breger, and P. Elosegui, "Nonlinearity in sensor fusion: Divergence issues in ekf, modified truncated sof, and ukf," in *AIAA Guidance, Navigation and Control Conference and Exhibit*, vol. 6514, 2007.
[21] M. S. Chen, Y. R. Hwang, and M. Tomizuka, "A state-dependent boundary layer design for sliding mode control," *Automatic Control, IEEE Transactions on*, vol. 47, no. 10, pp. 1677–1681, 2002.

Application of Decaying Boundary Layer and Switching Function Method Thorough Error Feedback for Sliding Mode Control on Spacecraft's Attitude

Hassrizal H. B.* and J. A. Rossiter[†]

* [†] Department of Automatic Control and Systems Engineering, The University of Sheffield,
Mappin Street, Sheffield, S1 3JD, UK

* School of Mechatronic Engineering, Universiti Malaysia Perlis, Malaysia

Email: * hbhassanbasri1@sheffield.ac.uk, [†] j.a.rossiter@sheffield.ac.uk

Abstract—**Effective operation of small spacecraft implies processors with low cost, energy efficiency and low computational burdens while retaining accurate output tracking. This paper presents the extension of work in [1] on eliminating the chattering for Sliding Mode Control (SMC) using a decaying boundary layer design which is able to achieve these small spacecraft operation needs. The extension is applied on a spacecraft's attitude control, while orbiting the earth with angular velocity, ω_0. In SMC, chattering is a main drawback as it can cause wear and tear to moving mechanical parts. Earlier work on a decaying boundary layer design was capable of reducing the chattering phenomena for a limited time only and hence this paper proposes a novel decaying boundary layer and switching function to improve the earlier version. The proposed technique is shown to reduce chattering permanently and also retain control output accuracy.**

Keywords: small spacecraft, spacecraft's attitude, SMC, chattering, decaying boundary layer, switching function, control accuracy

I. INTRODUCTION

A spacecraft or satellite is an object that is orbiting larger objects such as the earth. Currently there are more than 1000 operational man-made spacecraft and satellites in orbit around earth [2]. In this paper, the focus is on control strategies to maintain the spacecraft attitude; consequently there will be some discussion of dynamics and kinematics to determine the angular velocity with respect to the earth.

The spacecraft's attitude can be as important to control as its position. A spacecraft needs a motion control system to position and orientate itself correctly, especially when disturbances and uncertainties occur. The attitude motion of a spacecraft can be described as a set of differential equations [3]. The motion is given by the spacecraft body rotation with respect to different frames of motion. In space, there are disturbances and uncertainties that influence the coordinates of the spacecraft such as the gravitational force of the earth and moon and atmospheric drag in low earth orbits (LEO) [4]. Hence, a robust controller is required to make sure the spacecraft remains at the correct altitude and longitude and at the right time, moreover while producing high control accuracy.

Many control methods have been developed for a spacecraft's attitude. In this paper, Sliding Mode Control (SMC) is chosen as the basic control method for spacecraft's attitude control due to its advantages especially for small spacecraft space exploration, such as LunarSat [5]. Specifically, SMC is well-known as a robust controller, it is low complexity, can have low computational burden, low weight and low cost [6] [7]. Methods such as Adaptive Fuzzy Sliding Mode Attitude Control (AFSMC) [8], that is SMC combined with Adaptive Fuzzy rules and require a high computational load because of a complex fuzzy parameter and are not pursued. On the other hand, Minimum Sliding Mode Error Feedback Control (MSMEFC) [9] is an energy efficient, low complexity, low computational load, high control accuracy and robust control method. Moreover, MSMEFC is suitable for realistic disturbances and uncertainties experienced by a spacecraft in space and includes a cost function to offset the disturbances and uncertainties to improve the control performance.

In SMC, the controller input is $u(t) = u(t)_{eq} + u(t)_n$ where $u(t)_{eq}$ and $u(t)_n$ are denoted as equivalent control input and natural control input (switching function) respectively. $u(t)_{eq}$ is used to force the state trajectories to move to the sliding surface ($s_i(x) = 0$) as in figure 1 (in this time, $u(t)_n$ is off). When the state trajectories hit the sliding surface, $u(t)_n$ is on and ensures the state trajectories move along the sliding surface (in this time, $u(t)_{eq}$ is off). Unfortunately, using just the basis concept of SMC, chattering (figure 1) is a main drawback that can cause wear and tear in the moving mechanical parts. Chattering is produced by the switching function (1) inside the s-plane of the sliding surface ($s_i(x) = 0$).

$$u_i(t) = \begin{cases} u_i^+(x,t) & \text{with } s_i(x) > 0 \\ 0 & \text{with } s_i(x) = 0 \\ u_i^-(x,t) & \text{with } s_i(x) < 0 \end{cases} \tag{1}$$

In spacecraft operation a common actuation device is a reaction wheel. Reaction wheels consist of a rotating mass attached to an electric motor and are used to align the spacecraft's attitude on X (pitch), Y (roll) and Z (yaw) axis. Given the mechanical design, chattering will cause shorter lifespans to reaction wheels and reducing accuracy of the spacecraft's attitude. For example, in 2002, the Mars Odyssey
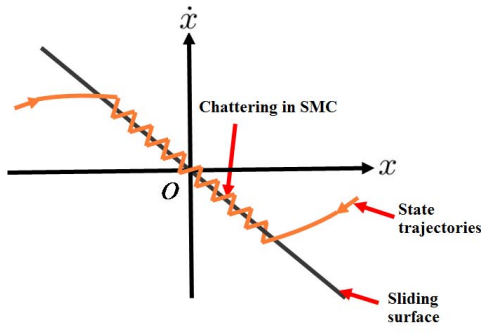
Figure 1. Chattering phenomena on s-plane in SMC

Figure 2. Constant boundary layer concept in SMC

Figure 3. Decaying boundary layer concept in SMC

spacecraft moved to safe mode because one of the reaction wheels produced unusual readings [10]. It took time before the recovery action was taken and this problem delayed the Mars Odyssey mission and increased the operational cost. Hence, many methods have been developed by researchers to overcome the chattering phenomena, while maintaining high control accuracy, such as a modification to the switching function.

A boundary layer technique is one of the most popular methods for chattering elimination in SMC. This technique strikes a trade off between invariance of system trajectories and smoothness of control [11]. The boundary layer is added inside $u(t)_n$ in $u(t)$. In [1], three boundary layer techniques around the sliding surface are introduced and discussed. The techniques are:

- A constant boundary layer (CBL): CBL (figure 2) is introduced to overcome the chattering problem but the control accuracy is dependent on the boundary layer width since the steady state error, $e_{ss} = 0$ if only if the state trajectory lies on $s = 0$.
- A decaying boundary layer (DBL): Subsequently, DBL (figure 3) was developed and this method produced greater control accuracy when the state trajectory lies on $s = 0$ but the chattering is only eliminated for a short period.
- A state-dependent boundary layer design (SDBL): Finally, for further improvement of DBL, SDBL was proposed which produces chattering-free and high control accuracy. However, SDBL requires a high complexity algorithm.

Hence, this paper proposes an alternative improvement method to the DBL work in [1] on eliminating chattering using a decaying boundary layer and switching function thorough error feedback (DBLSF) instead of using SDBL. DBLSF has less complexity compared to SDBL in [1] but produces chattering-free and high control accuracy.

Originally, in the DBL design, the boundary layer width varies with time. When the time approaches infinity, the boundary layer width becomes zero and hence the chattering reappears. Then, an initial improvement technique is proposed to the DBL, a decaying boundary layer thorough error feed-

back (DBLEF). DBLEF is proposed in order to introduce a boundary layer concept where the boundary layer width is not dependent on time. In this concept, boundary layer width will be generated every time when the error between the actual output and the required output, $|d_0| > 0$ to achieve high control accuracy.
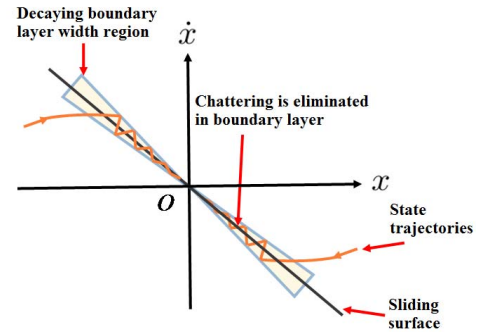
Finally, DBLSF is introduced. DBLSF is a method where the boundary layer width and switching function are proportional to and depends upon the $|d_0|$. In DBLSF, the boundary layer width reappears every time $|d_0| > 0$. Hence, the control accuracy ($|d_0| = 0$) can be guaranteed when the disturbances and uncertainties reappear. Then, when $|d_0| = 0$, the switching function will be off in order to eliminate the chattering in the controller input.

The remainder of this paper is organized as follows. Section II constructs the spacecraft's attitude model orbiting around earth. Section III reviews and examines the existing boundary layer designs of DBL and SDBL in a linear uncertain system. Section IV proposes and analyses the DBLEF. Next, Section V introduces and analyses the DBLSF. Finally, conclusions are presented in Section VI.

II. SPACECRAFT'S ATTITUDE MODEL ORBITING AROUND EARTH

In this section, the angular velocity of spacecraft's attitude is modelled and presented in state space form. A rigid body spacecraft, orbiting the earth with respect to an Earth Centered

Inertial (ECI) at an angular velocity, ω_0 with three rotational degrees of freedom is shown in Figure 4.
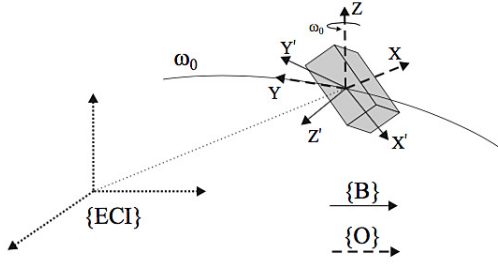
Figure 4. Spacecraft's attitude in moving frame B with respect to an orbiting reference frame O, both moving in ECI

The dynamic equations, concerning the effects of forces on the motion of the spacecraft [12] are:

$$J\dot{\omega} = J\omega \times \omega + \tau \qquad (2)$$

where $J = diag(J_x, J_y, J_z)$ is the constant inertia matrix in the body-fixed reference frame, ω is spacecraft angular velocity orbiting around Earth and $\tau = diag(\tau_x, \tau_y, \tau_z)$ is applied torque. The kinematics of the rigid body (Figure 4) using Euler's angles [12] ψ, θ and ϕ are denoted as yaw, pitch and roll angle respectively (Figure 5).
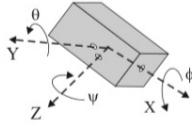
Figure 5. Sequence of Euler's angles according moving frame B orientation with respect to an orbiting frame O

The absolute angular velocity ω_B of moving frame B is:

$$\omega_B = \omega_{BO} + \omega_O \qquad (3)$$

where ω_{BO} is the velocity of B with respect to O and ω_O is the velocity of O with respect to ECI. ω_{BO} (4) depends on the sequence of rotations (Euler's angles sequence) that the orbit frame has to perform in order to reach the body frame and hence:

$$\omega_{BO} = \omega_{BO}'' + \omega_O''\omega_O' + \omega_O'\omega_O \qquad (4)$$

where ω_O' is the particular reference frame obtained from O after a first rotation of angle ψ along the first axis and ω_O'' is the angular velocity obtained from ω_O' after a second rotation of angle θ. Consequently:

$$\omega_{BO} = \begin{bmatrix} s\phi\dot{\theta} + c\theta c\phi\dot{\psi} \\ c\phi\dot{\theta} - c\theta s\phi\dot{\psi} \\ \dot{\phi} + s\theta\dot{\psi} \end{bmatrix} \qquad (5)$$

where s, c denote sine and cosine, $\dot{\psi} = \omega_O'\omega_O$, $\dot{\theta} = \omega_O''\omega_O'$ and $\dot{\phi} = \omega_{BO}''$. ω_O must be expressed in body coordinates as

in eqn.(7) below. R is the rotation matrix with sequence 1-2-3 that synodic frame O to frame B and ω_O is the angular velocity of O with respect to ECI. Hence, ω_B is given in eqn.(8).

$$\omega_O = R \begin{bmatrix} 0 \\ 0 \\ \omega_O \end{bmatrix} = \begin{bmatrix} (s\psi s\theta - c\psi s\theta c\phi)\omega_O \\ (s\psi c\phi + c\psi s\theta s\phi)\omega_O \\ c\psi c\theta\omega_O \end{bmatrix} \qquad (6)$$

$$R = \begin{bmatrix} c\theta c\phi & s\psi s\theta c\phi + c\psi s\phi & s\psi s\phi - c\psi s\theta c\phi \\ -c\theta s\phi & c\psi c\phi - s\psi s\theta s\phi & s\psi c\phi + c\psi s\theta s\phi \\ s\theta & -s\psi c\theta & c\psi c\theta \end{bmatrix} \qquad (7)$$

$$\omega_B = \begin{bmatrix} s\phi\dot{\theta} + c\theta c\phi\dot{\psi} + (s\psi s\theta - c\psi s\theta c\phi)\omega_O \\ c\phi\dot{\theta} - c\theta s\phi\dot{\psi} + (s\psi c\phi + c\psi s\theta s\phi)\omega_O \\ \dot{\phi} + s\theta\dot{\psi} + c\psi c\theta\omega_O \end{bmatrix} \qquad (8)$$

With a small angle displacement assumption between B and O, the following parameters can be linearised into $cos(\phi) = cos(\psi) = cos(\theta) \simeq 1$, $sin(\phi) \simeq \phi, sin(\psi) \simeq \psi, sin(\theta) \simeq \theta$. Then, eqn.(8) becomes:

$$\omega_B = \begin{bmatrix} \dot{\psi} - \omega_O\theta \\ \dot{\theta} + \omega_O\psi \\ p\dot{hi} + \omega_O \end{bmatrix} \qquad (9)$$

Finally, eqn.(9) is subsituted into eqn.(2) thus:

$$J_x\ddot{\psi} = (J_y - J_z)\omega_0^2\psi + (J_x + J_y - J_z)\omega_0\dot{\theta} + \tau_x \qquad (10)$$

$$J_y\ddot{\theta} = (J_z - J_y - J_x)\omega_0\dot{\psi} - (J_z - J_x)\omega_0^2\theta + \tau_y \qquad (11)$$

$$J_z\ddot{\phi} = \tau_z \qquad (12)$$

The model eqns. above are presented in state space form ($\dot{x}(t) = Ax(t) + Bu(t)$) as follows.

$$\begin{bmatrix} \dot{x_1}(t) \\ \dot{x_2}(t) \\ \dot{x_3}(t) \\ \dot{x_4}(t) \\ \dot{x_5}(t) \\ \dot{x_6}(t) \end{bmatrix} = \begin{bmatrix} 0 & 1 & 0 & 0 & 0 & 0 \\ h & 0 & 0 & i & 0 & 0 \\ 0 & 0 & 0 & 1 & 0 & 0 \\ 0 & j & k & 0 & 0 & 0 \\ 0 & 0 & 0 & 0 & 0 & 1 \\ 0 & 0 & 0 & 0 & 0 & 0 \end{bmatrix} \begin{bmatrix} x_1(t) \\ x_2(t) \\ x_3(t) \\ x_4(t) \\ x_5(t) \\ x_6(t) \end{bmatrix} + \begin{bmatrix} 0 \\ \frac{\tau_x}{J_x} \\ 0 \\ \frac{\tau_y}{J_y} \\ 0 \\ \frac{\tau_z}{J_z} \end{bmatrix} u(t) \qquad (13)$$

where

$$h = (\frac{J_y - J_z}{J_x})\omega_0^2; \qquad i = (\frac{J_x + J_y - J_z}{J_x})\omega_0;$$
$$j = (\frac{J_z - J_y - J_x}{J_y})\omega_0; \qquad k = -(\frac{J_z - J_x}{J_y})\omega_0^2;$$

$$[x_1(t) \ x_2(t) \ x_3(t) \ x_4(t) \ x_5(t) \ x_6(t)]^T = [\psi \ \dot{\psi} \ \theta \ \dot{\theta} \ \phi \ \dot{\phi}]^T$$

$$[\dot{x_1}(t) \ \dot{x_2}(t) \ \dot{x_3}(t) \ \dot{x_4}(t) \ \dot{x_5}(t) \ \dot{x_6}(t)]^T = [\dot{\psi} \ \ddot{\psi} \ \dot{\theta} \ \ddot{\theta} \ \dot{\phi} \ \ddot{\phi}]^T$$

III. EXISTING BOUNDARY LAYER DESIGNS FOR SMC

In this section, two existing boundary layer methods for controlling the angular velocity of a spacecraft's attitude are presented: (i) decaying boundary layer (DBL) for SMC [1] and (ii) state-dependent boundary (SDBL) layer for SMC [1]. The performance of the controller input and angular velocity output are observed in terms of chattering elimination and control output accuracy.

A. DBL or Decaying Boundary Layer Design for SMC

Consider a linear system with matching uncertainties is given as:

$$\dot{x}(t) = Ax(t) + B(u(t) + \Delta Ex(t) + d(t)) \qquad (14)$$

where $x(t) \in R^n$ is the system state, $u(t)$ is the scalar control input, $A \in R^{n \times n}$ and $B \in R^n$ are the nominal system matrices satisfying the controllability condition, uncertainty ΔE is possibly time varying and $d(t)$ an unknown disturbance. The system uncertainties are bounded by two unknown constants:

$$||\Delta E|| \leq \bar{E} \qquad ||d(t)|| \leq \bar{D} \qquad (15)$$

The controller input equation for a DBL was introduced in [1] as in (16) below where $-\rho(x)f_1(s)$ is $u(t)_n$ while the rest of the parameter is $u(t)_{eq}$.

$$u(t) = -\sigma s(t) - c_0 x_1(t) - CAx(t) - \rho(x)f_1(s) \qquad (16)$$

where $s(t)$ (17) is a sliding variable, C (18) incorporates coefficients c_i who's values are chosen such that the differential equation (19) is stable (poles in the left half plane), $\rho(x) = \rho_0(\bar{E}||x|| + \bar{D})$ with $\rho_0 > 1$ and $f_1(s)$ (20) is a switching function with DBL design.

$$s(t) = Cx(t) + c_0 v(t) \qquad (17)$$

$$C = [c_1, c_2, c_3, ..., 1] \qquad (18)$$

$$s(t) = x_1(t)^{n-1} + c_{n-1}x_1(t)^{n-2} + \cdots + c_1 x_1(t) + c_0 \int_0^t x_1 d\tau \qquad (19)$$

$$f_1(s) = \frac{s(t)}{|s(t)| + \epsilon_0 e^{-\pi t}} \qquad (20)$$

B. Application of DBL to a Spacecraft's Attitude Model

For the DBL design [1], consider a linear system with matching uncertainties (14) with $\omega_0 = 0.0011 rads^{-1}$, $J = diag(35, 16, 25)kgm^2$, $|\tau|_{max} = 1 \times 10^{-3}N$, the disturbance $d(t) = sin(t)$ and system uncertainties $\Delta E = 0$. The boundary layer parameters are applied to the system with $\pi = 0, \rho_0 = 1.5, \sigma = 2, \bar{E} = 0, \bar{D} = 1$ and the coefficients c_i are $C = [29, 57, 58, 32, 19, 1]$ with $c_0 = 6$. The boundary layer width tested in this example is $\epsilon_0 = 0.1$. These values are replaced in eqns.(12,14,16).

From figure 6 it is seen that the DBL can eliminate the chattering for a while (here upto $t = 25s$). However, in this technique, the boundary layer width depends on a time determined by $\epsilon_0 e^{-\pi t}$ and thus, as time approaches infinity, then this term becomes close to zero and the chattering appears again. Nevertheless, the control accuracy (figure 7) is guaranteed.
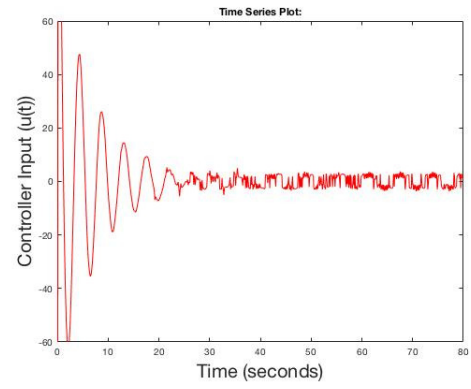
Figure 6. DBL Technique for Spacecraft's Attitude Controller Input
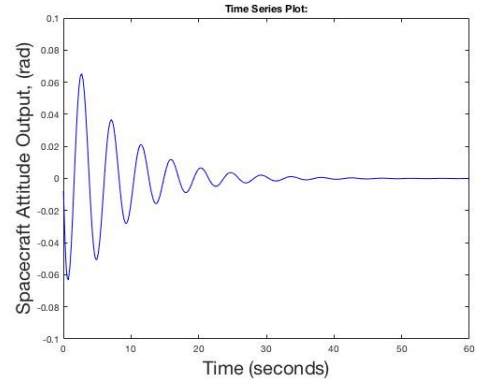
Figure 7. DBL Technique for Spacecraft's Attitude Output

C. SDBL or State-Dependent Boundary Layer Design for SMC

An alternative SDBL design for SMC is proposed in [1]. This will be used as a benchmark for proposed controller design of section V. In SDBL the controller input defined as follows:

$$\begin{aligned} u(t) = &-\sigma s(t) - c_0 x_1(t) - CAx(t) - \rho(x)f_4(s) \\ &+ \eta_1^2 G^T Pz(t) + \eta_0 \eta_1 G^T Pe_z(t) \end{aligned} \qquad (21)$$

where $P \in R^{n \times n}$ is a positive definite matrix satisfying the Lyapunov inequality (22) with F as in (23), G as in (24), $z(t)$ as in (25), η_1 as in(26), η_0 as in (27), $e_z = z(t)/||z(t)||_p$ and $f_4(s)$ as in (28) below.

$$(-F - \sigma I)^T P + P(-F - \sigma I) \leq 0 \qquad (22)$$

$$F = \begin{bmatrix} 0 & 1 & \cdot & \cdot \\ \cdot & 0 & 1 & \cdot \\ \cdot & \cdot & \cdot & \cdot \\ -c_0 & \cdot & \cdot & -c_{n-1} \end{bmatrix} \qquad (23)$$

$$G = \begin{bmatrix} 0 & 0 & \cdots & 1 \end{bmatrix}^T \qquad (24)$$

$$z(t) = \begin{bmatrix} \int_0^t x_1 d\tau & x_1 & \cdots & x_{n-1} \end{bmatrix}^T \in R^n \qquad (25)$$

$$\eta_1 = \frac{\epsilon_1}{\rho_0 - 1} > 0 \tag{26}$$

$$\eta_0 = \frac{\epsilon_0}{\rho_0 - 1} > 0 \tag{27}$$

$$f_4(s) = \frac{s(t)}{|s(t)| + \epsilon_1 ||z(t)||_p + \epsilon_0} \tag{28}$$

D. Application of SDBL to a Spacecraft's Attitude Model

Consider the same parameters value and analysis as in section III-B. Here try $\epsilon_0 = 0.001$ and $\epsilon_1 = 0.1$ while $||z||_p \equiv \sqrt{z(t)^T P z(t)}$. Figures 8,9 show that the chattering is eliminated and control output accuracy is maintained.
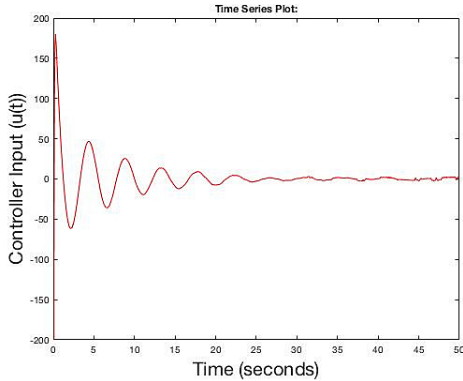
Figure 8. SDBL Technique for Spacecraft's Attitude Controller Input
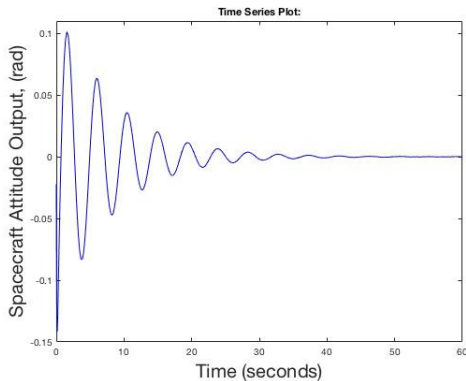
Figure 9. SDBL Technique for Spacecraft's Attitude Output

E. Conclusion

Overall, the DBL design has a simpler controller input compared to the SDBL design which has a more complicated controller input, however the former is not a chattering-free technique. Using SDBL one is able to eliminate the chattering in the controller input but there are many parameters (21) which have to be determined thus increasing the complexity of the controller input algorithm. Hence, an alternative controller input algorithm which has less controller input complexity but is still an improvement of the DBL technique is proposed. Critically, both existing boundary layer methods produce high

control output accuracy for angular velocity in the spacecraft's attitude.

IV. DECAYING BOUNDARY LAYER THOROUGH ERROR FEEDBACK (DBLEF) FOR SMC

In this section, a minor modification is made to the DBL technique. DBLEF is an initial improvement technique to the DBL. In DBL, the boundary layer width is dependent on time and chattering reappears when time approaches infinity. However, in DBLEF, the boundary layer width is dependent on the error between the actual output and the required output, $|d_0|$. Ideally, in this concept, the boundary layer width reappears every time $|d_0| > 0$. Hence, the control accuracy can be guaranteed even when disturbances and uncertainties reappear. Thus, DBLEF is defined below. Controller input and control output accuracy performances are observed by using similar analysis as in Section III.

Algorithm DBLEF: The boundary layer width will be permanently on and proportional to the error between the desired output and actual output , $|d_0| > 0$. Function $f_1(s)$ in (16) is replaced with $f_2(s)$ as in (29).

$$u(t) = -\sigma s(t) - c_0 x_1(t) - CAx(t) - \rho(x)f_2(s) \tag{29}$$

where the time t in (20) is replaced with $\frac{1}{|d_0|}$ in (30).

$$f_2(s) = \frac{s(t)}{|s(t)| + \epsilon_0 e^{\frac{-\pi}{|d_0|}}} \tag{30}$$
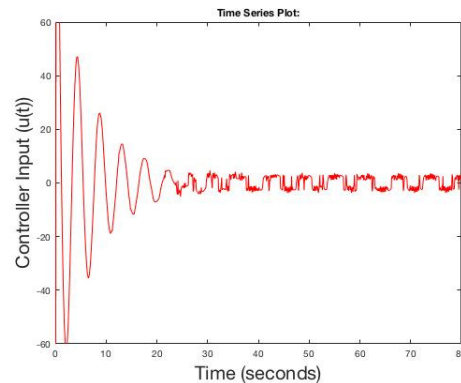
Figure 10. DBLEF Technique for Spacecraft's Attitude Controller Input

Figure 10 shows that the chattering in controller input start around $t = 23s$ when error, $|d_0 = 0|rad$ but the chattering pattern is uniformly shaped compared to DBL. The spacecraft's angular velocity output converges to zero (figure 11) with similar performance to the DBL. In summary, the minor modification inside the switching function produced minor significant change in controller input performance compared to the DBL.
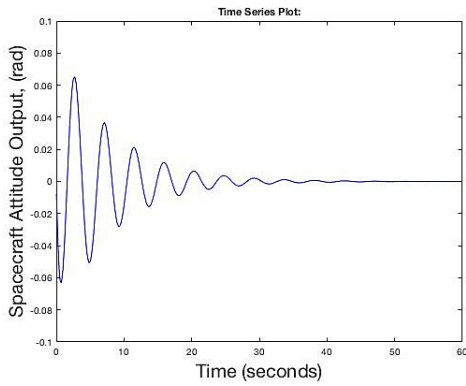
Figure 11. DBLEF Technique for Spacecraft's Attitude Output
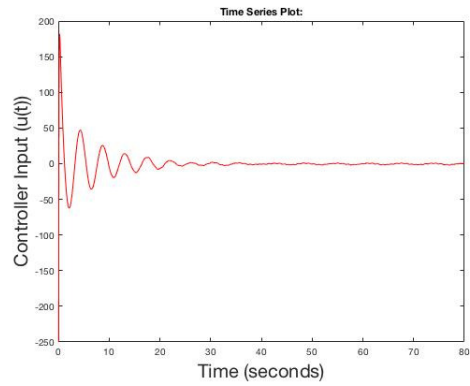
Figure 12. DBLSF Technique for Spacecraft's Attitude Controller Input

V. Decaying Boundary Layer and Switching Function Thorough Error Feedback (DBLSF) for Sliding Mode Control

In section IV, the DBLEF design shows the chattering pattern is uniformly shaped compare to the DBL but unable to eliminate the chattering in spacecraft's attitude controller input. Hence, another modification based on DBLEF method is required to achieve the aims of this research. At the end of this section, the controller input and control output accuracy performance are investigated.

A. Proposed SMC algorithm

In figure 6, the DBL for SMC is seen to eliminate the chattering until $t = 25s$ and a new decaying boundary layer thorough error feedback for SMC, the chattering appeared at $t = 23s$. Thus, a new decaying boundary layer and switching function thorough error feedback (DBLSF) for sliding mode control is introduced to overcome this problem. This proposed method is less complex compared to the state-dependent boundary layer for SMC technique in Section VI.

Algorithm DBLSF: The boundary layer and switching function in control input (31) will occur when $|d_0| > 0$ (32). When $|d_0|$ approach to zero, the boundary layer will converge to zero while switching function will decaying off. Thus the input is given as

$$u(t) = -\sigma s(t) - c_0 x_1(t) - CAx(t) - \rho(x)f_3(s) \quad (31)$$

where the DBL $f_1(s)$ (20) is replaced by the DBLSF

$$f_3(s) = \frac{s(t)e^{\frac{-\pi}{|d_0|}}}{|s(t)| + \epsilon_0 e^{\frac{-\pi}{|d_0|}}} \quad (32)$$

Figure 12 shows that the chattering is totally eliminated in the spacecraft's attitude controller input while the control accuracy is good, see figure 13. This control method is thus proven able to eliminate the chattering while maintain the control output accuracy.
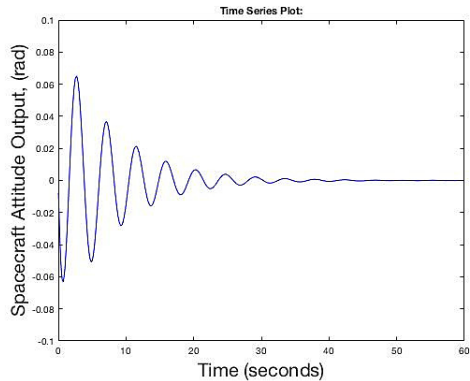
Figure 13. DBLSF Technique for Spacecraft's Attitude Output

B. Review of all four SMC algorithms

Overall, four SMC controller input algorithms for spacecraft's attitude control are discussed in this paper. DBL is a simple controller input algorithm (16) but the chattering (figure 6) is reappears when time approaches infinity. SDBL is an improvement to the DBL which produces chattering-free (figure 8) for controller input performance but SDBL requires high complexity (21) controller input algorithm. Hence, the DBLEF and DBLSF are proposed as the alternative methods of SDBL in order to eliminate the chattering for SMC in spacecraft's attitude system.

The first proposed design, DBLEF is unable to eliminate the chattering (figure 10) since the chattering reappears when $|d_0| = 0$. Then, DBLSF is proposed to eliminate the chattering (figure 12). DBLSF performances are comparable to the SDBL design but have a less complex algorithm (31) which thus is suitable to be implemented on small spacecraft operation. On the other hand, all four SMC controller input algorithms produce high control accuracy (figure 7,9,11,13).

VI. Conclusions and Future Recommendations

SMC approaches can produce high control accuracy but the occurrence of chattering phenomena is a significant drawback. The proposed DBLSF method in this paper is able to elimi-

nate chattering to a level comparable with more complicated methods such as SDBL.

However, in space, there are a few substantive and rigorous scenarios such as fault tolerant cases (actuator degradation scenario where the actuator work efficiency degrades by time (LOE), actuator fault after a certain time scenario (LIUT) and actuator failure for a short time period scenario (FFPT) [13], debris (encompasses by natural (meteoroid) and artificial (man-made) particles) avoidance in space [14] and spacecrafts formation [15]. Future work intends to investigate and justify the capability and robustness of DBLSF design on these scenarios. The spacecraft's attitude and orientation controller design must be low cost, robust, achieve high precision, high efficiency and low computational in order to be suitable to be implemented on small spacecraft.

VII. Acknowledgements

References

[1] M. S. Chen, Y. R. Hwang, and M. Tomizuka, "A state-dependent boundary layer design for sliding mode control," *Automatic Control, IEEE Transactions on*, vol. 47, no. 10, pp. 1677–1681, 2002.

[2] U. of Concerned Scientists, "Ucs satellite database," http://www.ucsusa.org/nuclear-weapons/space-weapons/satllite-database, 2016.

[3] N. S. Hussain, H. H. Basri, and S. Yaacob, "State-dependent boundary layer method for attitude control of satellite," *Jurnal Teknologi*, vol. 76, no. 12, 2015.

[4] M. Schmidhuber, S. Löw, K. Müller, S. Scholz, F. Chatel, R. Faller, and J. Letschnik, "Flight dynamics operations," in *Spacecraft Operations*. Springer, 2015, pp. 124–126.

[5] Y. Gao, A. Phipps, M. Taylor, I. A. Crawford, A. J. Ball, L. Wilson, D. Parker, M. Sweeting, A. da Silva Curiel, P. Davies *et al.*, "Lunar science with affordable small spacecraft technologies: Moonlite and moonraker," *Planetary and Space Science*, vol. 56, no. 3, pp. 368–377, 2008.

[6] T. Nguyen, J. Leavitt, F. Jabbari, and J. Bobrow, "Accurate sliding-mode control of pneumatic systems using low-cost solenoid valves," *IEEE/ASME Transactions on mechatronics*, vol. 12, no. 2, pp. 216–219, 2007.

[7] A. Sofyalı and E. M. Jafarov, "Integral sliding mode control of small satellite attitude motion by purely magnetic actuation," *IFAC Proceedings Volumes*, vol. 47, no. 3, pp. 7947–7953, 2014.

[8] X. Liu, P. Guan, and J. Liu, "Fuzzy sliding mode attitude control of satellite," in *Decision and Control, 2005 and 2005 European Control Conference. CDC-ECC'05. 44th IEEE Conference on*. IEEE, 2005, pp. 1970–1975.

[9] L. Cao, X. Li, X. Chen, and Y. Zhao, "Minimum sliding mode error feedback control for fault tolerant small satellite attitude control," *Advances in Space Research*, vol. 53, no. 2, pp. 309–324, 2014.

[10] S. Staff, "Mars odyssey spacecraft goes into standby after malfunction," http://www.space.com/16094-mars-odyssey-orbiter-safe-mode.html, 2012.

[11] P. V. Suryawanshi, P. D. Shendge, and S. B. Phadke, "A boundary layer sliding mode control design for chatter reduction using uncertainty and disturbance estimator," *International Journal of Dynamics and Control*, pp. 1–10, 2015.

[12] F. Bacconi, "Spacecraft attitude dynamics and control," *Florence: Florence university*, vol. 2006, pp. 1–0, 2005.

[13] L. Cao, X. Chen, and T. Sheng, "Fault tolerant small satellite attitude control using adaptive non-singular terminal sliding mode," *Advances in Space Research*, vol. 51, no. 12, pp. 2374–2393, 2013.

[14] D. J. Kessler and B. G. Cour-Palais, "Collision frequency of artificial satellites: the creation of a debris belt," *Journal of Geophysical Research: Space Physics*, vol. 83, no. A6, pp. 2637–2646, 1978.

[15] L. Felicetti and M. R. Emami, "A multi-spacecraft formation approach to space debris surveillance," *Acta Astronautica*, vol. 127, pp. 491–504, 2016.

Feasibility Study of Switching Function Approaches in Sliding Mode Control for a Spacecraft's Attitude Control System

Hassrizal H. B.[*], J. A. Rossiter[†] and A. R. Firdaus[‡]

[*] [†] [‡] Department of Automatic Control and Systems Engineering, The University of Sheffield,
Mappin Street, Sheffield, S1 3JD, UK
[*] School of Mechatronic Engineering, Universiti Malaysia Perlis, Malaysia
Email: [*] hbhassanbasri1@sheffield.ac.uk, [†] j.a.rossiter@sheffield.ac.uk, [‡] arfirdaus2@sheffield.ac.uk

Abstract—Sliding Mode Control (SMC) is well known as a robust control approach and is proven to be able to deal with nonlinear systems. To achieve this capability, the SMC controller input design is divided into two parts: a sliding surface design (continuous control) and a switching function design (discontinuous control). A spacecraft's attitude model is a multi-input and multi-output (MIMO) system and thus control design is difficult for some methodologies, however, in this case a SMC, is straightforward to construct. In this paper, for the continuous part, a reduction of order method (ROOM) is used to construct the sliding surface. For the discontinuous control, three different switching functions are designed and evaluated such as relays with constant gains, relays with state dependent gains and linear feedback with switched gains. The main contribution of this paper is to both analyse and investigate the limitations of these three switching functions at two different points (critical gains and proper gains) on a spacecraft's attitude model. The gains are selected using trial and error techniques as long as these gains meet the sufficiency conditions for the existence of a sliding mode. The discontinuous control is a high-speed switching function that produces chattering in the control input; however, solutions for chattering drawbacks are not discussed here. The best switching function is chosen based on the spacecraft's attitude transient performance requirements.

Keywords: SMC, switching function, sliding surface, spacecraft's attitude

I. INTRODUCTION

In space, spacecraft positioning is challenged by disturbances and uncertainties such as sun UV, solar storms, atmospheric drag in low earth orbits and, sun and moon gravitational forces [1]. Hence, a robust controller is required to maintain the orientation of the spacecraft when these challenges occur. Criteria such as computational time, control power consumption and control output accuracy must be considered when designing an appropriate robust controller. These criteria are very important to make sure a spacecraft is successfully able to accomplish its missions in the prescribed period.

Among the possible robust control strategies, Sliding Mode Control (SMC) attributes such as low complexity, low computational burden, less weight and low cost control method make this a suitable approach to be implemented as a spacecraft attitude controller [2]. Adaptive Fuzzy SMC [3], Minimum Sliding Mode Error Feedback [4] and Integral SMC [5] have been successfully proposed for spacecraft attitude and orientation model. Furthermore, as spacecraft's attitude model is a multi-input and multi-output (MIMO) system, using SMC, the compensated system is easy to design. Thus, in this paper, SMC is chosen as the base methodology for designing a spacecraft attitude and orientation control law.

SMC control law design can be divided into two characteristic features (as expanded in Section III); the continuous and discontinuous control parts. The continuous part will drive the state trajectories of the controlled system onto the sliding surface in a prescribed manner while the discontinuous feature will maintain the states on the sliding surface [6]. There are various approaches to design the continuous part such as regular form and the reduced order dynamics, method of hierarchy and diagonalization methods [7] for a MIMO system. This paper, however, will use the reduction of order method (ROOM) to design the continuous part. The rationale for this is that in the ROOM method, the sliding surface coefficients can be chosen flexibly and thus looser assumptions can be made as long as the characteristic equation of the compensated system is comparable to the design criteria. For the discontinuous part (switching function), three approaches (relays with constant gain, relays with state dependent gains and linear continuous feedback) are evaluated on a known spacecraft attitude model [7].

It is important to understand the range of limitations of these SMC methods before further improvements can be made. Hence, the main novelty of this paper is to design and investigate the SMC control law with a focus on the switching function (SFD) characteristics and capability at two different points (critical gains and proper gains) for a spacecraft's attitude control. A notable part of the proposed approach is that some of the gains can be tuned using trial and error while satisfying some mild conditions to ensure the existence of a sliding mode. Characteristics such as chattering in the control inputs and transient response in the outputs are observed. Consequently, the switching function with most advantages is chosen as a basis for proposed improvements. On the other hand, ideally, the discontinuous control law must produce chattering due to a fast switching mechanism and discontinuous control across the sliding surface [8]. In this paper, approaches for chattering attenuation are not discussed and elimination techniques are proposed for future work.

The remainder of this paper is organized as follows. Section

II constructs the spacecrafts attitude model orbiting around earth. Section III designs and examines the SMC control law (ROOM and SFD) in a nonlinear uncertain MIMO system at two different situations. Next, Section IV analyses and evaluates the designed methods with special attention on potential improvements. Finally, conclusions and future proposals are presented in Section V.

II. SPACECRAFT'S ATTITUDE AND ORIENTATION MODEL

In this section, the rotational equation of motions (EOM) [9] of a spacecraft's rigid body in the body-fixed frame orbiting the earth with respect to an Earth Centered Inertial (ECI) (figure 1) are presented.
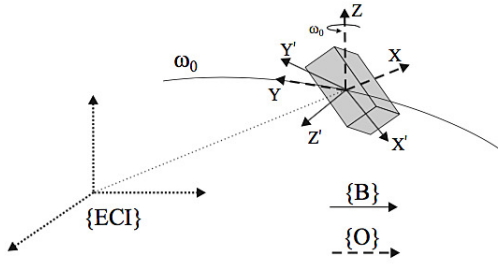
Figure 1. Spacecraft's attitude orbiting reference frame O, in moving frame B. Both are moving in ECI [10].

Consider the general form of a nonlinear system in state-space as in (1).

$$\dot{x}(t) = f(t, x) + B(u(t) + d(t)) \tag{1}$$

where $x(t) \in R^n$ is a set of state variables, $f(t, x) \in R^n$ is a nonlinear function, $B \in R^{m \times n}$ matrix, $u(t) \in R^m$ is a set of inputs and $d(t) \in R^m$ is the disturbances. Then, the EOM of a spacecraft are summarised as:

$$\boldsymbol{J\dot{\omega}} = \boldsymbol{J\omega} \times \boldsymbol{\omega} + \boldsymbol{\tau} \tag{2}$$

where $\boldsymbol{J}$=diag$(J_x, J_y, J_z) \in R^{N \times M}$ is the inertia tensor of rigid body, $\boldsymbol{\omega} \in R^M$ is spacecraft angular velocity, $\dot{\boldsymbol{\omega}} \in R^M$ is angular acceleration and $\boldsymbol{\tau} \in R^M$ is torque control input generated by the spacecraft's actuators. The vector $\boldsymbol{\omega}$ has three rotational degrees of freedom (Z, Y, and X axes are denoted as yaw (ψ), pitch (θ) and roll (ϕ) respectively).

The absolute angular velocity $\boldsymbol{\omega_B}$ of moving frame $\boldsymbol{B}$ is represented as follows where $\boldsymbol{\omega_{BO}}$ is the velocity of B respect to O and $\boldsymbol{\omega_O}$ is the velocity of O with respect to ECI.

$$\boldsymbol{\omega_B} = \boldsymbol{\omega_{BO}} + \boldsymbol{\omega_O}; \quad \boldsymbol{\omega_B} = \begin{bmatrix} \dot{\psi} - \omega_o \theta \\ \dot{\theta} + \omega_o \psi \\ \dot{\phi} + \omega_o \end{bmatrix} \tag{3}$$

Then, (3) is substituted into (2) with ω replaced by ω_B. Finally, the nonlinear spacecraft's attitude system is given by a form similar to (1) with:

$$
\begin{aligned}
\dot{x}(t) &= \begin{bmatrix} \dot{x_1} & \dot{x_2} & \dot{x_3} & \dot{x_4} & \dot{x_5} & \dot{x_6} \end{bmatrix}^T \\
f(t, x) &= \begin{bmatrix} x_2 & \bar{j} & x_4 & \bar{k} & x_6 & \bar{l} \end{bmatrix}^T \\
B &= \begin{bmatrix} 0 & 0 & 0 \\ 1 & 0 & 0 \\ 0 & 0 & 0 \\ 0 & 1 & 0 \\ 0 & 0 & 0 \\ 0 & 0 & 1 \end{bmatrix} \\
u(t) &= \begin{bmatrix} \frac{\tau_x}{J_x} & \frac{\tau_y}{J_y} & \frac{\tau_z}{J_z} \end{bmatrix}^T
\end{aligned}
\tag{4}
$$

where $\begin{bmatrix} \psi & \dot{\psi} & \theta & \dot{\theta} & \phi & \dot{\phi} \end{bmatrix}$ are replaced by $\begin{bmatrix} x_1 & x_2 & x_3 & x_4 & x_5 & x_6 \end{bmatrix}$ respectively and

$$
\begin{aligned}
\bar{j} &= (\frac{J_y - J_z + J_x}{J_x})\omega_o x_4 - (\frac{J_y - J_z}{J_x})(x_4 x_6 + x_1 x_2 \omega_o + x_1 \omega_o^2); \\
\bar{k} &= (\frac{J_z - J_x - J_y}{J_y})\omega_o x_2 + (\frac{J_z - J_x}{J_y})(x_2 x_6 - x_3 x_5 \omega_o - x_3 \omega_o^2); \\
\bar{l} &= (\frac{J_x - J_y}{J_z})(x_2 x_4 - x_3 x_4 \omega_o + x_1 x_2 \omega_o - x_1 x_3 \omega_o^2);
\end{aligned}
$$

In conclusion, the spacecraft's attitude model is a MIMO system where the inputs $u(t)$ are the torques τ_x, τ_y, τ_z generated by actuators while the outputs are the spacecraft's angular velocity in the X, Y and Z directions.

III. CONTROL LAW DESIGN IN SMC

In this section, the constructions of SMC control law are presented. There are two stages to design the control law (U_i) that is continuous (U_{eq}) and discontinuous (U_N) control.

$$U_i = U_N + U_{eq} \tag{5}$$

In this paper, the first part (continuous control (U_{eq})) is designed by manipulating the inputs of the uncompensated system using ROOM by introducing sliding surfaces. ROOM is chosen because this method is suitable and easy to design for a MIMO system.

The main contribution of this paper is focussed on the second part of the control design. In the discontinuous control (U_N) component, three alternative approaches are designed and deployed; relays with constant gains (RCG), relays with state dependent gains (RSG) and linear feedback with switched gains (LFSG) [7]. Practically, the gains are estimated adapting upper bound of the matching uncertainties [11]. Hence, the specific novelty in this section is the construction of the switching function at two different gain points (critical gains and proper gains) in order to observe their constraints. The critical gains are referred to the conditions where the spacecraft's angular velocity produces uniform steady state chattering outputs when torques and disturbances are given to the system while for the proper gains, the steady state error of the outputs are zero. For both situations, the gains for all approaches are estimated using trial and error technique by observing the outputs pattern until fulfill the critical gains and proper gains

criteria. The gains are tuning using trial and error techniques as long as the values are fulfill the conditions for the existence of a sliding mode (as expanded in Section III-C). Thereafter, the performances of the alternative switching functions are evaluated and compared.

A. Switching Surface Design using Reduction of Order Method

The basic method in SMC is to design a set of switching surfaces ($\sigma(x)$). The switching surface equation and the dynamics equation where S is the switching surface coefficients are summarised as:

$$\sigma(x) = Sx = 0 \tag{6}$$

$$\dot{\sigma}(x) = S\dot{x} = 0 \tag{7}$$

The spacecraft's attitude model is a multi-input (3 inputs) and multi-output (3 outputs) system. Hence, three set of switching surface coefficients (S_1, S_2, and S_3) are required for the spacecraft's attitude model:

$$S = \begin{bmatrix} S_1 \\ S_2 \\ S_3 \end{bmatrix} = \begin{bmatrix} s_{11} & s_{12} & s_{13} & s_{14} & s_{15} & s_{16} \\ s_{21} & s_{22} & s_{23} & s_{24} & s_{25} & s_{26} \\ s_{31} & s_{32} & s_{33} & s_{34} & s_{35} & s_{36} \end{bmatrix} \tag{8}$$

In this paper, and with the spacecraft's attitude model to be used, it is appropriate to have the characteristic equation at $\lambda^3 + 6\lambda^2 + 11\lambda + 6$ with poles at -1, -2 and -3; the selection of the characteristic equation is made in order to allow the spacecraft's attitude converge to the zero less than 100 seconds [12]. Thus, some assumptions on the switching surface coefficients (s_{ij}) are needed to ensure this characteristic equation is achieved.

B. ROOM design

The switching surface design using ROOM is as follows. Firstly, (1) is replaced in (7) and produces:

$$S\dot{x} = S(f(t,x) + B(U_{eq} + d(t))) = 0 \tag{9}$$

Now, $u(t)$ become control law U_{eq} (the continuous part). Hence:

$$U_{eq} = -(SB)^{-1}(Sf(t,x) + SBd(t)) \tag{10}$$

Then, (10) is substituted into (1) and produces :

$$\dot{x} = [I - B(SB)^{-1}S]f(t,x) \tag{11}$$

In ROOM, assumptions can be made on the s_{ij} values and can be chosen flexibly. First define SB

$$SB = \begin{bmatrix} s_{12} & s_{14} & s_{16} \\ s_{22} & s_{24} & s_{26} \\ s_{32} & s_{34} & s_{36} \end{bmatrix} \tag{12}$$

The determinant of SB can be set to any value as long as $|SB| \neq 0$ and $s_{ij} \geq 0$. To simplify the design process, assume $|SB| = 1$. One of the combinations to set $|SB| = 1$ is to let

$s_{12} = s_{14} = s_{22} = s_{26} = s_{32} = s_{34} = s_{36} = 1$, $s_{24} = 2$ and $s_{16} = 0$.

Thus, based on these selections, then:

$$(SB)^{-1} = \begin{bmatrix} 1 & -1 & 1 \\ 0 & 1 & -1 \\ -1 & 0 & 1 \end{bmatrix} \tag{13}$$

Next, substitute (4), (8) and (13) into (11) so the dynamic model is reduced to:

$$\begin{bmatrix} \dot{x_1} \\ \dot{x_2} \\ \dot{x_3} \\ \dot{x_4} \\ \dot{x_5} \\ \dot{x_6} \end{bmatrix} = \begin{bmatrix} 0 & 1 & 0 & 0 & 0 & 0 \\ 0 & a & 0 & b & 0 & c \\ 0 & 0 & 0 & 1 & 0 & 0 \\ 0 & d & 0 & e & 0 & f \\ 0 & 0 & 0 & 0 & 0 & 1 \\ 0 & 0 & 0 & h & 0 & i \end{bmatrix} \begin{bmatrix} x_1 \\ x_2 \\ x_3 \\ x_4 \\ x_5 \\ x_6 \end{bmatrix} \tag{14}$$

where

$$
\begin{array}{llll}
a &=& s_{21} - s_{11} - s_{31}; & \quad b &=& s_{23} - s_{13} - s_{33}; \\
c &=& s_{25} - s_{15} - s_{35}; & \quad d &=& s_{31} - s_{21}; \\
e &=& s_{33} - s_{23}; & \quad f &=& s_{35} - s_{25}; \\
g &=& s_{11} - s_{31}; & \quad h &=& s_{13} - s_{33}; \\
i &=& s_{15} - s_{35}; & &
\end{array}
$$

Finally, using (7) and (14), the reduced order model of the spacecraft's attitude system is:

$$\dot{\hat{x}} = \begin{bmatrix} \dot{\hat{x}_1} \\ \dot{\hat{x}_2} \\ \dot{\hat{x}_3} \end{bmatrix} = \begin{bmatrix} a & b & c \\ d & e & f \\ g & h & i \end{bmatrix} \begin{bmatrix} \hat{x}_1 \\ \hat{x}_2 \\ \hat{x}_3 \end{bmatrix} \tag{15}$$

where $\dot{\hat{x}_1} = \dot{x_2}$, $\dot{\hat{x}_2} = \dot{x_4}$ and $\dot{\hat{x}_3} = \dot{x_6}$.

In this design, the characteristic equation of (15) is matched to $\lambda^3 + 6\lambda^2 + 11\lambda + 6$, in order to achieve zero steady state error less than 100 seconds [12]. Hence, the expanded characteristic equation of (15) is given as:

$$
\begin{aligned}
\Delta(\dot{\hat{x}}) = \quad & \lambda^3 + (s_{11} - s_{15} - s_{21} + s_{23} + s_{31} - s_{33} + s_{35})\lambda^2 \\
& + (s_{11}s_{23} - s_{13}s_{21} - s_{11}s_{25} + s_{15}s_{21} + s_{13}s_{25} \\
& - s_{15}s_{23} - s_{11}s_{33} + s_{13}s_{31} + 2s_{11}s_{35} - 2s_{15}s_{31} \\
& - s_{13}s_{35} + s_{15}s_{33} - s_{21}s_{35} + s_{25}s_{31} + s_{23}s_{35} \\
& - s_{25}s_{33})\lambda + (s_{11}s_{23}s_{35} - s_{11}s_{25}s_{33} - s_{13}s_{21}s_{35} \\
& + s_{13}s_{25}s_{31} + s_{15}s_{21}s_{33} - s_{15}s_{23}s_{31})
\end{aligned} \tag{16}
$$

and the implied constraints on the values s_{ij} are given as:

$$s_{11} - s_{15} - s_{21} + s_{23} + s_{31} - s_{33} + s_{35} \qquad = \quad 6$$

$$
\begin{aligned}
& s_{11}s_{23} - s_{13}s_{21} - s_{11}s_{25} + s_{15}s_{21} + s_{13}s_{25} \\
& - s_{15}s_{23} - s_{11}s_{33} + s_{13}s_{31} + 2s_{11}s_{35} - 2s_{15}s_{31} \\
& - s_{13}s_{35} + s_{15}s_{33} - s_{21}s_{35} + s_{25}s_{31} \\
& + s_{23}s_{35} - s_{25}s_{33} \qquad\qquad = \quad 11
\end{aligned}
$$

$$
\begin{aligned}
& s_{11}s_{23}s_{35} - s_{11}s_{25}s_{33} - s_{13}s_{21}s_{35} \\
& + s_{13}s_{25}s_{31} + s_{15}s_{21}s_{33} - s_{15}s_{23}s_{31} \qquad = \quad 6
\end{aligned} \tag{17}
$$

In this paper we will define $s_{13} = 0.5$, $s_{15} = 4$, $s_{23} = 3$, $s_{25} = 2$, $s_{31} = 1$ and $s_{35} = 2$ and then use these values in combination with (17) to solve for the remaining coefficients s_{ij}. Thus:

$$
\begin{aligned}
s_{11} - s_{21} - s_{33} + 2 &= 6 \\
5s_{11} + 1.5s_{21} + 2s_{33} - s_{11}s_{33} - 11.5 &= 11 \\
6s_{11} - s_{21} - 2s_{11}s_{33} + 4s_{21}s_{33} - 11 &= 6
\end{aligned}
\tag{18}
$$

Solving (18), then $s_{11} = 5.5303$, $s_{21} = 0.0623$ and $s_{33} = 1.468$. Finally, the switching surface design of (8) is given as follows:

$$
S = \begin{bmatrix} 5.5303 & 1 & 0.5 & 1 & 4 & 0 \\ 0.0623 & 1 & 3 & 2 & 2 & 1 \\ 1 & 1 & 1.468 & 1 & 2 & 1 \end{bmatrix}
\tag{19}
$$

In conclusions, using the ROOM approach there are 18 coefficients which have to be selected to define the switching surface design. This gives a huge amount of flexibility to the designer. In principle one can meet the required dynamics for the sliding mode by choosing 15 coefficients and then solving for the remaining 3 to ensure sure the compensated system meets the design criteria. This paper does not explore how this flexibility might be exploited in general. However, the further details can be referred in [7].

C. Switching Function Design (SFD)

There are three popular variants of SFD (RCG, RSG and LFSG) which are discussed in this section and for two different scenarios which are critical gains and proper gains. The general form of RCG, RSG and LFSG are shown in Table I.

Table I
EXISTING SWITCHING FUNCTION CONTROL ALGORITHM

SFD	Algorithm	Condition
RCG	$U_{iN}(x) = \begin{cases} \alpha_i sgn(\sigma_i(x)), \\ 0 \end{cases}$	$\sigma_i(x) \neq 0$ $\sigma_i(x) = 0$
RSG	$U_{iN}(x) = \begin{cases} \alpha_i(x) sgn(\sigma_i(x)), \\ 0 \end{cases}$	$\sigma_i(x) \neq 0$ $\sigma_i(x) = 0$
LFSG	$U_N(x) = -L\sigma(x)$	L is symmetric positive definite constant matrix

1) Relays with constant gains (RCG): The rules to meet the sufficiency condition for the designed SMC is $\sigma\dot{\sigma} = \alpha_i\sigma_i(x)sgn(\sigma_i(x)) < 0$, if $\sigma_i(x) \neq 0$. α_i is a constant tuning gain ($\|\alpha_i\| \leq \bar{D}$, $\bar{D}$ is upper bound of matching uncertainties) where the value must be negative $\alpha_i < 0$. The stability condition for RCG is:

$$
\begin{aligned}
\sigma_i(x)\dot{\sigma}_i(x) &= \alpha_i\sigma_i(x)sgn(\sigma_i(x)) < 0 \\
&= \alpha_i \frac{\sigma_i^2(x)}{|\sigma_i(x)|}
\end{aligned}
$$

Let,

$$
\alpha_i < 0
\tag{20}
$$

Then,

$$
\begin{aligned}
\sigma_i(x)\dot{\sigma}_i(x) &= -\alpha_i \frac{\sigma_i^2(x)}{|\sigma_i(x)|} \\
&< 0
\end{aligned}
$$

Thus, the switching surface is meet the sufficiency conditions for the designed SMC. By observing the pattern outputs (as expanded in Section I), the critical gains and proper gain values for RCG are shown in Table II.

2) Relays with state dependent gains (RSG): The stability rules for the RSG controller are $\sigma\dot{\sigma} = \alpha_i(x)\sigma_i(x)sgn(\sigma_i(x)) < 0$, if $\sigma_i(x) \neq 0$. $\alpha_i(x)$ is a variable states function where $\alpha_i(x) = \beta_i(\sigma_i^{2k}(x) + \gamma_i)$ with $\beta_i < 0$, $\gamma_i > 0$ and k is an integer number.

$$
\begin{aligned}
\sigma_i(x)\dot{\sigma}_i(x) &= \alpha_i(x)\sigma_i(x)sgn(\sigma_i(x)) < 0 \\
\alpha_i(x) &= \beta_i(\sigma_i^{2k}(x) + \gamma_i)
\end{aligned}
$$

Let,

$$
\beta_i(x) < 0, \gamma_i > 0, k = \text{positive integer}
$$

Then,

$$
\begin{aligned}
\sigma_i(x)\dot{\sigma}_i(x) &= -\beta_i(\sigma_i(x)^2k + \gamma_i)\frac{\sigma_i(x)^2}{|\sigma_i(x)|} \\
&< 0
\end{aligned}
\tag{21}
$$

Hence, the stability rules are fulfill in term of sliding mode existence. Table II shows the critical gains and proper gains as discussed in Section I.

3) Linear feedback with switched gains (LFSG): The stability condition for LFSG is $\sigma^T(x)\dot{\sigma}(x) = -\sigma^T(x)L\sigma(x) < 0$, if $\sigma(x) \neq 0$, L is a symmetric positive definite constant matrix, $L \in R^{m \times m}$. In this paper, L is a 3×3 matrix

$$
L = \begin{bmatrix} w & y & z \\ y & w & y \\ z & y & w \end{bmatrix}
\tag{22}
$$

w, y and z values are given in Table II in order to produce uniform chattering and zero steady state in spacecraft's angular velocity outputs for critical gains and proper gains analysis respectively.

Table II
GAIN SELECTION FOR SFD

SFD	RCG	RSG		LFSG
	α_i	β	γ	L
Critical Gain	-0.01	-1	0.01	w=0.02, y=0.01, z=0
Proper Tuning	-0.000001	-1.0	0.000001	w=0.000002, y=0.000001, z=0

4) Critical Gains and Proper Gains: There are two different gains (critical gains and proper gains) where analysis of performance are made on these switching functions designs listed in Table I. The aims is to explore the limitations of

the SFD performances an gain insight into how alternative proposals may be better suited to the given application. A particular noteworthy point is that the gains in Table II are typically selected using trial and error techniques to meet the conditions in Table I and there is clearly a need for a more systematic approach and insight into the repercussions of the decisions taken.

IV. RESULTS

To perform and evaluate the designed control law with a real case situation, next this paper considers the spacecraft's attitude model in (4) with numeric parameters as in Table III. The selection of inertia tensor, J_x, J_y and J_z is based on the International Space Station (ISS) [9] values. This section will present the simulation results of the nonlinear system with and without the SMC switching function approaches. The results are divided into two parts; angular rate response at critical gains, and proper gains and control input. For the first subsection the transient response of the angular rate for both gains selections are observed while the chattering phenomena is analyzed in the second subsection.

Table III
NUMERIC PARAMETERS OF SPACECRAFT'S ATTITUDE SYSTEM

Parameter	Value	Unit
ω_o	0.0011	$rads^{-1}$
J_x	127538483.85	kgm^2
J_y	201272329.17	kgm^2
J_z	106892554.98	kgm^2
τ_x, τ_y, τ_z	1×10^{-3}	N
$d(t)$	$sin(t)$	N

A. Angular Velocity of Spacecraft's Attitude System

Figures 2 and 3 show the angular rate response of the uncompensated (open-loop) spacecraft's attitude system and the same system in closed-loop with RCG, RSG and LFSG, for critical gains and proper gains respectively.

- For critical gains, the uncompensated system shows that the outputs for yaw, pitch and roll do not settle at zero steady state error and thus closed-loop control is needed.
- For RCG, the outputs settle around 120 seconds with chattering at an amplitude at $0.02~rads^{-1}$.
- RSG shows a chattering amplitude similar to RCG (0.02 $rads^{-1}$) but converges faster in around 40 seconds.
- With LFSG, the angular velocity shows no chattering in the outputs, but the convergence is somewhat slower at 280 seconds.

For the proper gains selections in figure 3, all the SFD methods show zero steady state error with no discernible chattering. With RCG and LFSG the angular rates converge to the equilibirium point in around 10 seconds whereas RSG takes around 100 seconds to achieve the equilibirium point. Again the open-loop response does not converge. The summary of SFD performances is summarised in Tables IV and V.
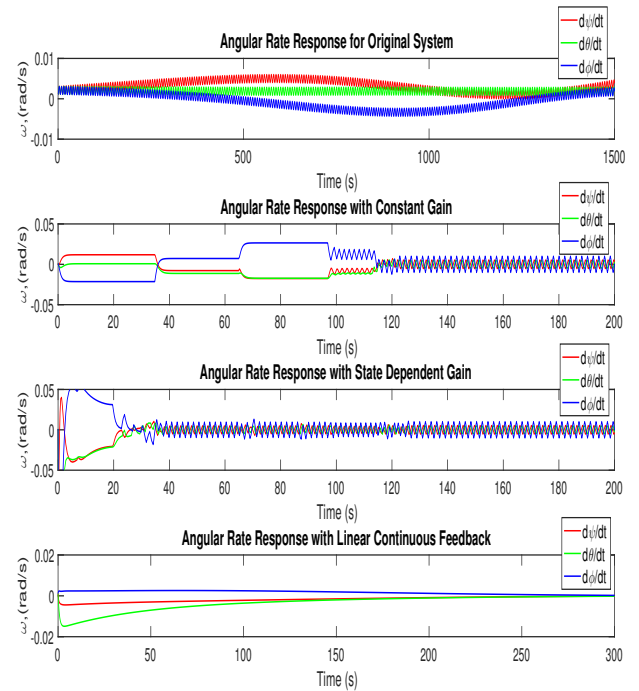
Figure 2. Angular Rate Response of the Uncompensated and Compensated System at the Critical Gain
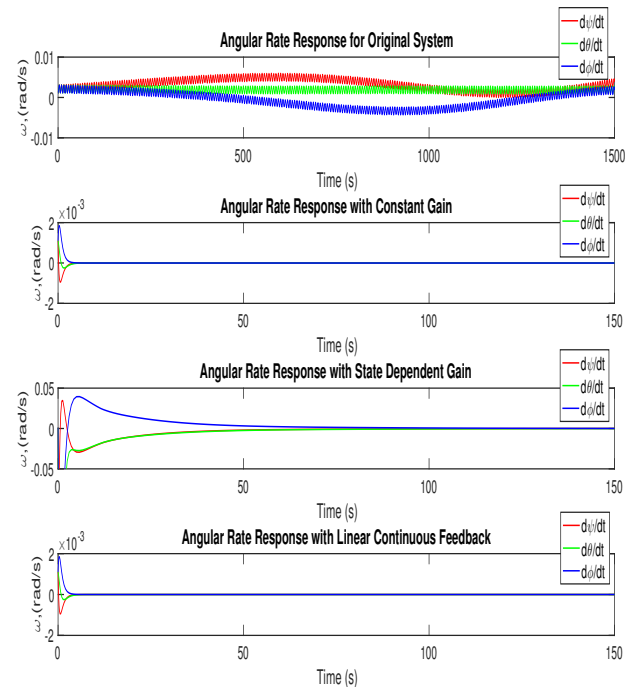
Figure 3. Angular Rate Response of the Uncompensated and Compensated System at the Proper Gain

Table IV
ANGULAR RATE RESPONSE AT THE CRITICAL GAIN

	Original System	RCG	RSG	LFSG
Steady State Error	Yes	Yes	Yes	No
Chattering	Yes	Yes	Yes	No
Chattering Amplitude		$0.02 rads^{-1}$	$0.02 rads^{-1}$	0
Settling Time		120 s	40 s	280 s

Table V
ANGULAR RATE RESPONSE AT THE PROPER GAIN

	Original System	RCG	RSG	LFSG
Steady State Error	Yes	No	No	No
Settle Time		10 s	100 s	10 s

B. Control Inputs of Spacecraft's Attitude System

Looking at the control inputs in figure 4, all the SFD methods show some chattering with an amplitude of 0.1 $rads^{-}1$. RSG, however, takes 5 seconds to converge to the chattering amplitude compared to RCG and LFSG methods where the chattering begins immediately.
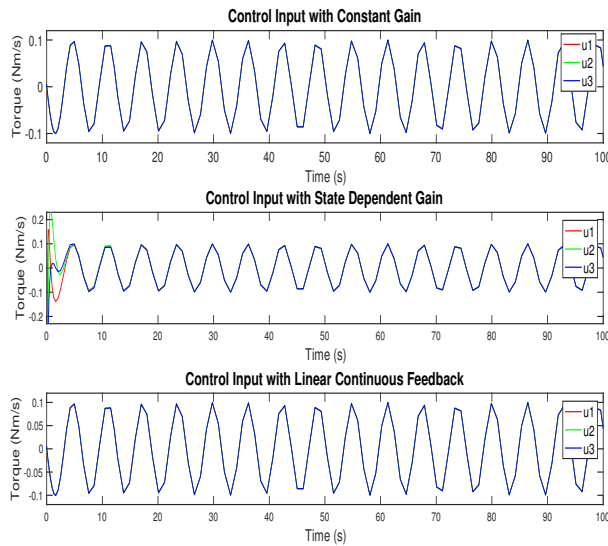
Figure 4. Control Input of the Compensated System

V. CONCLUSIONS AND FUTURE RECOMMENDATIONS

This paper has focused on the potential uses of SMC methods for spacecraft attitude control and specifically designs and contrasts three common algorithms.

In conclusion, the LFSG method shows a better performance as there is no chattering in the angular velocity outputs at the critical gains compared to RCG and RSG (both are producing chattering in the outputs) for spacecraft's attitude model (see Table IV). Thus, LFSG will be the preferred option to design the SMC control law for this system. However, it is noted that a modification in LFSG is required in order to attenuate the chattering in the control input. Some of the modifications to eliminate the chattering can cause high complexity to the control input. Hence, a proper approach must be chosen to make sure the control input is low complexity algorithm. It is important to reduce the operating power consumption in spacecraft. Thus, some possible modifications to explore include higher order sliding mode control [13], variable gain supertwisting sliding mode control [14] and decaying boundary layer, and switching function method thorough error feedback [2]. Besides that, the most difficult part in this design is tuning the critical gains. However, as long as the range of matching uncertainties are known, thus it can reduce the probability number of the gains since the gains are bounded in the matching uncertainties (see Section II).

VI. ACKNOWLEDGEMENTS

REFERENCES

[1] H. Hassrizal and J. Rossiter, "A survey of control strategies for spacecraft attitude and orientation," in *Control (CONTROL), 2016 UKACC 11th International Conference on*. IEEE, 2016, pp. 1–6.

[2] ——, "Application of decaying boundary layer and switching function method thorough error feedback for sliding mode control on spacecraft's attitude," in *Control and Automation (MED), 2017 25th Mediterranean Conference on*. IEEE, 2017, pp. 1250–1256.

[3] X. Liu, P. Guan, and J. Liu, "Fuzzy sliding mode attitude control of satellite," in *Decision and Control, 2005 and 2005 European Control Conference. CDC-ECC'05. 44th IEEE Conference on*. IEEE, 2005, pp. 1970–1975.

[4] L. Cao, X. Li, X. Chen, and Y. Zhao, "Minimum sliding mode error feedback control for fault tolerant small satellite attitude control," *Advances in Space Research*, vol. 53, no. 2, pp. 309–324, 2014.

[5] A. Sofyalı and E. M. Jafarov, "Integral sliding mode control of small satellite attitude motion by purely magnetic actuation," *IFAC Proceedings Volumes*, vol. 47, no. 3, pp. 7947–7953, 2014.

[6] A. Chalanga, S. Kamal, and B. Bandyopadhyay, "A new algorithm for continuous sliding mode control with implementation to industrial emulator setup," *IEEE/ASME Transactions on Mechatronics*, vol. 20, no. 5, pp. 2194–2204, 2015.

[7] R. A. DeCarlo, S. H. Zak, and G. P. Matthews, "Variable structure control of nonlinear multivariable systems: a tutorial," *Proceedings of the IEEE*, vol. 76, no. 3, pp. 212–232, 1988.

[8] H. Song, Y. Yu, M. Yang, and D. Xu, "A novel smc-fuzzy speed controller for permanent magnet brushless dc motor," in *Applied Power Electronics Conference and Exposition, 2003. APEC'03. Eighteenth Annual IEEE*, vol. 1. IEEE, 2003, pp. 281–285.

[9] A. Tewari, *Advanced control of aircraft, spacecraft and rockets*. John Wiley & Sons, 2011, vol. 37.

[10] F. Bacconi, "Spacecraft attitude dynamics and control," *Florence: Florence university*, vol. 2006, pp. 1–0, 2005.

[11] G. Wheeler, C.-Y. Su, and Y. Stepanenko, "A sliding mode controller with improved adaptation laws for the upper bounds on the norm of uncertainties," *Automatica*, vol. 34, no. 12, pp. 1657–1661, 1998.

[12] R. Stengal, "Spacecraft attitude control," http://www.princeton.edu/ stengel/MAE342.html, 2016.

[13] J. Gao and Y. Cai, "Higher order sliding mode control with fast transient performance," in *Measuring Technology and Mechatronics Automation (ICMTMA), 2015 Seventh International Conference on*. IEEE, 2015, pp. 524–528.

[14] T. Gonzalez, J. A. Moreno, and L. Fridman, "Variable gain supertwisting sliding mode control," *IEEE Transactions on Automatic Control*, vol. 57, no. 8, pp. 2100–2105, 2012.

Particle Swarm Algorithm Sliding Mode Control on Spacecraft's Attitude with Switching Function Method Thorough Error Feedback

To cite this article: H. B. Hassrizal *et al* 2019 *IOP Conf. Ser.: Mater. Sci. Eng.* **705** 012039

View the article online for updates and enhancements.

Particle Swarm Algorithm Sliding Mode Control on Spacecraft's Attitude with Switching Function Method Thorough Error Feedback

Hassrizal H. B.[†], J. A. Rossiter[‡], Siti Marhainis Othman[§] and M. N. Ayob[¶]

[† ‡] Department of Automatic Control and Systems Engineering, The University of Sheffield, Mappin Street, Sheffield, S1 3JD, UK
[† § ¶] School of Mechatronic Engineering, Universiti Malaysia Perlis, Malaysia

E-mail: [†]`hassrizal@unimap.edu.my`, [‡]`j.a.rossiter@sheffield.ac.uk`,
[§] `marhainis@unimap.edu.my`, [¶]`nasirayob@unimap.edu.my`

Abstract. Small spacecraft requires capable processors with energy efficiency, low cost and low computational burden while maintaining the output tracking accuracy. This paper presents the extension of work in [1], to enhance the transient performance using particle swarm optimization (PSO) on decaying boundary layer and switching function thorough error feedback (DBLSF) in Sliding Mode Control (SMC). Generally, SMC is known for having chattering as the main drawback which can introduce wear and tear to moving mechanical parts. As a solution, a DBLSF proposed in [1] and capable of eliminating the chattering in SMC while considering the essential requirements for small spacecraft operation. Then, the extension implemented on spacecraft's attitude, which is one-of-six subsystems in spacecraft, used to orient the spacecraft referred to reference objects and control the dynamics of a spacecraft time-to-time according to the needs. However, the SMC's transient response can be tuned using some coefficients in the SMC algorithm. The parameters in [1] were tuned using outputs observation technique. In this paper, then, an improvement is introduced to optimize the outputs by adding a PSO in the SMC-DBLSF in term of transient performances and accuracy while reducing the chattering permanently.

Keywords: small spacecraft, spacecraft's attitude, SMC, chattering, switching function error feedback, PSO, control accuracy

1. Introduction

A spacecraft or satellite is an object that is orbiting larger objects such as the earth. Currently, there are more than 1000 operational human-made spacecraft and satellites in orbit around earth [2]. One of the spacecraft operations in space is position control. Then, a spacecraft critically needs a motion control system to position and orientate itself correctly, mainly when disturbances and uncertainties occur. Hence, a robust control method is required to ensure that this task successfully is done.

A small spacecraft needs processors with energy efficiency, low cost and low computational burden while operating in space. Thus, Sliding Mode Control (SMC) is one of the robust control methods, capable of providing the requirements [3][4][5]. SMC, however, produces chattering in

the controller inputs, specifically in the switching function (Eq. 1) which it can cause wear and tear to the actuator [6].

$$u_n = \begin{cases} -1 & \text{for} \quad s > 0 \\ 0 & \text{for} \quad s = 0 \\ 1 & \text{for} \quad s < 0 \end{cases} \tag{1}$$

where s is a sliding surface as in Eq. 2.

$$s = (\frac{d}{dt} + \lambda)^{n-1} e \tag{2}$$

with λ represents as a set of sliding surface coefficients, n denotes the order of the system and e is the error between the desired input and the measured output.

Thus many researchers proposed a modification in SMC techniques to overcome this problem [7][8][9][5]. One of the solutions is implementing a boundary layer around the sliding surface.

A boundary layer technique is one of the most popular methods for chattering elimination in SMC. Initially, a constant boundary layer (CBL) introduced by the researchers, but the control output accuracy cannot be maintained [10]. Then, a decaying boundary layer (DBL) where the boundary layer existing is dependent on time is proposed to solve the accuracy issue. As results, the chattering only can be eliminated for finite time [11]. As a solution, thus, a decaying boundary layer and switching function thorough error feedback (DBLSF) is proposed in [1] to eliminate the chattering while maintaining the accuracy outputs. DBLSF, however, needs an optimization algorithm to enhance the transient performances by tuning the λ parameter (Eq. 2) in the DBLSF control algorithm. Hence, in this paper, a particle swarm optimization (PSO) is introduced to the DBLSF to improve the small spacecraft attitude and orientation (SAOM) transient performance.

PSO is a straightforward concept, requires only primitive mathematical operators and needs less memory and speed of computational load where can be coded using only a few lines in the program code. Besides, PSO also suitable implements on nonlinear functions [12]. In PSO, there are two primary components used to determine the optimization of the state, which is particle and swarm. Each particle updates their coordinates referred to the best solution (fitness) it has achieved so far, which known as *pbest*. On the other hands, the swarm keeps tracking the best value and location so far among all the particles in the population, known as (*gbest*).

Since SMC and PSO sharing similar important specifications (simple mathematical operators, required low computational load and inexpensive), thus, the combination of the PSO-DBLSF is suitable to implement on small spacecraft operation.

The paper is organised as follows. Section 2 describes the orbits relative to the earth with possible disturbances and uncertainties in state-space form. Section 3 describes the SMC general model and introduces the DBLSF control algorithm. Section 4 elaborates the PSO techniques and the development control strategies for SAOM alongside the PSO-DBLSF. Section 5 demonstrates the comparison results between DBLSF and PSO-DBLSF. In Section 6, brief conclusions are given along with proposals for future work, that is where improvements of the control strategies are possible.

2. Spacecraft's Attitude and Orientation Model around Earth

In this section, the angular velocity of the spacecraft's attitude is designed and translated into state-space form. Figure 1(a) represents a rigid body spacecraft, orbiting the earth concerning Earth Centered Inertial (ECI) at an angular velocity, ω_O with three rotational degrees of freedom. The general dynamics equation [13] for Figure 1(a) as in Eq. 3.

5th International Conference on Man Machine Systems

IOP Conf. Series: Materials Science and Engineering **705** (2019) 012039

IOP Publishing

doi:10.1088/1757-899X/705/1/012039

(a)

(b)
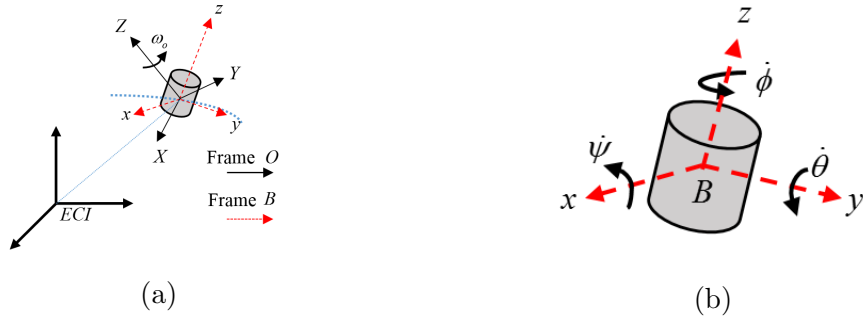
Figure 1. (a) Spacecraft's attitude in moving frame B with respect to an orbiting reference frame O and both are moving in ECI
(b) Sequence of Euler's angles,$(R_x(\psi) \to R_y(\theta) \to R_x(\psi))$, according moving frame B orientation relative to an orbiting frame O

$$J\dot{\omega} = J\omega \times \omega + \tau \tag{3}$$

where $J = diag(J_x, J_y, J_z)$ represents the constant inertia matrix in the body-fixed frame, $\tau = diag(\tau_x, \tau_y, \tau_z)$ is the applied torque and ω is the spacecraft angular velocity orbiting around the Earth.

The kinematics of the rigid body (Figure 1(a)) are designed using Euler's angles with the sequence rotation (Figure 1(b)) as in Eq. 4 with each axis denoted as angular velocity for $\dot{\psi}$ (roll), $\dot{\theta}$ (pitch) and $\dot{\phi}$ (yaw).

$$
\begin{aligned}
Q &= R_Z(\phi) * R_Y(\theta) * R_X(\psi) \\
&= \begin{bmatrix}
c\phi c\theta & c\psi sin\phi + c\phi sin\psi s\theta & s\psi s\phi - c\psi c\phi s\theta \\
-c\theta s\phi & c\psi c\phi - s\psi s\phi s\theta & c\phi s\psi + c\psi s\phi s\theta \\
s\theta & -c\theta s\psi & c\psi c\theta
\end{bmatrix} \\
&= \begin{bmatrix}
c\phi c\theta & c\psi s\phi + c\phi s\psi s\theta & s\psi s\phi - c\psi c\phi s\theta \\
-c\theta s\phi & c\psi c\phi - s\psi s\phi s\theta & c\phi s\psi + c\psi s\phi s\theta \\
s\theta & -c\theta s\psi & c\psi c\theta
\end{bmatrix}
\end{aligned}
\tag{4}
$$

with $(c\psi \ c\theta \ c\psi)$ and $(s\psi \ s\theta \ s\psi)$ denote the sin and cos for each axis respectively.

Finally, the spacecraft's attitude model [1] in state-space form as in Eq. 5.

$$
\begin{bmatrix}
\dot{x}_1(t) \\
\dot{x}_2(t) \\
\dot{x}_3(t) \\
\dot{x}_4(t) \\
\dot{x}_5(t) \\
\dot{x}_6(t)
\end{bmatrix}
=
\begin{bmatrix}
0 & 1 & 0 & 0 & 0 & 0 \\
h & 0 & 0 & i & 0 & 0 \\
0 & 0 & 0 & 1 & 0 & 0 \\
0 & j & k & 0 & 0 & 0 \\
0 & 0 & 0 & 0 & 0 & 1 \\
0 & 0 & 0 & 0 & 0 & 0
\end{bmatrix}
\begin{bmatrix}
x_1(t) \\
x_2(t) \\
x_3(t) \\
x_4(t) \\
x_5(t) \\
x_6(t)
\end{bmatrix}
+
\begin{bmatrix}
0 \\
\frac{\tau_x}{J_x} \\
0 \\
\frac{\tau_y}{J_y} \\
0 \\
\frac{\tau_z}{J_z}
\end{bmatrix}
u(t)
\tag{5}
$$

where

$$
\begin{aligned}
h &= (\tfrac{J_y - J_z}{J_x})\omega_O^2; & i &= (\tfrac{J_x + J_y - J_z}{J_x})\omega_O; \\
j &= (\tfrac{J_z - J_y - J_x}{J_y})\omega_O; & k &= -(\tfrac{J_z - J_x}{J_y})\omega_O^2;
\end{aligned}
$$

$$[x_1(t) \ x_2(t) \ x_3(t) \ x_4(t) \ x_5(t) \ x_6(t)]^T = [\psi \ \dot{\psi} \ \theta \ \dot{\theta} \ \phi \ \dot{\phi}]^T$$

$$[\dot{x}_1(t) \ \dot{x}_2(t) \ \dot{x}_3(t) \ \dot{x}_4(t) \ \dot{x}_5(t) \ \dot{x}_6(t)]^T = [\dot{\psi} \ \ddot{\psi} \ \dot{\theta} \ \ddot{\theta} \ \dot{\phi} \ \ddot{\phi}]^T$$

3. Sliding Mode Control

In this section, the general SMC's approach is elaborated. Then, the advantages and disadvantages of the DBLSF are discussed with a possible solution. In SMC, a compensated system guaranteed to achieve the robustness once hitting around a sliding surface (determine the transient performance) and achieve the equilibrium point by the switching surface (u_n) expression. The switching function, however, produces chattering in control input as a drawback. Hence, many modifications in switching function developed and proposed to overcome this issue. Then, a decaying boundary layer and switching function thorough error feedback (DBLSF) [1] is proposed and can solve the chattering problem. The DBLSF used outputs observation techniques to determine the λ parameter (Eq. 8) in the sliding surface, which influenced the transient output characteristics.

Consider a linear system with matching uncertainties in (6).

$$\dot{x}(t) = Ax(t) + B(u(t) + d(t)) \tag{6}$$

with $x(t) \in R^n$ is the system state, $u(t)$ is the scalar input, $A \in R^{n \times n}$ and $B \in R^m$ are the nominal system matrices satisfying the controllability condition and $d(t)$ an unknown bounded disturbance.

In general, SMC's control input algorithm (u_{smc}) (7) is construct by two parts; sliding surface (continuous, u_{eq}) and switching surface (discontinuous, u_n).

$$u_{smc} = u_{eq} + u_n \tag{7}$$

with u_{eq} is an equivalent estimation control (Eq. 8) derived from Eq. 6 [1] and u_n from Eq. 1 which can be simplified into Eq. 9. However, Eq. 9 generates chattering in the control inputs.

$$u_{eq} = -(\lambda B)^{-1}(\lambda Ax(t)) - d(t) \tag{8}$$

where λ is a set of sliding surface coefficients.

$$u_n = \frac{s}{|s|} \tag{9}$$

Initially, the CBL in SMC can eliminate the chattering, however, reduce the output accuracy, which depends on the boundary layer width [1]. Thus, the DBLSF (Eq. 10) is introduced to solve this disadvantage where the boundary layer width is dependent on the error, d_0. In DBLSF, when the time converges to finite, then the $d_0 \approx 0$. As a result, the output accuracy is guaranteed [1].

$$u_{ndblsf} = \frac{se^{\frac{-\pi}{|d_0|}}}{\left|s + \epsilon_0 e^{\frac{-\pi}{|d_0|}}\right|} \tag{10}$$

where $|d_0|$ is the error between actual output and desired output and ϵ_0 is the boundary layer width.

Finally, the SMC-DBLSF control strategy as in Eq. 11.

$$u_{smc} = -(\lambda B)^{-1}(\lambda Ax(t)) - d(t) - \frac{se^{\frac{-\pi}{|d_0|}}}{\left|s + \epsilon_0 e^{\frac{-\pi}{|d_0|}}\right|} \tag{11}$$

Besides, the transient response of the SAOM outputs depends on the λ value in Eq. 11. In [1], an output observation technique is used to determine the λ value, which did not optimize the outputs transient. As a solution, the λ can be tuned using the PSO approach to enhance transient optimization.

4. Particle Swarm Optimization

In this section, the PSO concept is elaborated, and the control strategies for PSO-DBLSF on SAOM is developed. In PSO, a swarm represents by a population while a particle denotes by an individual [14]. Each particle produces two parameters, which are position and velocity. The relationship between the current position and next iteration position, and velocity as in Eq. 12.

$$s_i(k+1) = s_i(k) + v_i(k+1) \tag{12}$$

where i is the particle number, k refers to the number of iteration, $s_i(k+1)$ and $v_i(k+1)$ represent the next iteration value for particle's position and velocity respectively and s_i is the current iteration for particle's position.

Then, the $v_i(k+1)$ term can be obtained using Eq. 13 [14].

$$v_i(k+1) = wv_i(k) + c_1 r_1 (pbest_i - s_i(k)) + c_2 r_2 (gbest_i - s_i(k)) \tag{13}$$

where w denotes the inertia weight for current particle's velocity, $v_i(k)$ represents the current iteration for velocity of particle, c_1, and c_2 are the cognitive and social component which are known as learning factors and r_1 and r_2 are random number between 0 and 1.

In this paper, the objective function in the SAOM model is to minimize the error value for each state (ψ, θ, ϕ). Hence, the PSO used the error values from the simulation to tuning the λ, which act as the particle to improve the transient performance.

5. Results

In this section, the spacecraft's position model (Eq. 5) is analyzed using DBLSF and PSO-DBLSF. Then, the transient performances and the outputs accuracy for both approaches are compared. The numeric parameters are set up for the SAOM, as shown in Table 1.

Table 1. Numeric parameters of the spacecraft's attitude system and PSO

Parameter	Value	Unit
ω_O	0.0011	$rads^{-1}$
J_x	35	kgm^2
J_y	16	kgm^2
J_z	25	kgm^2
$\tau_{x,y,z}$	0.001	Nm
$d(t)$	$sin(t)$	$-$
$c_1,\ c_2$	1.42	$-$
w	0.9	$-$

Next, the λ values for all axis $(\psi, \theta$ and $\phi)$ using PSO (13) and output's observation technique are represent in Table 2. There are two periodic inputs given to each axis with the state's initial condition as in Table 3.

Table 2. The λ values using DBLSF and PSO-DBLSF

	DBLSF	PSO-DBLSF
λ_ψ	0.2500	2.4567
λ_θ	0.2500	2.1442
λ_ϕ	0.2500	1.6229

Table 3. Inputs characteristics on the SAOM with states initial condition

	Initial Condition	Inputs	
		$0 \leq t < 75s$	$75 \leq t \leq 150s$
Roll (ψ)	-0.50	0.50	1.00
Pitch (θ)	-0.87	1.05	0.25
Yaw (ϕ)	0.35	-1.57	-0.25

Figure 2 shows the SAOM's outputs using the DBLSF (Figure 2(a)) and the PSO-DBLSF (Figure 2(b)) techniques. It clearly can be seen that the transient response of the PSO-DBLSF improved compared to the DBLSF. The rise time for the PSO-DBLSF's first periodic input ($0 \leq t < 75s$) are $2.746s$, $3.912s$ and $3.207s$ for ψ, θ and ϕ respectively but the DBLSF shows over than $8s$ for all states. In term of accuracy, the outputs error compared to the desired inputs are slightly comparable for both methods. The PSO-DBLSF recorded less maximum-error among the states (0.2095%) compared to the DBLSF (2.0200%) algorithm. On the other hand, both methods effectively eliminate the chattering in the control inputs (Figure 3(b) and Figure 3(c)) compared to the classical SMC algorithm (Figure 3(a)). The detailed summary for both observations in term of the outputs accuracy comparison and transient characteristics between the DBLSF and the PSO-DBLSF is shown in Table 4 and Table 5.
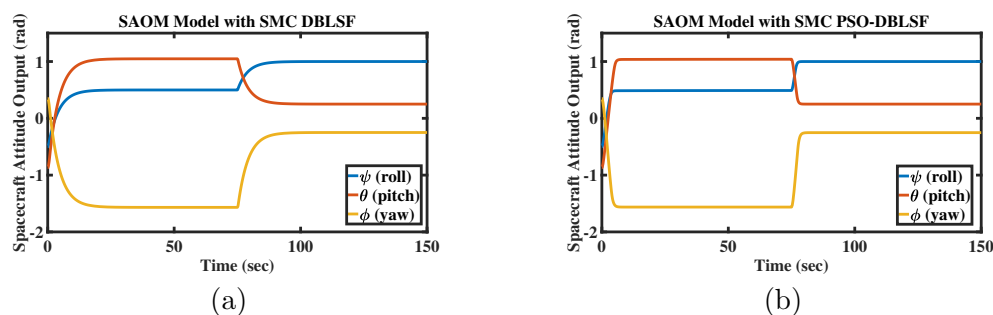
Figure 2. The SAOM's outputs using the DBLSF (a) and the PSO-DBLSF (b)

Table 4. The outputs accuracy comparison between the DBLSF and the PSO-DBLSF compared to the target output

Output Parameters	Time (s)	Desired Outputs (rad)	DBLSF		PSO-DBLSF	
			Output (rad)	Error (%)	Output (rad)	Error (%)
Roll (ψ)	75	0.5000	0.4899	2.0200	0.4991	0.1800
	150	1.000	0.9997	0.0300	0.9999	0.0100
Pitch (θ)	75	1.0500	1.0402	0.9333	1.0478	0.2095
	150	0.2500	0.2503	0.1200	0.2504	0.1600
Yaw (ϕ)	75	-1.5700	-1.5628	0.4586	-1.5678	0.1401
	150	-0.2500	-0.2521	0.8400	-0.2496	0.1600

(a)

(b)

(c)

Figure 3. The SAOM's control inputs using the classical SMC (a), the DBLSF (b) and the PSO-DBLSF (c)

Table 5. The transient comparison between the DBLSF and the PSO-DBLSF

	Rise Time / Fall Time (s)	
	$0 \leq t < 75s$	
SMC Approaches	DBLSF	PSO-DBLSF
Roll (ψ)	8.713	2.746
Pitch (θ)	8.753	3.912
Yaw (ϕ)	8.753	3.207

6. Conclusions and Future Recommendations

SMC approaches can produce high control accuracy, but the occurrence of chattering phenomena is a significant drawback. The proposed DBLSF method in [1] can eliminate chattering; however, did not offer optimization in the transient characteristics. Implementing a PSO on a DBLSF, then, capable of optimizing the performance of the output while maintaining the accuracy and eliminate the chattering in the control input.

In space, however, some scenarios and applications need drastic changing in the inputs, for instance, debris (encompasses by natural and artificial particles produced from meteoroid and human-made respectively) avoidance in space [15], spacecraft formation [16] and spacecraft rendezvous and docking manoeuvres (SRDM) [17]. Then, PSO-DBLSF is proposed to validate the robustness and capability to encounter the challenges on these scenarios for future research.

References

[1] Hassrizal H B and Rossiter J A 2017 *Control and Automation (MED), 2017 25th Mediterranean Conference on* (IEEE) pp 1250–1256

[2] of Concerned Scientists U 2016 Ucs satellite database http://www.ucsusa.org/nuclear-weapons/space-weapons/satllite-database

[3] Guldner J and Utkin V I 1993 *Proceedings of 32nd IEEE Conference on Decision and Control* (IEEE) pp 424–429

[4] Nguyen T, Leavitt J, Jabbari F and Bobrow J 2007 *IEEE/ASME Transactions on mechatronics* **12** 216–219

[5] Sofyalı A and Jafarov E M 2014 *IFAC Proceedings Volumes* **47** 7947–7953

[6] Hassrizal H B, Rossiter J A and Firdaus A R 2018 *Proceedings of CoDIT'18* (IEEE)

[7] Liu X, Guan P and Liu J 2005 *Decision and Control, 2005 and 2005 European Control Conference. CDC-ECC'05. 44th IEEE Conference on* (IEEE) pp 1970–1975

[8] Cao L, Chen X and Sheng T 2013 *Advances in Space Research* **51** 2374–2393

[9] Cao L, Li X, Chen X and Zhao Y 2014 *Advances in Space Research* **53** 309–324

[10] Utkin V I 1993 *IEEE transactions on industrial electronics* **40** 23–36

[11] Chen M S, Hwang Y R and Tomizuka M 2002 *Automatic Control, IEEE Transactions on* **47** 1677–1681

[12] Eberhart R and Kennedy J 1995 *MHS'95. Proceedings of the Sixth International Symposium on Micro Machine and Human Science* (IEEE) pp 39–43

[13] Bacconi F 2005 *Florence: Florence university* **2006** 1–0

[14] Ayob M N, Yusof Z M, Adam A, Abidin A F Z, Ibrahim I, Ibrahim Z, Sudin S, Shaikh-Husin N and Hani M K 2010 *2010 2nd International Conference on Computational Intelligence, Communication Systems and Networks* (IEEE) pp 49–53

[15] Kessler D J and Cour-Palais B G 1978 *Journal of Geophysical Research: Space Physics* **83** 2637–2646

[16] Felicetti L and Emami M R 2016 *Acta Astronautica* **127** 491–504

[17] Fehse W 2003 *Automated rendezvous and docking of spacecraft* vol 16 (Cambridge university press)